CONCEPTUAL DESIGN OF GASIFICATION-BASED BIOREFINERIES USING THE C-H-O TERNARY DIAGRAM

by

Lefu Andrew Litheko (50 14 67 18)

submitted in accordance with the requirements

for the degree of

Master of Technology

in the subject

Chemical Engineering

at the

UNIVERSITY OF SOUTH AFRICA

Supervisor: Professor Bilal Patel

October, 2017

DECLARATION

I declare that **Conceptual design of gasification-based biorefineries using the C-H-O ternary diagram** *is my own work and that all the sources that I have used or quoted have been indicated and acknowledged by means of complete references.*

I further declare that I submitted the thesis to originality checking software. The result summary is attached.

I further declare that I have not previously submitted this work, or part of it, for examination at UNISA for another qualification or at any other higher education institution.

.....

Lefu Andrew Litheko

.....day of.....2017

ACKNOWLEDGEMENTS

I would first and foremost like to express my heartfelt appreciation and gratitude to my supervisor and promoter, Professor Bilal Patel. His guidance, insight, expertise and motivation have been invaluable over the course of the research project. I will forever remain grateful to him for the contribution he made from the start to the finish of my master's degree.

I would also like to thank my fellow students as well as part of UNISA staff body at the department of Civil and Chemical Engineering, in particular KB, Rudzani, Pinky and Corina for their pleasant conversations, support and encouragement. Many thanks are also due to the Process and Laboratory section at the Water and Sewage Company (WASCO) Pty (Ltd), particularly my Manager Mr Mpho Mokoatleng for the support he afforded me to complete my master's degree.

My sincere appreciation also goes to my sister, Mamthimk'hulu Mafaesa for my upbringing and her steadfast support. I will always be indebted to her for all the sacrifices she made. I am also appreciative to my best friend and life companion, Mpho Mokone. Her constant support, encouragement and editorial efforts on my dissertation have been invaluable and greatly appreciated. Words are not enough to express my indebtedness to my dear friend Morris Karumazondo, whose friendship and support has contributed significantly towards the completion of my research.

Last but not least, I would like to acknowledge and appreciate the financial support from the University of South Africa (UNISA) as well as the Chemical Industries Education & Training Authority (CHIETA) which allowed me to finish my study.

ABSTRACT

This dissertation develops a systematic targeting method based on the C-H-O ternary diagram for the conceptual design of gasification-based biorefineries. The approach is applied using dimethyl ether (DME) as case study. A stoichiometric equilibrium model is presented for calculation of the C-H-O chemical equilibria to evaluate and predict equilibrium syngas composition, operating temperature, type and amount of oxidant required in biomass gasification. Overall atomic species balances are developed and process targets are plotted on the C-H-O ternary diagram. Sustainability metrics are incorporated to provide useful insights into the efficiency of biorefinery process targets. It was found that syngas at 1200 and 1500 K is predominantly H_2 and CO. Moreover, DME biorefineries have two main process targets, based on the indirect and direct synthesis routes. Gasification at 1200 K and 1 atm. using H_2O/CO_2 = 2.642 (w/w) and H_2O/CH_4 = 1.645 (w/w) achieved syngas composition targets for the direct and indirect methods respectively. Comparatively, the integrated biorefinery based on indirect route was more efficient, producing 1.903 ton of DME per ton of biomass feedstock. The process is 100% carbon-efficient and recycles 1.025 tons of H_2O.

Keywords: biorefinery, gasification, C-H-O ternary diagram, chemical equilibria, dimethyl ether (DME), process targets, sustainability metrics

TABLE OF CONTENTS

LIST OF FIGURES

LIST OF TABLES

CHAPTER 1

INTRODUCTION

1.1. BACKGROUND

A cursory examination of the current energy patterns (i.e. the energy supply and demand) challenges any notion of sustainable global development for a number of reasons: The world's economy is almost entirely dependent on fossil fuel resources which are non-renewable. Specifically, 86% of the world's energy and 96% of organic chemicals are currently being supplied from fossil fuels (Waldron, 2014). Significant pressure is constantly being put on these resources as a result of the world currently experiencing a period of unprecedented growth in the main drivers of energy (i.e. economic activity, population and technological advancement). This means that these fossil fuel resources are headed for an inevitable depletion in the next few decades (BP, 2015). Furthermore, the net anthropogenic CO_2 and other greenhouse gases (GHGs) released as a result of the combustion of fossil fuels are said to contribute substantially to global warming and other climate issues (Johansson et al., 2012).

Therefore, as a way to deal with the abovementioned challenges and attenuate some of the impact, more attention has been paid to alternative renewable energy sources like biomass, wind, solar, geothermal, etc. Biomass is the only source of renewable carbon and therefore the only viable option to crude oil and natural gas for the production of fuels and material products. It is estimated that woody biomass worldwide, can supply over 56 EJ of the global primary energy (World Energy Council, 2016). The World Bioenergy Association (2014) also reports that agricultural residues such as corn stover, straw, husks, cobs, bagasse, etc. have a potential to provide approximately 17 EJ to 128 EJ. These amounts of potential energy from some of the biomass resources, underscore the general potential that biomass has as a sustainable source of fuels and chemicals.

1.2. THE CHALLENGE OF SUSTAINABILITY IN BIOREFINERIES

The processing of biomass feedstock into marketable products and fuels is called bio-refinery and it is analogous to contemporary petroleum-refinery (Kamm et al., 2006). Because the concept of biorefineries is still new, biorefineries are faced with the challenge of sustainability. Efficient utilization of energy and raw materials as well as improved environmental performance form part of the indices for sustainable biorefineries. For the past few decades, many well-established conversion technologies have been developed for processes that convert biomass to value added products. Examples include the production of biodiesel from the transesterification of vegetable oil as well as production of bio-alcohols from corn. These biorefinery technologies mostly comprise of standalone plants which focus on the production of a single product from a single feedstock. Even though these processes may be productive and have proven to be technically viable, they may still not be sustainable.

Fernando et al. (2006) suggest a more efficient framework for the valorization of biomass based on the use of multiple feedstock and integration of various conversion processes to produce a wide spectrum of products. This is referred to as integrated biorefineries and it enhances the overall process efficiency as well as economic performance of biorefineries by minimizing waste and maximizing energy and material recovery. However, given the broad portfolio of available biomass feedstock, potential products, reaction pathways and processing technologies, integrated biorefinery configurations are open and extremely complex (Yuan et al., 2013).

Gasification is one of the technologies that are remarkably adaptable to integrated biorefineries because it is robust, feedstock-neutral and produces an intermediated platform that has multiple industrial functions and applications (Demirbas, 2010). It involves the thermochemical, partial oxidation of biomass feedstock by means of an oxidant to produce a combustible gaseous product and/or platform called synthesis gas. Syngas produced from biomass gasification can be used for heat and power generation, and as a precursor for producing a broad portfolio of products such as dimethyl ether (DME), mixed alcohols, diesel, gasoline, etc.

Each of the various downstream applications of syngas platform in gasification-based biorefineries requires specific syngas composition. For instance, downstream application of syngas for the synthesis of methanol requires syngas with a H_2/CO ratio of 2 (Tay et al., 2011). Optimizing and tailoring the composition of syngas for application in these technologies, in turn, requires manipulation of a number of process parameters including reactor temperature and pressure, feedstock material and dimensions, type of gasifying agents, reactor design etc. The optimum selection of these process conditions cannot be overemphasized as it impacts the economics as well as the overall efficiency of the gasification-based biorefinery process.

1.3. APPROACH: CONCEPTUAL DESIGN OF SYNGAS-BASED INTEGRATED BIOREFINERIES

One of the ways to addressing the issue surrounding sustainability in integrated biorefineries is through efficient process design. Effective design of integrated biorefineries should focus on synthesis, integration and screening of alternatives (El-Halwagi, 2012). Since there are a large number of available alternatives involved in gasification-based integrated biorefineries, systematic tools and/or methods are required for the synthesis and evaluation of potential bio-based products, conversion technologies and process parameters.

In particular, systematic methodologies based on physical (thermodynamic) insight offer a useful means to determine the performance benchmarks of biorefinery processes early in the conceptual stage of the design process. These benchmarks/targets define the theoretical limits that can be achieved in the process (Patel et al., 2007). Insights-based tools are based on fundamental principles such as mass, energy and entropy/exergy balance to (i) provide overall insight into the process, (ii) set performance benchmarks prior to designing the process flowsheet, and (iii) identify opportunities for improvement in the process at the conceptual stage of the design *(ibid.*). That is, the application of these methods ranges from grassroots design to retrofitting and evaluation of existing processes and flowsheets.

Insight-based methods use minimum data in calculations based on algebraic, graphical or mathematical optimization techniques to achieve the set target or optimum flowsheet (El-

Halwagi, 2006). An important aspect of the insights approach that renders it extremely useful is that it considers a holistic or macroscopic view of the process and not the individual units of the process. This enables the designer to dictate the overall process material balance instead of allowing the process to dictate the material balance (Patel, 2015).

1.4. AIMS AND OBJECTIVES

This study addresses the issue of sustainability in the context of gasification-based integrated biorefinery through process synthesis and integration. Specifically, a systematic process synthesis tool is developed for the conceptual design of a gasification-based biorefinery. A graphical targeting approach based on C-H-O ternary diagrams is used to determine the maximum potential for the biorefinery as defined in terms of material balance targets (i.e. maximum yield of the desired final product) according to the technique proposed by Tay et al. (2011).

The study consists of two main aims:

Firstly, it presents a stoichiometric equilibrium model for biomass gasification which can be used to evaluate and predict the equilibrium composition of syngas. This is useful for analyzing and optimizing the gasification process in order to increase the overall performance of the entire gasification-based integrated biorefinery. Specific objectives that are deemed important to realize this aim are:

1. Analyze, and formulate the complex chemical equilibrium for the C-H-O system.
2. Solve and provide gaseous equilibrium composition and carbon deposition boundaries for the C-H-O system.

Secondly, a graphical targeting approach that applies the equilibrium gas composition with carbon deposition boundaries is presented for the conceptual synthesis of a syngas-based biorefinery. Based on syngas composition targets, C-H-O ternary diagrams with carbon deposition boundaries are systematically used to design the integrated biorefinery. The

approach is illustrated by means of a case study for the synthesis of DME with respect to a number of specific objectives, namely,

1. To determine the maximum targets for DME synthesis in a syngas-based integrated biorefinery.
2. To determine the syngas composition target required for the application in the synthesis of DME.
3. To investigate the optimum reacting conditions for biomass gasification, including the type of gasifying agents, as well as the gasifying temperature.

The study is entirely theoretical and investigates process targets for the actual syngas-based biorefinery process with the goal to optimize the production of syngas for application in a downstream process. Fundamental concepts and thermodynamic principles are applied to define the limits within which syngas-based biorefineries can be better understood, optimized and operated. The approach is suitable for preliminary evaluation of gasification-based biorefineries prior to the detailed design of the process.

The research work will add to the patchwork of developments in the synthesis and design of biorefineries by evaluating and comparing the process targets for the DME production routes. The overall study will comprise of five chapters and its outline structure is provided in the following section.

1.5. DISSERTATION STRUCTURE

Chapter 1 - Introduction

This chapter gives a brief background on the traditional paradigm of meeting the current energy demand and looks at the drivers for the development of biorefineries. The challenges related to the sustainability of biorefineries as well as the approach to improve current and future biorefineries are presented. The chapter then elaborates the research aim(s) and

identifies the main objectives to achieve the aim(s). In conclusion, the value and contribution of the research work are presented.

Chapter 2 - Literature Review

This chapter sets out by discussing the current factors that are propelling the modern economy to make a transition from fossil fuel resources to cleaner, renewable sources. It then proceeds to describe the uniqueness of biomass as a renewable carbon source, and then defines the concept of biorefineries. The three types of biorefineries according to their feedstock, process and product targets are discussed. A way of enhancing sustainability and efficiency of biorefineries is explored further under the topic - integrated biorefineries.

The chapter then focuses on a technology that is adaptable to the concept of integrated biorefineries, i.e. gasification: The fundamentals of biomass gasification process, including the effects of operating conditions, reaction chemistry, gasifier performance and modelling are discussed. The last section of the chapter deals with the design of syngas-based biorefineries, looking into the targeting and conceptual phase of the design process.

Chapter 3 – Methodology/Research Methods

The chapter provides an overview of the concepts that will be used in the dissertation, including the C-H-O ternary plot/diagram, material balance and inverse lever rule, C-H-O thermodynamic equilibrium, etc. In particular, it is shown how valuable these concepts are in designing biorefinery processes at a conceptual stage. The chapter then provides a brief delineation of the analysis and calculation of the chemical equilibria for the C-H-O system as well as how it will be applied in the conceptual design of a syngas-based DME biorefinery.

Chapter 4 - Results and discussions

Chapter 4 of the dissertation provides a discourse of the results of the C-H-O chemical equilibria calculation, focusing on the model validation, general trends of the equilibrium syngas composition and carbon deposition boundaries. It then moves on to discuss the

application of material balance and the equilibrium syngas composition in the case study for the conceptual design of DME biorefinery.

Chapter 5 - Conclusions

The chapter concludes the dissertation by providing a summary of key findings and recommendations for future work.

REFERENCES

1. BP. 2015. *BP Statistical Review of World Energy June 2015*. http://www.bp.com/statisticalreview 15 July 2015.

2. Demirbas, A. 2010. *Biorefineries: for biomass upgrading facilities*. Dordrecht; New York: Springer.

3. El-Halwagi, M.M. 2006. *Process integration*. Amsterdam: Elsevier Academic Press.

4. El-Halwagi, M.M. 2012. *Sustainable design through process integration: fundamentals and applications to industrial pollution prevention, resource conservation, and profitability enhancement*. Boston, MA: Butterworth-Heinemann.

5. Fernando, S., Adhikari, S., Chandrapal, C. & Murali, N. 2006. Biorefineries: Current Status, Challenges, and Future Direction. *Energy & Fuels*, 20(4): 1727–1737.

6. Johansson, T.B., Patwardhan, A., Nakićenović, N., Gomez-Echeverri, L. & International Institute for Applied Systems Analysis eds. 2012. *Global Energy Assessment (GEA)*. Cambridge: Laxenburg, Austria: Cambridge University Press ; International Institute for Applied Systems Analysis.

7. Kamm, B., Gruber, P.R. & Kamm, M. eds. 2006. *Biorefineries - industrial processes and products: status quo and future directions*. Weinheim: Wiley-VCH.

8. Patel, B. 2015. A Thermodynamic Targeting Approach for the Synthesis of Sustainable Biorefineries. In *Computer Aided Chemical Engineering*. Elsevier: 1283–1288.

9. Patel, B., Hildebrandt, D., Glasser, D. & Hausberger, B. 2007. Synthesis and Integration of Chemical Processes from a Mass, Energy, and Entropy Perspective. *Industrial & Engineering Chemistry Research*, 46(25): 8756–8766.

10. Tay, D.H.S., Ng, D.K.S., Kheireddine, H. & El-Halwagi, M.M. 2011. Synthesis of an integrated biorefinery via the C–H–O ternary diagram. *Clean Technologies and Environmental Policy*, 13(4): 567–579.

11. Waldron, K.W. ed. 2014. *Advances in biorefineries: biomass and waste supply chain exploitation*. Amsterdam: Elsevier/Woodhead Publishing.

12. World Bioenergy Association. 2014. WBA Global Bioenergy Statistics 2014. http://worldbioenergy.org/uploads/WBA%20Global%20Bioenergy%20Statistics%202014.pdf 20 February 2018.

13. World Energy Council. 2016. World Energy Resources 2016. http://www.worldenergy.org/wp-content/uploads/2016/10/World-Energy-Resources-Full-report-2016.10.03.pdf 15 February 2018.

14. Yuan, Z., Chen, B. & Gani, R. 2013. Applications of process synthesis: Moving from conventional chemical processes towards biorefinery processes. *Computers & Chemical Engineering*, 49: 217–229.

CHAPTER 2

LITERATURE REVIEW

2.1. BACKGROUND

Serious implications arise from the fact that the world is heavily dependent on resources which are non-renewable. Fossil fuels such as coal, crude oil as well as natural gas supply approximately 86% of the global energy and 96% of organic chemicals (Waldron, 2014). According to Johansson et al. (2012), the demand for these resources is mainly driven by economic activity, population, and technological advancement. With the world undergoing a period of dramatic growth in these three parameters, it is estimated that by 2025, our energy demands are expected to increase by 50% (Ragauskas, 2006). This will result in significant strain on these conventional resources and the question of how long we can depend on them as our primary energy source arises.

A report by BP (2015), reveals that the quantities of oil and natural gas from proven reserves reached 1.7 trillion barrels and 187.1 trillion cubic meters respectively at the close of 2014. These reserves are sufficient to meet 52.5 years of global production for oil and 54.1 years for natural gas (*ibid.*). In addition, the use of fossil fuels has been the cause of several debilitating concerns. Evans (2015) maintains that the current use of fossil fuels on a large-scale is putting significant stress on our environment. Fossil fuels are converted to energy in power plants, vehicles, industrial facilities, etc. through combustion reactions that lead to a net emission of CO_2 and other greenhouse gases (GHGs), and air pollutants into the atmosphere.

For instance, IPCC (2007, cited in Edenhofer et al., 2012) has confirmed that the anthropogenic activities from energy production, industrial processes and transport has raised the atmospheric concentration of the main greenhouse gas, CO_2, from a pre-industrial level of around 280 ppm to nearly 370 ppm today. This represents a total atmospheric carbon concentration of about 760 Gt added to the atmosphere (Evans, 2015). The main consequence of the increased concentration is the global mean temperature (GMT) increase

of 0.74°C $\pm$ 0.18°C, which has been associated with other climate issues such as severe storms, melting of the ice caps, and more frequent droughts (Johansson et al., 2012).

Another matter of concern is the fear over the availability of sufficient, reliable supply of energy at affordable prices in the decades ahead. Yergin (2006) refers to this as energy security. One of the main risks to energy security is the instability of the energy market. This, in turn, is also compounded by the uneven distribution of the primary energy sources *viz*. crude oil, natural gas and coal. For instance, the world's proven conventional oil reserves are concentrated in a small number of countries and regions commonly referred to as the Organization for the Petroleum Exporting Countries (OPEC) which account for approximately 71.6% of total oil reserves (BP, 2015).

However, part of the challenge is that despite this uneven distribution of oil reserves, the top 10 largest oil consuming countries do not have sufficient oil production capacity to meet their internal consumption, and therefore have to import more than 35% of the world oil demand (Lehman Brothers, 2008). This leaves the global oil supply vulnerable to the conditions of the OPEC countries and regions as well as the demand dynamics of the major consumers. As such, if anything were to disrupt the oil supply, whether due to natural, political or economic causes, this would destabilize the supply-demand balance and lead to increased fuel prices or even short-term physical scarcity of fuels.

In view of these concerns, it becomes evident that one of the main challenges facing the modern world today is the ability to supply its primary demands without compromising the ability for future generations to satiate their own needs. In this regard, both adaptation, in which mankind simply learns to adjust to these situations, and mitigation, in which measures are taken to counteract the severity of these situations have been proposed (Evans, 2015). Adaptation is seldom an option favoured by most scientists, engineers and policy makers despite arguments that mankind is adaptable. Therefore alternative renewable sources are being researched and considered for sustainable future supply of energy and material products.

Renewable resources refer to any form of solar, geo-physical, or biological source that is replenished by natural processes at a rate that equals or exceeds its rate of use. Examples include biomass, hydro, solar, wind, geothermal and ocean energy. Edenhofer et al. (2013) indicate that the theoretical supply as well as the technical potential of these renewable energy sources exceed the current energy demand. Thus, the renewable energy resource base is more than sufficient to supply our energy demands as it stands. This prospect has led to an increase in the global contribution of renewables from 1,784 Mtoe in 2014 to 1,823 Mtoe in 2015, and is currently representing 13.4% of the 13,647 Mtoe of global primary energy supply (International Energy Agency (IEA), 2017). Figure 2.1 shows the contribution of renewal energy in the global primary energy supply. A significant portion of renewable energy comes from the traditional use of biomass (9.4%) and larger-scale hydropower (2.5%), while the remaining 1.5% is supplied by other renewable forms (*ibid.*).

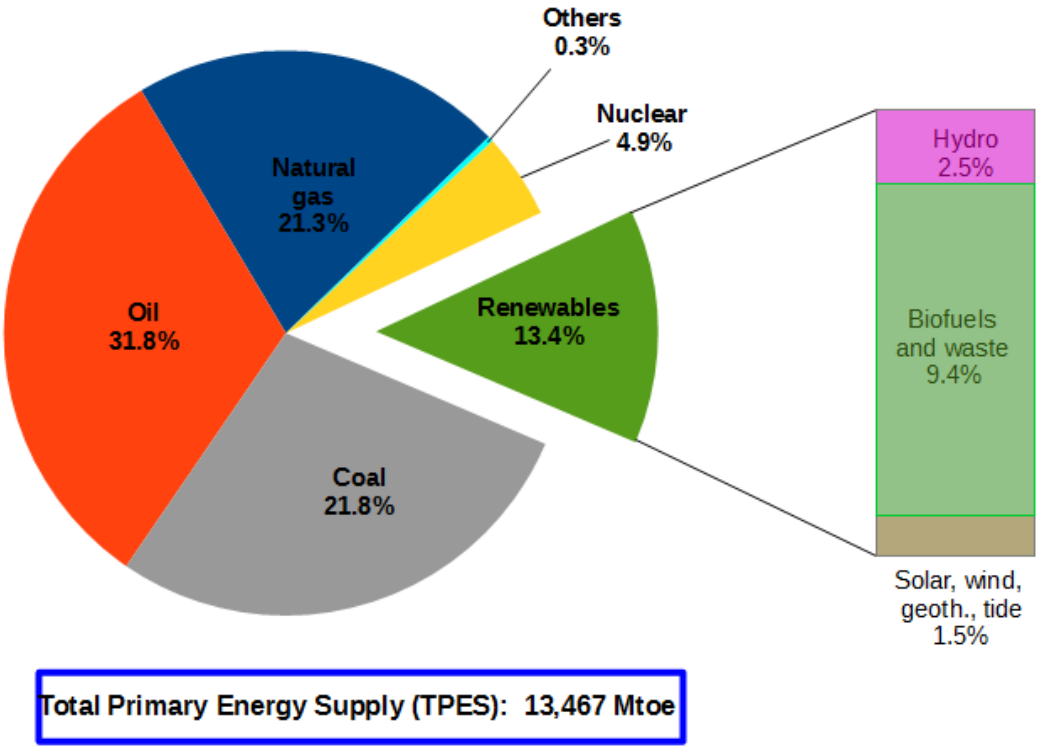

Figure 2.1. Contribution of renewable energy in the primary energy supply (International Energy Agency (IEA), 2017)

2.2. BIOMASS AS A RENEWABLE SOURCE OF CARBON

Amongst the renewable resources, biomass has a striking uniqueness of being the only source of renewable carbon, thereby making it the most attractive alternative to modern-day petroleum. Sims (2004) defines biomass as,

"The organic matter contained in plant and animal based products (including organic wastes) that can be captured and used as a source of stored chemical energy". (p.14)

The annual global production of biomass is 220 billion oven dry tons (odt), which is about 4500 EJ of solar energy captured each year (*ibid.*). This energy which is stored in biomass through photosynthesis represents approximately eight times the current total global energy of 571 EJ/year (International Energy Agency (IEA), 2017). This gives an indication of the vast potential biomass has as the world's largest and sustainable source of fuels and chemicals.

Currently, the dominant utilization of biomass (mostly as firewood) lies in inefficient, traditional applications like cooking and heating, especially in developing countries. However, when exploited sustainably, biomass can be converted to modern fuels and chemical products that are clean, convenient and with little or no associated greenhouse gas (GHG) emissions (Strezov and Evans, 2015). This is because biomass is carbon-neutral and as a result, any CO_2 produced from its combustion is subsequently consumed through photosynthesis for biomass regrowth and regeneration.

Biomass also has very low sulphur content; therefore, very low SO_2 emissions are released when utilized for energy production. It is also a widely held view that another reason behind the renewed interest in biomass world-wide is the prospect of improving the economy in countries that accept the challenge of making the transition from fossil fuels. Serrano-Ruiz et al. (2010) highlight that the economies of such countries would be less susceptible to changes in oil prices and they would also be stronger because jobs will be created in sectors such as agriculture, forest management, and oil/chemical industries.

Biomass differs from other renewable sources in that, though they both can provide other energy forms such as electricity and heat, it is the only renewable alternative to fossil fuels for the production of transportation fuels, biomaterials, and chemicals. Given the flexibility and

variety of potential use of biomass, it is important that the most promising option be selected under environmental, economic and resource consideration. For this reason, Agrawal and Singh (2010) and Marquardt et al. (2010) argue that electricity should primarily be generated from other renewable sources, whereas the use of biomass should be directed to production of biofuels and carbon-based chemical products on the premises that biomass has lower energy conversion efficiency and a lower energy density relative to fossil fuels.

2.3. THE CONCEPT OF BIOREFINERIES

The possibility of replacing fossil-based carbon with renewable carbon from biomass has led to the development of biorefineries. Amongst several definitions of biorefinery, the International Energy Agency (IEA) (2009) developed one of the most exhaustive definitions, i.e.

"Biorefining is the sustainable processing of biomass into a spectrum of bio-based products (food, feed, chemicals and/or materials) and bioenergy (biofuels, power and/or heat)".

It appears from this definition that the main impetus behind biorefinery is sustainability. The sustainability of biorefineries can be assessed for the entire value chain based on environmental, economic as well as social considerations. Therefore, a biorefinery can be a concept, a process, a facility, a plant or even a cluster of facilities depending on the scope under consideration.

Biorefineries are in principle analogous to the present-day petroleum refinery, in that it produces energy and chemicals (Spellman, 2012). Whilst refineries use crude oil as the raw material, biorefineries use biomass feedstock, ranging from wood and agricultural crops, plant and animal-derived organic residues, to forest residues as well as aquatic biomass (algae and sea weeds). Since fossil fuels originated from biomass centuries ago, biorefining can therefore produce direct substitutes for almost all the products that are derived from petroleum processing. These products can be intermediates as well as final and include transportation fuels, specialty and platform chemicals, pharmaceuticals, polymers, etc. as shown in Figure 2.2.

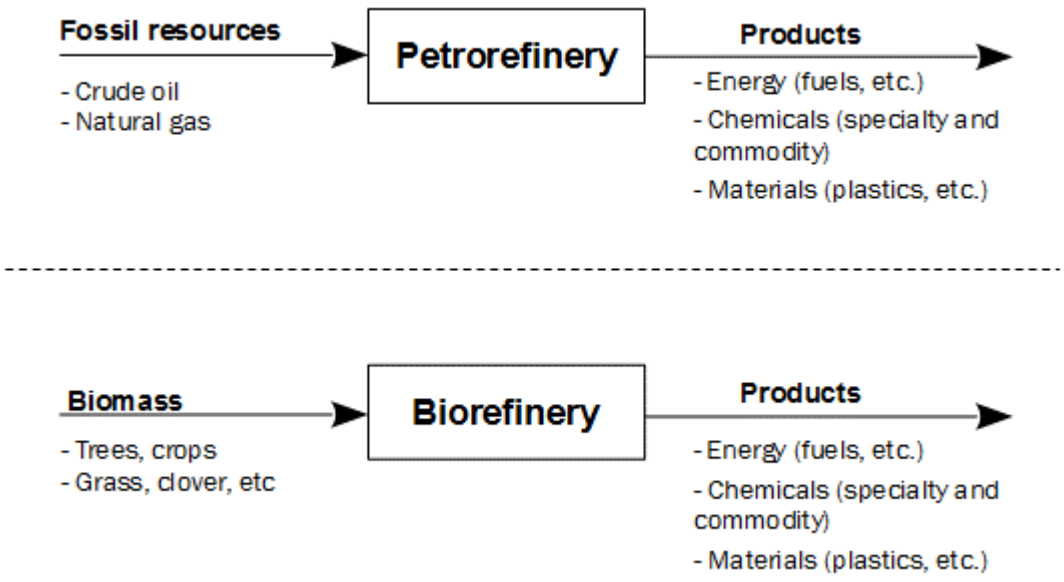

Figure 2.2. Illustration of biorefinery versus petro-refinery (Clark and Deswarte, 2015:p.11)

2.3.1. Biorefinery feedstock and potential products

Regarding biomass-derived products from biorefineries, Aresta (2012) explains that products can be categorized into energy and chemical/material products. Energy products are primarily used for their energy content in producing secondary energy carriers in the form of biofuels, power and/or heat. In order to optimize profitability as well as get the most out of the energy-based biorefineries, the residual products generated are mostly sold as feed or better still, upgraded to value-added products. The main driver for developments in biorefineries is energy, and most precisely biofuels (Luque et al., 2011). Therefore, the past decade has seen industrial production of biofuels rapidly grow in many parts of the world. Examples of important energy products and platforms that can be produced from biorefineries are:

- Gaseous biofuel – bio-hydrogen, syngas, biogas, bio-methane, etc.
- Liquid biofuels – pyrolysis/bio-oil, bio-diesel, FT-fuels, bio-methanol, etc.
- Solid biofuels – pellets, charcoal, etc.

In the case of chemical/material-based biorefineries, biomass is fractionated into a range of valorized products that have maximum value and overall environmental benefits as far as their functionalities are concerned, based on physical and/or chemical properties (Luque et al., 2011). In such biorefineries, process residue is used as utility for power and/or heat production for both internal use as well as for selling of the surplus to national grids. Typically, potential chemical/material products that can be produced from biomass include:

- Bio-materials – pulp, paper, cellulose, etc.
- Resins and polymers – plastics, furan and phenol resins, etc.
- Organic acids – lactic, succinic, etc.
- Chemicals – bulk chemicals, building blocks, etc.

Many reviews on the types of feedstock utilized in biorefineries reveal that biomass feedstock rich in carbohydrates are currently the pillars of biorefineries (Xu et al., 2008). That is, the commercial success experienced in biorefineries is primarily based on the use of edible agricultural commodities such as wheat, grain, sugarcane, corn, oil seeds, vegetable oil and animal fat (Clark et al., 2012). These biorefineries are referred to as primary biorefineries. Bio-ethanol and biodiesel are the most common biofuel products derived from primary biorefineries and are potential substitutes for gasoline and diesel respectively. Other biofuels such as bio-butanol, biomass-derived hydrocarbon fuels and hydrogen are still under investigations.

Despite the potential that exists in biorefineries which are based on these biomass feedstock, there are several drawbacks that need to be addressed. The most hard-hitting challenge has to do with the criticism that these raw materials compete directly with food production. Graham-Rowe (2011) explains that the price for many food commodities have increased drastically in the past few years as they were diverted to biofuels. Furthermore, there seems to be a general consensus amongst analysis of public policy issues relating to science and technology that the use of edible feedstocks for production of fuels and chemicals have a detrimental impact on greenhouse emissions, biodiversity, land use, water usage and water fouling (Baldwin, 2007).

These reasons have triggered a paradigm shift towards the development of biorefinery systems that use non-food substances such as municipal solid wastes, lignocellulosic crops and residues. Among these feedstock materials, the use of lignocellulosic (woody) biomass is considered to be advantageous because of the vast abundance of lignocellulosic biomass (Xu et al., 2008). Lignocellulosic biomass feedstock is made up of a mixture of varying structural constituents, mostly hemicellulose (20-30%), cellulose (40-50 %), and lignin and minor fractions of extractives, depending on their source (Klass, 1998; Lange, 2007).

Biorefinery systems that utilize lignocellulosic feedstock are still at the developmental stage and their products (mostly fuels) have only been produced at laboratory level and/or pilot stage. However, Clark et al. (*op. cit*) believe that the commercialization of these biorefineries is expected to be fully realized within the next 15-20 years given the intense research and scale up activities that are taking place. For instance, there is a high interest in novel biorefinery technologies such as gasification, Fischer–Tropsch synthesis and methanol synthesis, pyrolysis, etc. and some of these technologies are gaining ground and are being implemented industrially. Future projections show that 90% of all liquid biofuels (26 EJ) used for transportation will be derived from these technologies in 2050 (International Energy Agency (IEA), 2008).

2.3.2. Conversion technologies in biorefineries

As mentioned earlier, the main impetus behind biorefinery development is energy. Therefore, the conversion of biomass feedstock into advanced biofuels in biorefineries is primarily achieved via thermochemical and biochemical pathways as illustrated in Figure 2.3.

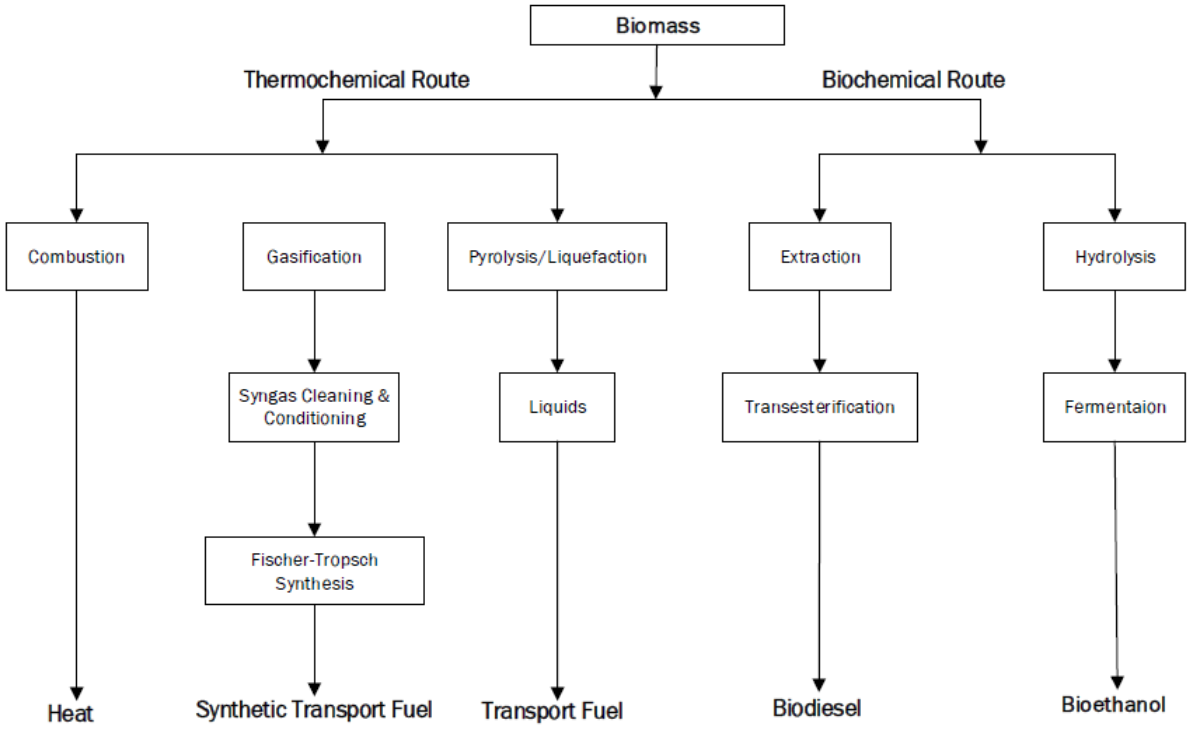

Figure 2.3. Simplified schematic of the two main biofuel production pathways (Damartzis and Zabaniotou, 2011)

2.3.2.1. Bio-chemical processes

In biochemical processes, lignocellulosic biomass is initially pretreated using liquid catalyst like ammonia, sulphuric acid or water at temperatures between 100 and 200 ^{o}C. Biomass pretreatment essentially breaks down the cell wall and alters the biomass ultra-structure and chemistry, thereby improving enzymatic accessibility. The pretreated biomass is subsequently subjected to enzymatic or microbial catalysts to convert carbohydrates to sugars which are then converted to fuels. In biochemical conversion, combined pretreatment and enzymatic hydrolysis serve to overcome lignocellulose recalcitrance, the inability to degrade lignin, which is the major barrier in this process (Clark et al., 2012). The last step in biochemical conversion, which is currently undergoing active research, involves co-fermentation of pentose and hexose sugars to alcohols (mainly ethanol), as well as anaerobic digestion of organic materials to biogas using bacteria.

The low processing temperatures and high product selectivity make biochemical processes better than its counterpart (i.e. thermochemical processing). However, the process has poor space-time yields and suffers from pre-processing stages and difficulty in downstream processes like distillation, making it more energy intensive (*ibid.*).

2.3.2.2. Thermochemical process

Thermochemical conversion on the other hand is based on thermal decomposition of lignocellulose, usually in the presence of varying concentrations of oxygen. The salient trait of thermochemical processing is the capability to convert essentially all the organic components of the biomass into products instead of selectively converting polysaccharides, which is the case in biochemical processing (Gomez et al., 2008).

There are different thermochemical conversion method/technologies to produce advanced biofuels from biomass. One of the most arguably developed thermochemical process is gasification. Gasification heats carbonaceous biomass feedstock at high temperatures (>700 °C) and low levels of oxygen (typically 35 %) into combustible gases called syngas (Basu, 2010). The syngas can be further processed to liquid fuels like diesel and gasoline by Fischer-Tropsch synthesis or converted to other chemical intermediates.

Another relatively well-understood and commercial thermochemical process is combustion. It is the burning of biomass in air and in the process, converting stored chemical energy of biomass into heat, electricity and mechanical power through various equipment such as stoves, boilers, steam turbines, furnaces, etc. It is an older method of utilizing biomass for production of energy on a small scale for domestic purposes like cooking and space heating, as well as for large-scale industrial applications such as generation of steam in turbines and producing heat in boilers and furnaces. One of the drawbacks of this process, especially in small scale application, is that it can be very inefficient, with a heat transfer loss of 30 to 90% (Pandey, 2009).

Other two processes which are more or less similar are thermal liquefaction and pyrolysis. Both these processes produce bio-oil – an important intermediate for the production of biofuels and chemicals. In thermal liquefaction, biomass is converted to gaseous and/or liquid bio-crude oil which exists mainly as biochar and non-condensable gases. The lignocellulosic feedstock is mixed with water in the presence of a basic catalyst such as sodium carbonate. The process usually takes place at temperatures between 252-472 °C, high pressures of 50-150 atm. and longer residence time, usually 5-30 minutes. Even though the liquid product obtained from liquefaction is relatively pure and contains less oxygen (i.e. 12-14 %), Elliott (1994) asserts that the process is more expensive than pyrolysis.

Pyrolysis generally refers to thermal decomposition in the absence of oxygen. The biomass feedstock is fed into a pyrolysis chamber which has hot solids and is heated rapidly to the peak/pyrolysis temperature of approximately 500 ^{o}C. Heating and vapor condensation take place in only 1 or 2 seconds, resulting in decomposition of biomass to high condensate yield of up to 75%. In general, up to two thirds of the biomass can be converted into a dark brown, viscous liquid called “bio-oil” or “bio-crude”. Bio-oil can be used directly in simple boilers and turbines for heat and electricity production and it is also an important source of renewable chemicals.

2.4. TYPES OF BIOREFINERIES

Biorefineries can be classified into three types, namely, Phase I, Phase II and Phase III biorefineries according to feedstock, process and product targets (Cherubini et al., 2009). The three types are summarized in Figure 2.4.

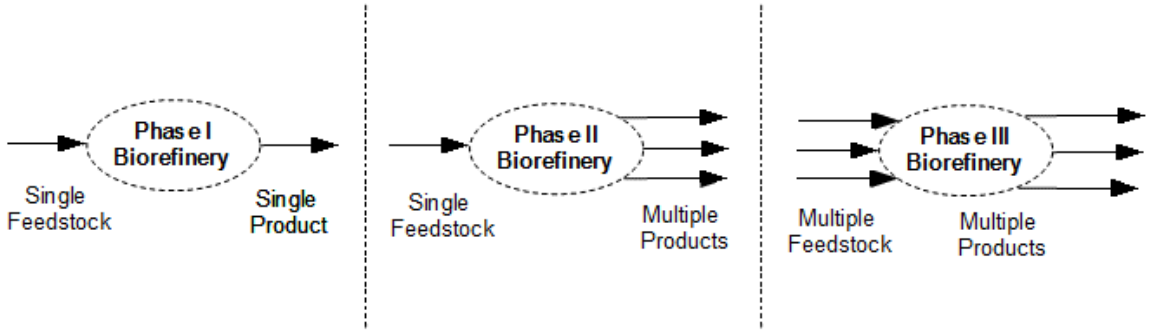

Figure 2.4. Different types of biorefineries (Ptasinski, 2016:p.677)

The following section discusses the three phases of biorefineries.

2.4.1. Phase I Biorefineries

Phase I Biorefineries are based on the use of a single feedstock and involve one processing unit that is designed to produce a single major product. They are well-developed and commercialized worldwide since they are technically and economically feasible. The production of fatty acid methyl ester (FAME) or biodiesel through transesterification of oil extracted from rapeseed or sunflower is an example of a Phase I biorefinery as illustrated in Figure 2.5. The production of ethanol from corn is another example of a phase I biorefinery.

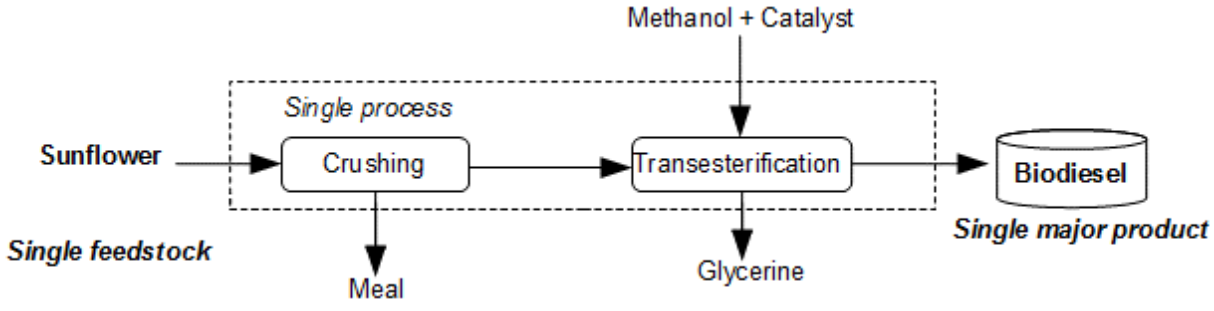

Figure 2.5. Biodiesel (FAME) production – An example of a Phase I biorefinery (Clark and Deswarte, 2015:p.12)

2.4.2. Phase II Biorefineries

The difference between phase I and II is the number of product outputs. Although Phase II biorefineries like Phase I, use a single feedstock, they however target different end-products (chemical, materials and energy). Phase II biorefineries therefore have an advantage of being efficient and economical because they are adaptable/amenable to market demands, prices as well as plant operation (Bozell and Petersen, 2010). A typical example of a Phase II biorefinery is the production of starch, ethanol and lactic acid together with high fructose, syrup, corn syrup, corn oil and corn meal from corn wet mill operations (Fernando et al., 2006). The Novemont plant (Italy) is an example of a phase II biorefinery which produces various chemical products including bio-plastics and bio-lubricant and greases from corn starch (Clark and Deswarte, 2015).

2.4.3. Phase III Biorefineries

Phase III biorefineries involve processing a range of biomass feedstock into multiple industrial products (energy, chemicals, and materials) using a combination of different technologies. This type of biorefineries has not yet been commercialized even though intensive work on their feasibility as well as their design is currently underway. Phase III biorefineries are further sub-divided into five phases which are currently under intensive research and development. The five phases are Lignocellulosic feedstock biorefinery, Green biorefinery, Whole crop biorefinery, Two-platform biorefinery and Marine biorefinery. These phases are described and reviewed in detail by Bonomi et al. (2016).

2.5. BIOREFINERY IN SOUTH AFRICA

Lynd et al. (2003) highlight that the history of biorefinery in South Africa can be summarized into two stages. The first stage, spanning from the late 1970s to the early 1990s, was characterized by intensive research and development (R&D) efforts which were mostly spearheaded by the Council for the Industrial and Scientific Research (CSIR). The impetus behind the intensive R&D in biomass conversion to fuels and product was the perpetual threat

of economic sanctions and oil price shocks. However, the early 1990s, ushered in what is referred to as the second chapter in the South African biorefinery industry, in which research and development in biomass conversion to value-added products, literally became dormant (*ibid.*). Ironically, the abandonment of biorefinery R&D efforts in South Africa came during a time of unprecedented global appreciation and interest in the potential offered by biomass conversion to fuels and commodity chemicals.

Currently, approximately 77% of the energy demand in South Africa is derived from coal, while the remaining 33% is mainly divided between nuclear and hydroelectric power (Khan et al., 2015). In keeping in step with the global need to deal with over-dependence on fossil fuels as well as curtailing anthropogenic greenhouse gas emissions, the South African government has put forward several initiatives and programs. One such initiative is the Renewable Energy Independent Power Producer Procurement Program (RWIPPP), which is aimed at increasing the existing electricity infrastructure by means of alternative energy sources such as solar, photovoltaic, biomass, etc (Eberhard et al., 2014). With regards to biomass, recent reports by Hugo (2016), shows that biomass in south Africa has an estimated energy equivalence of 487.24 Petajoules (PJ) per annum.

Biomass is primarily used in low-efficiency processes for cooking and space heating in rural areas. One of the established commercial utilization of biomass in South Africa involves the generation of electricity from bagasse (a waste fibre derived from sugar cane processing) by the sugar industry (Aliyu et al., 2018). Bagasse is also utilizes as feedstock to produce 20 000 ton of furfural per year, making South Africa one of the world's biggest furfural producers alongside China and the Dominican Republic (Machado et al., 2016). Technology for production of first-generation biofuels has also gained ground, with small to medium scale plants that produce biodiesel from waste vegetable oil (WVO) as well as ethanol from sugar cane and sorghum (Pradhan & Mbohwa, 2014). Examples of some of the biggest manufacturing sites for commercial production of biodiesel and ethanol respectively, include Phyto Energy (Eastern Cape) with a production capacity of over 500 ML per annum and Mabele Fuels (Free State) which produces 158 ML/annum (*ibid.*). There is also an ongoing research on some new and advanced technologies for second generation biofuels in various universities and research institutions such as the CSIR.

2.6. INTEGRATED BIOREFINERIES

The types of biorefineries previously discussed are mainly based upon a single conversion process in standalone plants for the production of various products. In this type of set-up, the biorefinery systems become extremely capital-intensive because the cost of the output produced becomes high (Damartzis and Zabaniotou, 2011). On top of the limited product portfolio, such biorefineries are also characterized by low energy efficiency (*ibid.*). As a result, a framework that integrates and uses the synergy of multiple conversion technologies was proposed in an effort to improve the overall process efficiency as well as the economic performance of biorefineries (Fernando et al., 2006). This is commonly referred to as integrated biorefineries and its underlying principle is extrapolated from the petroleum industry.

The basic idea in integrated biorefineries is to employ multiple processing technologies in order to target a wider scope of biomass feedstock, extend flexibility in product generation and also to attain a state of self-sustainability as far as energy is concerned. Figure 2.6 shows a schematic representation of an integrated biorefinery where three distinct platforms, *viz*. sugar platform, thermochemical platform as well as current technologies are systematically combined. Integration of petroleum industry into biorefineries involves designs in which biomass processing units are followed by conventional technologies as in the case of gasification. The syngas produced from biomass gasification is taken and converted into chemicals and fuels using current technology.

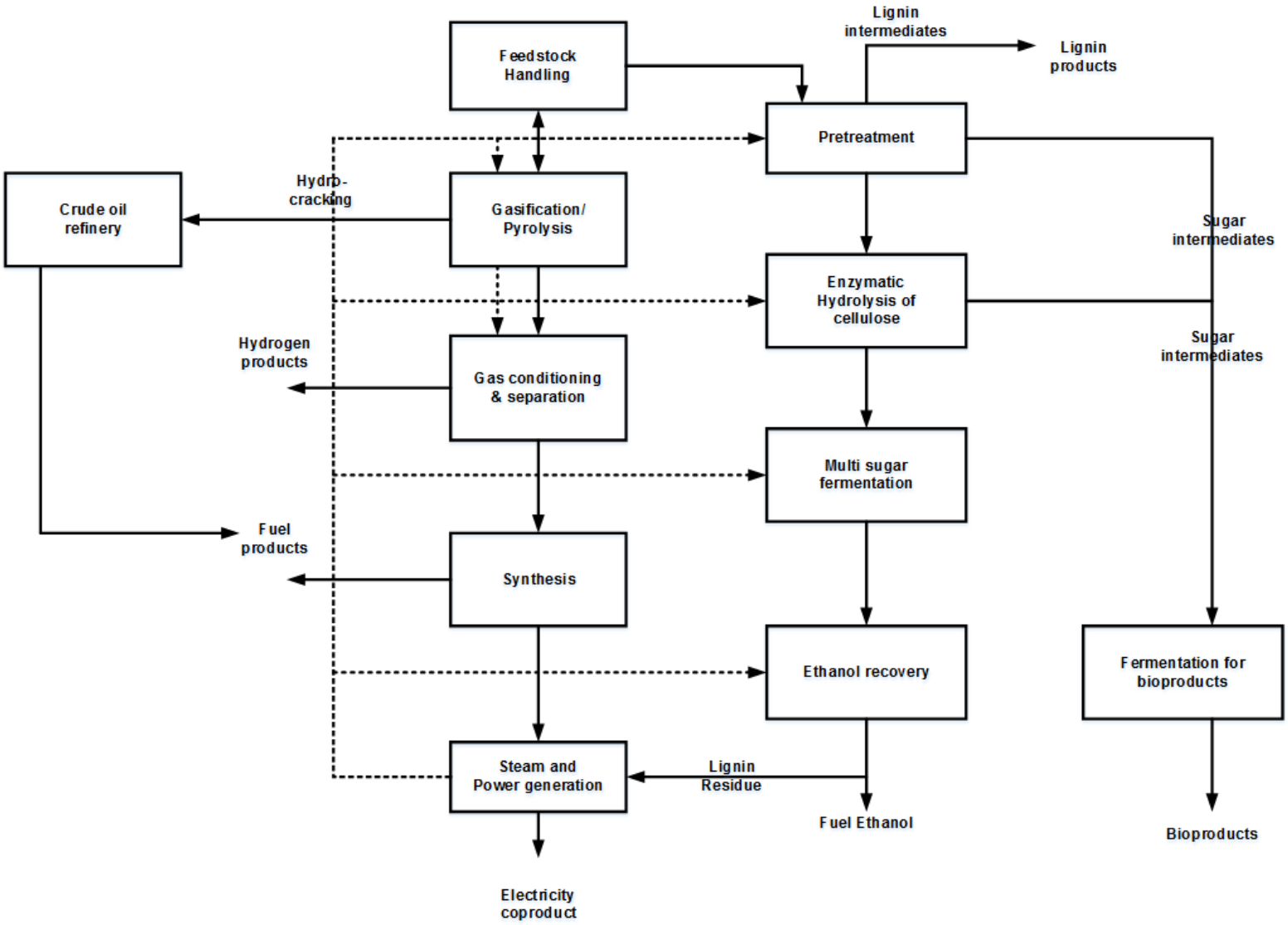

Figure 2.6. Schematic of an integrated biorefinery (Fernando et al., 2006)

Integrated biorefineries can also be achieved through process retrofitting (Kokossis and Yang, 2010). Retrofitting is described by Stuart and El-Halwagi (2013, p.5) as, "an integration of new technology within an existing operating plant structure". Thus, retrofitting biorefinery systems and technologies into the current industrial facility can improve the efficiency of energy utilization while simultaneously varying the product portfolio and minimizing emissions (*ibid*). Cohen et al. (2010) highlights the substantial reduction in the initial capital cost as one of the major benefits derived from integrating biorefinery systems with the existing petroleum facility and supply chain.

2.6.1. Syngas-based integrated biorefineries

Gasification is an attractive and robust technology for the primary processing of biomass into value-added products and energy platforms for a number of reasons. Its capacity to process a wide range of feedstock materials makes it attractive (Demirbas, 2009). Other marked advantages associated with biomass gasification include high thermal efficiency, reduced CO_2 emissions, and accurate combustion control (Marsh et al., 2007).

Gasification offers a remarkably broad variety of potential fuel products compared to other biomass conversion processes. A review by Rauch et al. (2014) reveals that research and development on syngas application has, over the past decade, focused on transportation fuels more than producing chemical products. Potential fuels that can be produced from biomass gasification span from liquid fuels like dimethyl ether (DME), methanol, gasoline, and diesel to gaseous fuels such as syngas or hydrogen as shown in Figure 2.7.

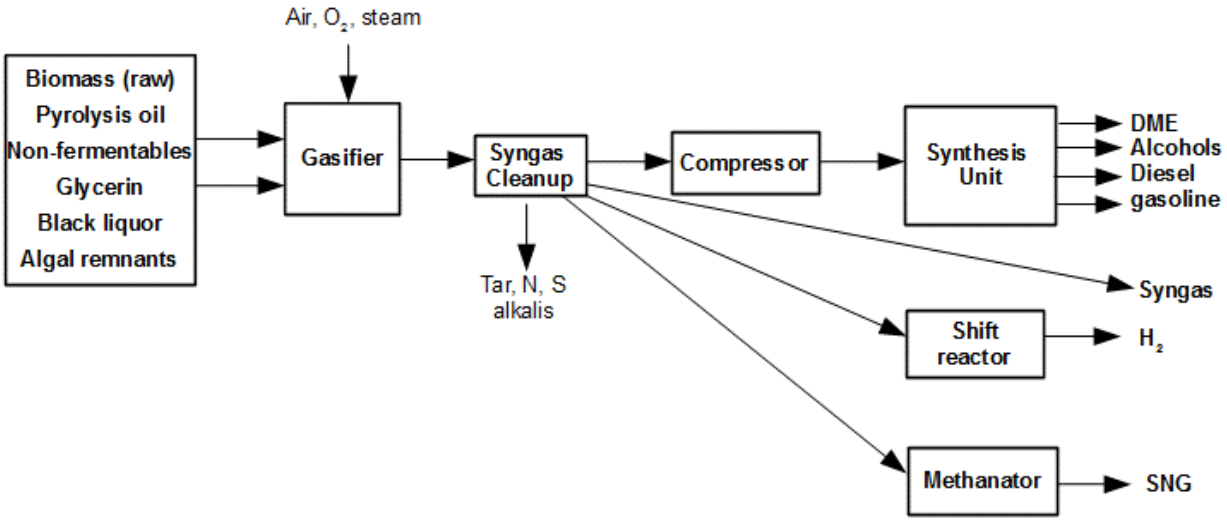

Figure 2.7. Main processes in biomass gasification and potential end product (Shaddix, 2011)

The different applications of bio-syngas are further discussed in the following section.

2.6.1.1. Fischer–Tropsch (FT) synthesis

FT synthesis basically involves the conversion of mixtures of hydrogen and carbon monoxide in syngas into liquid hydrocarbons according to the following chemical reactions:

$$(2n+1)H_2 + nCO \Longrightarrow C_nH_{(2n+2)} + nH_2O \quad (2.1)$$

$$2nH_2 + nCO \Longrightarrow C_nH_{2n} + nH_2O \quad (2.2)$$

FT synthesis using syngas primarily from coal and natural gas is predominantly used by Sasol in South Africa for the large-scale production of chemicals and synthetic fuels. Based on the reaction temperature, the FT synthesis process can be either high-temperature (HTFT) or low-temperature (LTFT). The HTFT process is characterized by temperatures of 300 – 350 ^oC whereas the LTFT functions at 200 – 260 ^oC. The FT synthesis process generally involves reaction pressure that ranges from 1 to several tens of atmospheres (Rauch et al., 2014). The FT synthesis process from syngas is depicted in Figure 2.8.

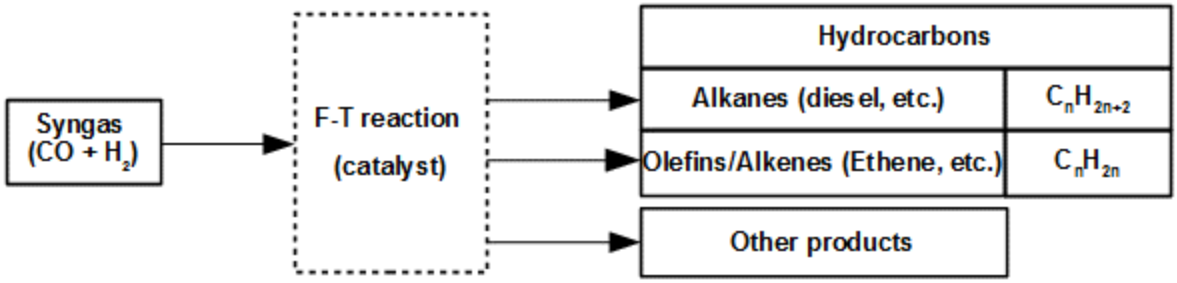

Figure 2.8. Schematic of FT synthesis

Amongst the number of different catalysts that can be used in FT synthesis, transition metals such as iron, cobalt and ruthenium are mostly common. Iron or cobalt-based catalysts are mostly utilized in LTFT while only iron-based catalysts are used in HTFT (Dry, 2002). A number of key process input variables including process conditions, catalyst, H_2/CO ratio, reactor type, determine the chain length of the product. For instance, high reaction temperature favors shorter chain molecules along with CH_4, olefins and aromatics, whereas increased pressure results in formation of more long-chained alkenes (Rauch et al., 2014). Reactions in FT synthesis are extremely exothermic and therefore require sufficient cooling to maintain constant reaction conditions.

2.6.1.2. Methanol synthesis

The use of methanol ranges from a transportation fuel to a blending stock as well as an intermediate/building block for other products such as DME, synthetic gasoline and ethanol. The technology for synthesizing methanol from syngas is well-established. Methanol synthesis is an exothermic equilibrium reaction that usually occurs at 220–275 ^{o}C and 50-100 bar in the presence of a catalyst that consists of a mixture of Cu, Zinc oxide and alumina according the following reactions (Stuart and El-Halwagi, 2013):

$$CO + H_2O \Leftrightarrow H_2 + CO_2 \quad (2.3)$$

$$CO_2 + 3H_2 \Longrightarrow CH_3OH + H_2O \quad (2.4)$$

Therefore, the overall reaction stoichiometry for this process is given by (Ptasinski, 2016)

$$CO + 2H_2 \Leftrightarrow CH_3OH \qquad \Delta H_{298\,K} = -90\ kJ/mole \tag{2.5}$$

2.6.1.3. Mixed alcohols

Mixed alcohols consist of a linear chain of various types of alcohols ranging from methanol to octanol. Mixed alcohols can be used in replacing gasoline as fuel in some fuel engines or blended with gasoline. The production of mixed alcohols from syngas is achieved through the use of metal catalysts such as molybdenum, rhenium or tungsten promoted with nickel, cobalt or iron (Strezov and Evans, 2015). The overall stoichiometry of the reaction can be summarized as

$$nCO + 2nH_2 \Rightarrow C_nH_{2n+1}OH + (n\text{-}1)H_2O \tag{2.6}$$

2.6.1.4. Dimethyl Ether (DME)

DME offers great potential as an alternative fuel to diesel in ignition engines (Namasivayam et al., 2010). It has higher octane number of about 55–66 and low auto-ignition temperature of 235 K compared to diesel which has an octane number of 40-50 and an ignition temperature of 250 K (Arcoumanis et al., 2008). Moreover, its physical properties resemble those of liquefied petroleum gas (LPG) and therefore can also be used to substitute LPG in household and industrial purposes. Some physical properties of DME compared to other fuels are presented in Table 2.1.

Table 2.1. Comparison of DME properties with other fuels (Ogawa et al., 2003)

Properties	Fuels				
	DME (CH_3OCH_3)	Propane (C_3H_8)	Methane (CH_4)	Methanol (CH_3OH)	Diesel
Boiling point (K)	247.9	231	111.5	337.6	180 - 370
Liquid density (g/cm^3)[a]	0.67	0.49	-	0.79	0.84
Specific gravity (*vs.* air)	1.59	1.52	0.55	-	-
Heat of vaporization (kJ/kg)	467	426	510	1097	-
Vapor pressure (atm)[a]	6.1	9.30	-	-	-
Ignition temperature (K)	623	777	905	743	-
Explosion limit	3.4 - 7	2.1 - 9.4	5.-15	5.5-36	0.6-6.5
Cetane number[b]	55-60	5[b]	0	5	40-55
Net calorific value (10^6 J/kg)	28.9	46.46	50.23	21.1	41.86

[a] 293 K
[b] Estimated value

The production of DME from syngas can be achieved through a two-step process (indirect synthesis) or a single step (direct synthesis), with the latter being the preferred option (Aguayo et al., 2007). The two routes are depicted in Figure 2.9.

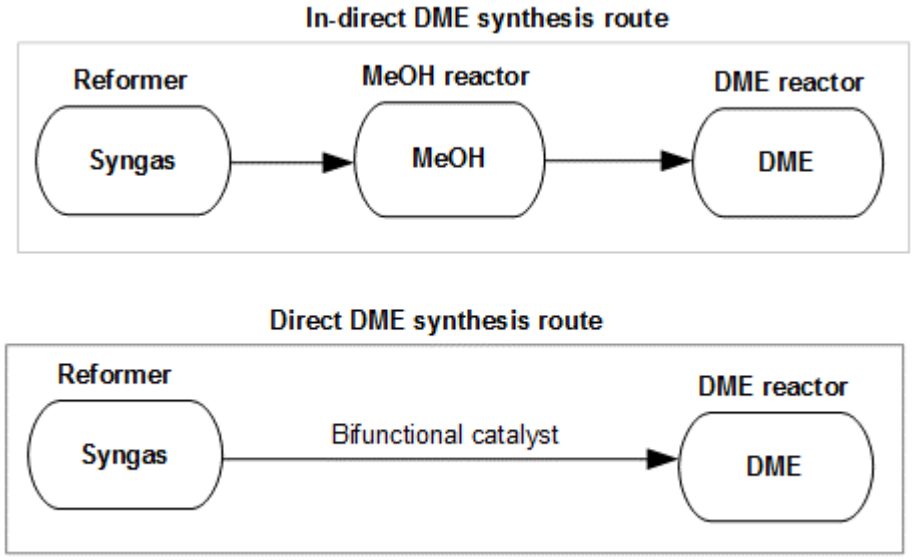

Figure 2.9. DME production routes (Luu et al., 2016)

In the conventional indirect synthesis of DME, CO from syngas is hydrogenated into methanol using a metallic catalyst. The initial reaction is given by,

$$CO + 2H_2 \Leftrightarrow CH_3OH \qquad \Delta H_{298\,K} = -90\ kJ/mol \tag{2.5}$$

The subsequent step of the process involves the dehydration of the methanol produced in the first step into DME on an acid catalyst (Zhu et al., 2010).

$$2CH_3OH \leftrightarrow CH_3OCH_3 + H_2O \qquad \Delta H^0 = -23.4\ kJ/mol \tag{2.6}$$

The two-step indirect DME production process is however limited by thermodynamics governing the initial methanol synthesis reaction. This therefore results in relatively low conversion of methanol, especially at high temperatures. Moreover, since methanol is an

expensive chemical product and feedstock, the indirect production of DME also implies high capital costs. These reasons have resulted in a tremendous shift of interest towards the direct, single step DME production route in industry.

The single-step production of DME uses a bi-functional catalyst with two active sites to simultaneously integrate the methanol synthesis reaction with the methanol dehydration (Sun et al., 2003). Thus, methanol that is generated from syngas in the catalyst is immediately dehydrated into DME in a single process. The instant dehydration of methanol enhances the forward reaction and reduces the reverse reaction of the process. At the same time, the water that is released during the methanol dehydration step reacts with CO in the water-gas shift reaction (WGSR) to produce H_2 as shown in Equation 2.3. These two reaction mechanisms complement each other in increasing the overall forward reactions for both the synthesis and dehydration of methanol. Consequently, the direct DME production process has high synergetic effect for the CO conversion to DME (*ibid.*).

$$\text{WGSR:} \quad CO + H_2O \rightleftharpoons CO_2 + H_2 \qquad \Delta H = -41.2 \text{ kJ/mol} \qquad (2.3)$$

The reaction conditions for the direct synthesis of DME from syngas is summarised in Table 2.2. The direct production of DME results in optimum conversion when syngas has a composition with a H_2/CO ratio of 1 (NEDO, 2015). The overall reaction for the sigle/direct synthesis process is given by

$$3CO + 3H_2 \Longrightarrow CH_3OCH_3 + CO_2 \qquad \Delta H = -246.9 \text{ kJ/mol} \qquad (2.7)$$

Table 2.2. Reaction conditions of direct DME synthesis (Ogawa et al., 2003)

Reaction condition	Temperature (°C)	Pressure (MPa)	Feed syngas H_2/CO ratio	W/F[a] ((kg.h)/kg)
Experimental	240-280	3.0-7.0	0.5-2.0	3.0-8.0
Standard	200	5.0	1.0	4.0

[a] W/F ≡ Ratio of catalyst weight (kg) to reactant gas flow rate (kg·mol/h)

2.6.1.5. Hydrogen production

Gas rich in hydrogen can be produced from biomass gasification using steam as the gasifying medium. Liu et al. (2014) and Fremaux et al. (2015) achieved syngas with 60-70 %vol. hydrogen concentration in a bench-scale fixed bed and pilot-scale fluidized bed gasification using a catalyst respectively. In biomass gasification, temperature significantly influences the production of hydrogen with increasing temperature resulting in increased hydrogen (Kumar et al., 2009). The hydrogen-rich syngas from biomass gasification can be converted to hydrogen through steam reforming and water gas shift reaction.

2.7. BIOMASS GASIFICATION PROCESS

In most syngas-based integrated biorefineries, the gasification technology can be considered as the groundwork for the entire biorefinery. Therefore, its efficient analysis and optimization is essential in terms of the overall performance of the biorefinery. But in order to optimize the gasification process, understanding the fundamentals of the process is important.

As mentioned earlier, gasification is basically a thermo-chemical process that involves a partial oxidation of biomass into a gaseous biofuel platform called syngas. The process makes

use of a gasifying agent such as air, steam or oxygen to rearrange the biomass molecules into a combustible gaseous product with high hydrogen-to-oxygen ratio. The produced syngas is more versatile and easy to use compared to its parent biomass and its quality can also be standardized. The chemistry involving biomass gasification is generally quite complex. However, it has been observed that biomass gasification proceeds in four steps, namely, drying, pyrolysis (devolatilization), oxidation (combustion) and reduction (char gasification) (Christopher, 2013).

Drying

The drying stage in biomass gasification takes place when biomass reaches the flaming zone at the surrounding temperature of about 100 – 200 ^{o}C. The moisture content of biomass is reduced to less than 5 percent. Optimum results in biomass gasification are obtained when the biomass feedstock has a moisture content well below 25 wt.%. At this condition, higher thermal efficiencies are achieved in the gasifier. The drying stage of the biomass gasification process can be represented by the following equation:

$$\text{Wet Biomass} + \text{Heat} \Longrightarrow CH_wO_xN_yS_z + H_2O \qquad (2.8)$$

Pyrolysis

Pyrolysis of the biomass occurs at temperatures of around 200 to 700 ^{o}C. Basically, part of the biomass is thermally decomposed in the absence of oxygen or air to condensable hydrocarbon gases, oils, methane as well as char. This stage of the process is endothermic and therefore usually lowers the temperature in the gasifier. The pyrolysis step can be represented as follows:

$$CH_wO_xN_yS_z + \text{Heat} \Longrightarrow C(\text{char}) + \text{tars/oils} + aNH_3 + bN_2 + cH_2S + dH_2O + eH_2 + fCH_4 \qquad (2.9)$$

Oxidation (combustion)

The introduction of oxygen into the gasifier results in the oxidation of the combustible substances to form CO_2 and H_2O. The oxidation of carbon and hydrogen is extremely exothermic and the temperature of the char and gas particles may go as high as 1800 ^oC. The following reactions take place at the oxidation (combustion) stage:

$$C + \frac{1}{2}O_2 \Longrightarrow CO \qquad \Delta H_r^o = -111 \text{ kJ/mol} \qquad (10)$$

$$H_2 + \frac{1}{2}O_2 \Longrightarrow H_2O \qquad \Delta H_r^o = -242 \text{ kJ/mol} \qquad (11)$$

$$CO + \frac{1}{2}O_2 \Longrightarrow CO_2 \qquad \Delta H_r^o = -283 \text{ kJ/mol} \qquad (12)$$

$$NH_3 + \frac{3}{4}O_2 \Longrightarrow \frac{1}{2}N_2 + \frac{3}{2}H_2O \qquad \Delta H_r^o = -383 \text{ kJ/mol} \qquad (13)$$

$$H_2S + \frac{3}{2}O_2 \Leftrightarrow SO_2 + H_2O \qquad \Delta H_r^o = -563 \text{ kJ/mol} \qquad (14)$$

Reduction

Several endothermic reduction reactions take place between 800 – 1000 ^oC (Puig-Arnavat et al., 2010). In the reduction step, combustible gases like CO, CH_4 and hydrogen are produced through a sequence of reactions. All the carbon is converted to CO and CO_2 in the case where complete gasification occurs while the residues that remain after this stage comprise of unburned carbon and ash. Four main reactions occur at this stage:

Water-gas shift reaction (WGSR):

$$CO + H_2O \Leftrightarrow CO_2 + H_2 \qquad \Delta H_r^o = -131.4 \text{ kJ/mol} \qquad (2.3)$$

Boudouard equilibrium:

$$C(s) + CO_2 \Leftrightarrow 2CO \qquad \Delta H_r^o = -172.6 \text{ kJ/mol} \qquad (2.15)$$

Heterogeneous water-gas shift reaction/shift reaction:

$$CO + H_2 \Leftrightarrow C(s) + H_2O \qquad \Delta H_r^o = -42 \text{ kJ/mol} \qquad (2.16)$$

Methane reaction (methanation)/Hydrogenating gasification:

$$C(s) + 2H_2 \Leftrightarrow CH_4 \qquad \Delta H_r^o = +75 \text{ kJ/mol} \qquad (2.17)$$

Given that biomass feedstock characteristically consists of C, H, O and N plus traces of other elements, biomass gasification reaction with steam (H_2O), air (0.79 N_2 and 0.21 O_2) and CO_2 can generally be represented by the following equation

$$C_aH_bO_cN_d + eH_2O + gH_2O + hO_2 + (79/21)hN_2 + jCO_2 \Longrightarrow n_1H_2 + n_2CO + n_3CO_2 + n_4H_2O + n_5CH_4 + n_6N_2 + n_7C \qquad (2.18)$$

where

a – d is the number of atoms for C, H, O and N respectively,

e, g, h and j respectively represent the stoichiometric coefficients of biomass moisture, steam, air and CO (per unit mole of biomass), and

n_1 – n_7 represent the stoichiometric coefficients of H_2, CO, CO_2, H_2O, CH_4, N_2 as well as solid carbon (C).

2.7.1. Effects of operating conditions in biomass gasification

The product syngas from biomass gasification is characterized by both its composition and yield which are in turn influenced by several input parameters and gasifier design. These parameters significantly influence the product quality and quantity in biomass gasification. The main parameters include reactor temperature and pressure, gasification medium, residence time and equivalent ratio.

2.7.1.1. Reactor temperature

Temperature has a significant impact on the conversion as well as the distribution of the product gas. Basically, the overall conversion of carbon increases as temperature increases such that at higher temperatures, there is higher yield of hydrogen and low yield of methane (Sikarwar et al., 2016). At higher gasification temperatures of more than 800 ^{o}C, high carbon conversion of the biomass feedstock is preferentially obtained along with clean syngas that has lower tar content (Strezov and Evans, 2015). The temperature dependence of the bio-syngas is a function of the thermodynamic behavior of the exothermic and endothermic reactions that are taking place in the gasifier.

In a study by Lv et al. (2004) on the effect of bed temperature on carbon conversion, gas yield and lower heating value (LHV), it was observed that the increase in temperature resulted in the carbon conversion efficiency increasing from 78.17 to 92.59% and the gas yield increasing from 1.43 to 2.53 m^3/kg. It was however observed that the increase in temperature from 700 to 900 ^{o}C caused a decrease in the LHV from 7.94 to 7.36 kJ/m^3. Moreover, increasing gasifier bed temperature from 700 to 900 ^{o}C in an air and air/steam biomass gasification increased the CO and H_2 production composition and reduced the CO_2 and CH_4 content (González et al., 2008). The same pattern of results were obtained by Qin et al. (2012) in an entrained biomass gasifier at the temperature range of 1000 to 1350 ^{o}C.

2.7.1.2. Gasification medium

One of the parameters that directly affect the heating value of the product syngas significantly is the gasifying medium. Biomass gasification can be performed by means of various oxidants or gasifying agents like air, pure O_2, CO_2, steam or a mixture of steam and oxygen (Basu, 2010). The fuel to gasifying medium is an important factor that influences the syngas product distribution and it is expressed in various ways for different gasification mediums (Table 2.3).

Table 2.3. Gasification mediums and characteristic parameters

Medium	Parameter
Air	Equivalent ratio (ER) = ratio of air used to stoichiometric air required for complete combustion
Steam	Steam-to-biomass (S/B) ratio
Carbon dioxide	CO_2-to-biomass ratio
Steam and oxygen	Gasification ratio (GR): (steam + O_2)-to-biomass ratio

Air is the cheapest gasifying agent even though it results in syngas with lower heating values due to the significant amount of nitrogen in air. Utilizing pure O_2 as a gasifying medium on the other hand produces syngas with increased heating values. The only major setback in using pure O_2 in gasification is the high operating cost associated with the production of oxygen.

The use of steam in biomass gasification results in syngas with high heating value and high H_2 content. Studies by Gil et al. (1999) and Rapagnà (2000) have shown that the product syngas heating value resulting from biomass gasification with steam is about 10–15 MJ/Nm^3. This is significantly high compared to 3-6 MJ/Nm^3 from biomass gasification with air (Zainal et al., 2002). Another gasifying medium that can be used in biomass gasification is CO_2. In the presence of catalyst like Ni/Al, CO_2 can increase the H_2 and CO content of syngas by transforming CH_4, tar, and char into CO and or/H_2 in a process called dry reforming (Devi et al., 2003; Garcia et al., 2001). This reaction is shown in Equation 2.19.

$$C_nH_x + nCO_2 \Longrightarrow 2nCO + (X/2)H_2 \qquad (2.19)$$

Alternatively, a combination of steam and O_2 can be used in biomass gasification. Adding O_2 to steam provides the heat required to make gasification reaction auto-thermal and also reduces tar formation (Lv et al., 2004). This reaction is characterized mainly by the steam-O_2 to biomass mass ratio, usually known as gasification ratio (GR). At higher GR, there is more tar reduction while light tars get formed at a low GR (Aznar et al., 1997).

2.7.1.3. Equivalence Ratio (ER)

Equivalence ratio describes the quantitative relationship that exists between air/oxygen and biomass. In essence, it provides the ratio of the amount of air/oxygen supplied to the gasifier to the stoichiometrically required air/oxygen for complete oxidation of biomass as expressed below:

$$ER = \frac{\text{air used(kg)/biomass used (kg)}}{\text{stoichiometric air (kg)/biomass used (kg)}} \qquad (2.20)$$

It is a design parameter that has significant influence on the syngas composition and syngas heating value. An ER of more than 1 implies that the gasification process approaches the combustion process, resulting in a product with a high CO_2 composition. A low ER (<0.25), on the other hand, signifies deficiency in air/oxygen and therefore favours the pyrolysis process with product characterized mainly by CO and H_2 (Damartzis et al., 2012). Even though ER depends on other factors such as operating temperature, design of gasifier, and moisture content of biomass, a review of literature generally reveals that the optimum ER ranges between 0.2 to 0.4 (Adhikari et al., 2012).

2.7.1.4. Steam to Biomass Ratio (S/B)

When biomass gasification is performed using steam as a gasifying agent, steam to biomass ratio (S/B) becomes an important basic operating parameter. It is defined as the steam flow rate divided by the biomass feedstock flow rate into the gasifier. High S/B ratio means that there is high partial pressure of steam in the gasifier and this typically promotes the water-gas shift reaction, the water gas reaction and methane steam reforming reaction, resulting in

additional hydrogen production. An investigation by Lv et al. (2004) on the biomass air-steam gasification in a fluidized bed reactor showed that bio-syngas yield, gas heating value and efficiency of carbon conversion are improved as the S/B ratio is increased.

Ruoppolo et al. (2012) also report that at higher steam to biomass ratio, the amount of tar in the producer gas is reduced. Operating the gasifier at higher S/B, however, may prove to be economically infeasible and/or unattractive because more heat needs to be supplied in order to maintain the high gasification temperature. Moreover, biomass steam gasification at a higher S/B ratio may also need simultaneous integration with CO_2-capture technologies in order to deal with the increased CO_2 concentration that accompanies the high H_2 generation from the water-gas shift and methane steam reforming reactions.

2.7.1.5. Biomass gasifier types and design

Reactor type is another important parameter that influences the composition of syngas as well as the level of undesirable components (tar, ash, etc.) produced from biomass gasification (Rauch et al., 2014). Biomass gasifiers can be classified into two primary types, namely, the fixed bed and fluidized bed. Fixed bed gasifiers can further be categorized into updraft, downdraft or cross-draft gasifiers depending on the direction and entry of airflow. Fluidized-bed gasifiers can, on the other hand, be divided into circulating fluidized-bed and bubbling fluidized-bed. Patra and Sheth (2015) provide an extensive review of the different types of gasifiers with their advantages and disadvantages. Fixed-bed gasifiers produce syngas with low calorific value and high tar content (*ibid.*). Gordillo et al. (2009) report that syngas from fixed-bed gasifier typically comprises of 12 – 20% H_2, 40 – 50% N_2, 10 – 15% CO, 10-15% CO_2 and 3-5% CH_4 and a net calorific value of 4-6MJ/Nm^3. In fluidized-bed reactors, however, syngas with lower tar content (<1-3 g/Nm^3) is produced as a result of the reaction of the hot bed material with the high molecular weight tar (Patra and Sheth, 2015).

2.7.2. Performance of biomass gasifiers

The gasification of biomass for the production of energy requires that the performance of the gasification system be determined in order to be able to manipulate the process variable such that the optimum economics of the process is achieved. The performance of a biomass gasifier can basically be described in terms of both the quantity as well as the quality of the gas product (Basu, 2010). These two criteria can further be sub-divided into four main performance criteria including: (1) syngas properties, (2) gas product yield, (3) efficiencies, and (4) carbon conversion.

2.7.2.1. Syngas properties

Syngas properties are usually characterized in term of the composition, amount of impurities (e.g. tar and alkali metals), higher and lower heating values. The composition of bio-syngas is influenced by a number of input parameters including gasifying medium, operating pressure and temperature, feedstock moisture content, etc. The numerous variables make the prediction of the exact composition of the final gas product challenging (Puig-Arnavat et al., 2010). Based on the downstream application of the bio-syngas, the level of cleaning can vary from as-received, to mild in case of application in engines and turbine, to strict cleaning in cases of synthesis application. Table 2.4 summarizes some syngas properties and characteristics required for particular applications.

Table 2.4. Requirements for different syngas applications (Ciferno and Marano, 2002)

	Synthetic fuel	Methanol	Hydrogen	DME	Fuel Gas	
	FT-Gasoline & Diesel				Boiler	Turbine
H_2/CO	*0.6*[1]	~2.0	High	1 - 2	Unimportant	Unimportant
CO_2	Low	Low[2]	Not Important[3]	Low	Not critical	Not critical
Hydrocarbons	Low[4]	Low[4]	Low[4]	Low[4]	High	High
N_2	Low	Low	Low	Low	Note[5]	Note5
H_2O	Low	Low	High[6]	Low	Low	Note[7]
Contaminants	<1 ppm Sulfur Low particulates	<1ppm Sulfur Low Particulates	<1ppm Sulfur Low particulates	< 1 ppm	Note[8]	Low particulates Low metals
High value	Unimportant[9]	Unimportant	Unimportant	Unimportant	High[10]	High
Pressure (bar)	~20-30	~50 (liquid phase) ~140 (vapor phase)	~28	30 – 70	Low	~400
Temperature (℃)	200-300[11] 300-400	300-400	100-200	240 – 280	250	500-600

[1] Depends on catalyst type, e.g. 0.6 is satisfactory for iron catalyst; ≈2.0 should be used for cobalt catalyst.
[2] A level of CO_2 is tolerable provided the H_2/CO ratio is more than 2.0 (as in the case of steam reforming of natural gas); if H_2 is present in excess, the CO_2 will be converted to methanol.
[3] Syngas is converted to H_2 through the water gas shift reaction which produces CO_2 as by-product; CO_2 in syngas can be removed along with the CO_2 produced from the water gas shift reaction.
[4] Heavier hydrocarbons and methane need to be recycled for conversion to syngas; they represent biomass gasification inefficiency.
[5] N_2 reduces the lower heating value, but level is unimportant provided syngas can be burned with a stable flame.
[6] The presence of water in syngas will enhance the water gas shift reaction to produce more H2; water is required for the water gas shift reaction.
[7] Relatively high-water levels can be tolerated.
[8] Small amount of contaminant can be tolerated.
[9] Heating value is not critical provided the H_2/CO and impurities levels are satisfied.
[10] High heating value improves the efficiency.
[11] Depends on catalyst type; iron catalysts typically operate at higher temperatures than cobalt catalysts.

The higher heating value (HHV) and lower heating value (LHV) are important syngas quality indices that are particularly important for syngas application in fuels. Both these syngas quality indices provide valuable information regarding the energy content of the syngas fuels. The LHV of the biomass gasification product can be calculated from the composition of the syngas using the following equation (Xianwen et al., 2000)

$$LHV_{gas}(KJ/m^3) = (30.0 \times CO + 25.7 \times H_2 + 85.4 \times CH_4 + 151.3 \times C_nH_m) \times 4.2\ kJ/m^3 \quad (2.21)$$

where H_2, CH_4, CO, C_nH_m are the molar fraction of the syngas component species

2.7.2.2. Syngas yield

The gas product yield is also a significant indicator of the biomass gasification process. It is usually expressed in terms of Nm^3/kg biomass fuel of CO, H_2, CO_2, and C_xH_y (total maximum hydrocarbon of C_3) present in the syngas. Qin et al. (2012) explain that syngas yield per biomass is expected to be maximized for H_2 and CO during the gasification process. Typical properties of syngas produced from steam-oxygen gasification are shown in Table 2.5.

Table 2.5. Typical producer gas properties and yield generated from an atmospheric bubbling fluidized-bed (BFB) gasifier (Strezov and Evans, 2015)

Gas composition (vol.%)							Tars (g/kg,daf)	Char (g/kg,daf)	Gas Yield (Nm^3/kg, daf)	LHV (MJ Nm^3)
H_2[a]	CO[a]	CO_2[a]	CH_4[a]	C_2H_n[a]	N_2[a]	Steam[b]				
13.8-31.7	42.5-52.0	14.4-36.3	6.0-7.5	2.5-3.6	0	38-61	2.2-4.6	5-20	0.86-1.14	10.3-13.5

[a] Dry basis
[b] Wet basis

2.7.2.3. Carbon conversion

The carbon conversion of biomass in gasification systems provides the utilization ratio of the biomass feedstock. Carbon conversion is expressed as follows (Neathery, 2010)

$$\text{Carbon conversion } \% = \left(1 - \left(\frac{m_{ash} \times \%C_{ash}/100}{m_{biom} \times \%C_{biom}/100}\right)\right) \times 100\% \qquad (2.22)$$

where

m_{ash} (kg/h) ≡ mass flow rate of residual ash leaving the gasifier;

m_{biom} (kg/h) ≡ mass flow rate of biomass feedstock;

$\%C_{ash}$ and $\%C_{biom}$ are carbon weight percentages in ash and biomass respectively

2.7.2.4. Efficiencies

(a) Cold-gas efficiency

The cold-gas efficiency (η) describes the ratio of the total output of the syngas heating value to the total output of the heating value of biomass. It provides the energy efficiency of the gasification system and it is expressed as follows:

$$\eta = \frac{LHV_{gas} \times f_{gas}}{LHV_{biom} \times f_{biom}} \times 100\% \qquad (2.23)$$

where,

LHV_{gas} (kJ/m^3) and LHV_{biom} (kJ/m^3) are the lower heating values of syngas and biomass respectively

f_{gas} and f_{biom} (m^3/h) are the flow rates of the syngas and biomass feedstock respectively.

The cold-gas efficiency can also be calculated using the higher heating value (HHV). Depending on other parameters such as the oxidizing agent, feedstock properties, operating

conditions as well as the reactor design and configuration used in the gasifiaction process, the cold-gas efficiency can range between 60 to 75% (Strezov and Evans, 2015).

(b) Exergy efficiency

Exergy defines the amount of work (i.e. entropy minus free energy) that a system can perform when it is brought into thermodynamic equilibrium with its environment. Thus, exergy efficiency with regards to biomass gasifieres, is the ratio of useful exergy output to the necessary exergy input into the gasifier (Abuadala et al., 2010). The exergetical analysis is effectively used in the design and analysis of biomass gasification flow using energy and mass balances with the second law of thermodynamics. For an adiabatic gasifier that uses air as a gasifying medium, the exergy efficiency is expressed as (Puig-Arnavat et al., 2010)

$$\psi = \frac{n_{gas} \times (e_{ch,gas}+e_{ph,gas})}{e_{ch,biom} + n_{air} \times e_{air}} \times 100\% \qquad (2.24)$$

where,

n_{gas} (kmol) is the number of moles for the sygas;

n_{air} (kmol) number of moles of air;

$e_{ch,gas}$ (kJ/kmol) is the chemical exergy of syngas;

$e_{ph,gas}$ (kJ/kmol) is the physical exergy of syngas

$e_{ch,biom}$ (kJ/kmol) is the chemical exergy of biomass; and

e_{air} (kJ/kmol) is the specific molar exergy of air

2.7.3. Biomass gasification modelling

As shown earlier, there are a number of operating parameters that influence the gasification process and consequently the quantity and quality of the syngas as well as gasifier performance. Moreover, different biomass feedstock have heterogenous composition and differing thermo-chemical properties which make investigations of biomass gasification a complicated task. Given the various input variables which also happen to show intricate interelation with each other, carrying out experiments to determine the optimum operating

conditions for a particular reactor design can prove to be expensive and time consuming. It is for this reason that modelling becomes an important tool when it comes to studying the behaviour of gasifiers for the purpose of optimizing their design as well as their operation. The models provide a representation of the physical and chemical phenomena that take place in the gasifiers. These, in turn, guide the chemical engineer as to how various design, operating and feedstock parameters affect the performance of the gasifier.

Basu (2010) underlines the significance of mathematical modelling or simulations in providing information regarding:

- The optimum operating conditions or design and configuration of a gasifier;
- Identifying the areas of potential concern in the operation;
- Give valuable information on extreme operating conditions, such as high temperature and pressure which are generally risky to experiment empirically;
- Assist in scaling up of the gasifier from one successful operating size to another, and from one feedstock to another;
- Improve the interpretation of experimental results and analyze abnormal behaviour of a gasifier.

It is however important to note that the efficacy and reliability of a gasification model depend on the ability of the model to mimic the process and its variables in the most realistic way possible. Otherwise, this compromises the results of the model. This is usually the case when modelers do not pay attention to some variables or at least make assumptions that over-simplify the gasification scenario in an attempt to reduce the complexity of the model. Thus, Baruah and Baruah (2014) caution that maximum care should be taken when formulating gasification models to ensure that reliable results are obtained. An excellent case in point is the study by Babu and Sheth (2006) who modeled the reduction zone of a downdraft biomass gasification, focusing on the effect of char reactivity factor (CRF). It was discovered that the model results, when varying the char reactivity factor (CRF) exponentially, were more agreeable to experimental results compared to assuming linear variation.

Much of the work done in gasification modelling has been categorized into two: kinetic and thermodynamic equilibrium modelling (Puig-Arnavat et al., 2010).

2.7.3.1. Kinetic modelling

Kinetic modelling is a useful tool for predicting the gas yield and product composition that can be achieved in a gasification system over a finite time or finite volume in a flowing medium (Basu, 2010). It basically makes use of kinetic mechanisms to represent the gasification process for design, evaluation and improving of gasifiers. It uses parameters such as residence time, reaction rates and hydrodynamics of the reactor. That is, for a particular gasifier configuration, this model can predict the gas compositon profile, temperature inside the gasifier as well as the overall perfomance of the gasifier. Kinetic modelling is therefore generally utilised for specific reactor types.

Kinetic modelling accounts for both the kinetics of the gasification process and the hydro-dynamics of the gasifier. Gasification kinetics deals with the mass and energy balances that is involved in the yield of the various products at the given operating conditions whereas hydro-dynamics has to do with the forces involved in the physical mixing of the particles in the gasification process. The simultaneous consideration of the kinetics and hydrodynamics renders the kinetic models remarkably accurate, especially at relatvely low temperatures (<800 ^{o}C) where the reaction rate is low and the residence time high (Altafini et al., 2003).

Nikoo and Mahinpey (2008) developed a comprehensive gasification model on reaction kinetics and reactor hydrodynamics using ASPEN PLUS simulator. The model was applied to determine the effect of equivalence ratio, biomass particle size, reactor temperature and steam-to-biomass ratio after the model was validated using experimental values. The results showed that increasing the reaction temperature improved the gasification process by enhancing the hydrogen production and carbon conversion efficiency. The production of CO_2 and carbon conversion efficiency increase proportionally with increasing equivalence ratio (ER). Various other researchers, including Wang and Kinoshita (1993), Fiaschi and Michelini

(2001) and Giltrap et al. (2003), have done extensive work on the kinetic modelling of biomass gasification.

However, since kinetic models do not perform well for reaction conditions at higher temperatures despite their intensive computation, equilibrium models come in handy in these situations. Better still, combining both the kinetic and thermodynamic approaches in designing and targeting processes would be ideal since each method offers its own merits in the design process.

2.7.3.2. Thermodynamic Equilibrium modelling

From a thermodynamics perspective, the state of equilibrium of a system provides the maximum conversion at the particular reaction condition (Li et al., 2001). It represents the most stable compositon of the system where the system entropy is maximum and its Gibbs energy is minimum. Thus, thermodynamic equilibrium models for gasification processes allows one to predict the maximum yield that can be achieved in the product stream. Compared to kinetic modelling, thermodynamic equilibrium models are less computationally intensive (Zhang, 2012). They are also more general and therefore suitable for for preliminary/conceptual studies (*ibid.*). On the other hand, equilibrium models are ideally suited for systems at high temperature ranges with residence times that are long enough to allow complete reaction. These condition are hard to come by in real gasifiers, therefore, equilibrium models may not estimate the syngas product composition and calorific value accurately at relatively low temperatures bettween 750 and 1000 ^{o}C (Basu, 2010).

There are general assumptions underlying equilibrium modelling. These assumptions work better in specific gasifier types for which this type of equilibrium model provides a better simulation of the process. Prins et al. (2007) discuss these assumptions:

- Perfect adiabatic conditions are assumed for the gasifier. In other words, the gasifier is considered to be perfectly insulated with no heat loses.
- It is assumed that the temperature is uniform and there is perfect mixing in the reactor.

- Reaction rates for the gasification process are assumed to be rapid enough and the residence time takes long enough to attain equilibrium.

Because of the assumptions made in equilibrium models, the model results tend to deviate from the experimental results under certain circumstances. This usually happens at relatively low gasification temperatures where it is mostly the case that H_2 and CO yields are overestimated while CO_2, CH_4, tars and char are underestimated. It is for this reason that equilibrium models are currently being modified to achieve better results. For example, Jarungthammachote and Dutta (2007) improved the results for the composition of the producer gas in a thermodynamic equilibrium model of a downdraft gasifier by using correction factors for equilibrium constants for the water-gas shift reaction and the methane reaction.

Equilibrum models are generally sub-divided into stoichiometric and non-stoichiometric models. Jarungthammachote and Dutta (*ibid.*) explain that the two approaches are fundamentally equivalent and provide similar results. Some typical characteristics of the two approaches are presented below.

(a) Non-stoichiometric equilibrium model

In non-stoichiometric models, no reaction mechanisms are required in formulating the gasification simulation. Only the elemental composition of the feedstock that is obtained from the ultimate analysis of the feed is needed in setting up the model (Li et al., 2004). The non-stoichiometric approach is developed based on the minimization of the Gibbs energy. The premise for the development of this model is that the stable equilibrium condition of a reactive system is reached when the Gibbs energy is at the minimum.

(b) Stoichiometric equilibrium model

Stoichiometric models are characterised by reaction mechanisms that incorporate the chemical reactions and species of the system. Specific chemical reactions are identified and used for the prediction of the composition of the syngas product. That is, only reactions that

are considered to have significance as far as the thermodynamics of the system is concerned, are used in the modelling process. Stoichiometric modelling is also developed on the basis of equilibrium constants (Giltrap et al., 2003). The formulation of the model is based on the chemical species that are present in significant amount and comprise of elements that predominate the system (e.g. C, H and O).

The elements that exist in small amounts in the product gas are not considered. The chemical species that are important in the system have lower values of the change in the Gibbs energy of formation under gasification conditions. Prins et al. (2003) have shown that for biomass gasification at temperatures between 600 and 1500 K, there are only seven chemical species present in concentrations higher that 10^{-4} mol%. These are CO, CO_2, CH_4, H_2O, N_2, H_2 and solid carbon in the form of graphite. According to the Duhem's theory, this system has three independent chemical reactions (Puig-Arnavat et al., 2010). If the system is homogeneous (with no carbon present), the number of independent reactions reduces to two (*ibid.*).

Zainal et al. (2001) employed the stoichiometric model to predict the performance of a downdraft gasifier and also to determine the producer gas for various biomass feedstock materials. The model managed to predict results that are reasonably close to the experimental values. For instance, the model predicted the producer gas composition with a combined H_2 and CO composition of 40.67% versus 38.27% for the experimental value.

2.8. DESIGN OF GASIFICATION-BASED INTEGRATED BIOREFINERIES

The design of integrated biorefineries, like other chemical processes, follows a series of design phases that are each characterized by different levels of details. Examining the available literature on the design of integrated biorefineries, reveals that the targeting phase and the conceptual phase of process design are mostly relevant to biorefineries (Kelloway and Daoutidis, 2014; Tang et al., 2013). Part of the reason is that the concept of biorefineries is in general at its early stages of development. Thus, the main focus of this review is on these two stages of process design applied to integrated biorefineries.

2.8.1. Targeting

Targets basically describe the possible theoretical limits for a given system. Thus, setting process targets (or targeting) in design allows one to identify the performance benchmarks for a system prior to carrying out the detailed design of a system (Patel, 2015). That is, at the targeting phase of process design, the extent to which a process can get relative to its ideal performance is determined from the onset. Process targets are usually developed based on fundamental principles such as mass and energy balance and therefore can provide insight into systems (El-Halwagi, 2012). Targeting can therefore be used as a decision-making tool for the determination of optimum conditions for process alternatives early in the design phase. One of its salient features that make it such a useful tool is that it is independent of the process structure or flowsheets, considering the system as a whole and disregarding the different process units and equipment.

2.8.2. Conceptual design

The next phase after the targeting stage is the conceptual phase. The conceptual stage of the design process is critical as it influences the overall economics of the process in a tremendous way. It is estimated that a decision taken at this stage of the process design fixes about 80 % of the total process cost (Biegler et al., 1997). It is essentially an iterative process consisting of four main stages*, viz*. problem formulation, synthesis, analysis and evaluation (Cano-Ruiz and McRae, 1998). Process synthesis is a central component of the entire process design activity (Nishida et al., 1981). It involves developing the flowsheet structure that meets the requirements of various process objectives, including the highest yield and energy efficiency. Process synthesis also deals with developing process topologies using the most sustainable and optimum path for transforming the raw materials to desired products. At this stage, the inputs and outputs of the process are known and the process flowsheet that meets the set objectives needs to be determined (Figure 2.10).

Figure 2.10. Schematic representation of process synthesis

The success of the design process largely depends on the efficient integration of the various technologies and conversion processes of raw materials to desired products. In designing integrated biorefineries, process synthesis can be considered under the premise that, given the set of available biomass feedstock, more conversion reactions and technologies that are becoming established, more and more process topology structures become available. Thus, the design of integrated biorefineries becomes more intricate as the degrees of freedom with regards to the selection of products, feedstock and conversion technologies increases (Andiappan et al., 2015). This subsequently makes the decision-making process in designing biorefinery systems an open and massively complex task.

Therefore, because of this large number of available alternatives in integrated biorefineries, there is a need to develop methodologies, concepts and models that can predict the performance and assist in decision-making regarding these biorefinery systems. In this regard, Dimian (2007) and Kokossis and Yang (2010) highlight the potential offered by process systems engineering (PSE) approaches in supporting the design and synthesis of biorefineries. These PSE approaches make use of various systematic computer-aided means for designing, controlling and optimizing physical, chemical and biological processes (Stephanopoulos and Reklaitis, 2011).

Different systematic tools have been developed and utilized for synthesis and design of integrated biorefineries. These techniques include classical process synthesis tools which have been used in the design of petroleum refineries. The same methods are applied in the synthesis and design of integrated biorefineries for screening and determination of optimum technology pathways and process configurations. A review of available literature reveals that

these methods can basically be distilled into three categories, namely, (a) Hierarchical approach, (b) Insights approach, and (c) mathematical programming (Yuan et al., 2013). Each of these has its own inherent advantages and disadvantages in terms of applicability. However, Mizsey and Fonyo (1990) also point out that there is a general development of applying a combination of these approaches in order to supplement the disadvantages of one technique with the strong-points of others. The approaches are briefly discussed below.

2.8.2.1. Hierarchical approaches

The underlying principle in hierarchical approaches involves decomposing the usually complex design problem into numerous sub-problems that can easily be dealt with (Barnicki and Siirola, 2004). The process is based on shortcuts models and calculations as well as heuristics at each sub-problem to search and reduce the available alternatives. The hierarchical technique was recently presented in screening potential alternatives in the conceptual design and synthesis of integrated biorefineries (Ng et al., 2009). In this work, two screening tools, namely, the forward-reverse synthesis tree and evolutionary technique were proposed to systematically reduce the process alternatives.

Mansoornejad et al. (2010) proposed the novel application of the hierarchical approach for the economic performance optimization of forest biorefineries through integration of process/product design portfolio, supply chain network and manufacturing flexibility. Although hierarchical methods offer a quick way of solving process design and synthesis problems, they do however have a major setback that compromises their ability to find the optimum solution (Li and Kraslawski, 2004). Because the method follows a particular order from one level to another in its solutions, the interaction that may exist between different levels is usually not considered.

2.8.2.2. Mathematical programming

Mathematical programming approaches in the synthesis and integration of processes entail determining the best process structures and conditions through various optimization

techniques. Depending on the complexity of the design as well as the level of details required, the design can be formulated and solved as a linear program (LP), nonlinear program (NLP) or mixed-integer linear programming models (MILP). In their study on optimization of biomass conversion to fuels and chemicals, Kelloway and Daoutidis (2014) formulated a biorefinery superstructure as a mixed integer nonlinear program (MILP). The synthesis problem was solved to determine the superstructure with the highest economic potential as well as the maximum efficiency of carbon.

Sammons et al. (2008) also introduced a framework that employs mathematical optimization for the allocation of biorefinery products with consideration for profitability using matrices based on the process technology and economy. The mathematical programming technique has the advantage of being able to handle many process alternatives at the same time and therefore generating quick solutions to process synthesis and design problems. The downside of mathematical programming methods is seen when the design problem is too complex and cannot be represented as a linear model. In such instances, there is no guarantee that the optimum solution can be found.

2.8.2.3. Insights-based approach

The insight approach typically uses thermodynamics and physical laws as basis for setting targets. These approaches are particularly useful in providing insight into the overall performance of the process early in the design stage before developing a flowsheet. Some well-known insight-based approaches include pinch analysis, ternary diagrams and distillation residue curve maps. Ng (2010) adopted an insight approach based on pinch analysis to come up with a targeting framework for determining the optimum biofuel production as well as revenue targets for an integrated biorefinery.

The automated targeting approach was developed further into a multiple-cascade automated targeting approach by Tay and Ng (2012). The method was applied to an integrated biorefinery based on gasification process where the highest performance of the process was assessed in terms of its economy. Furthermore, Tay et al. (2011) proposed the utilization of a C-H-O ternary

diagram in the conceptual synthesis of integrated biorefinery to evaluate the overall performance for the production of methanol from biomass gasification. Although the use of insights-based approaches in synthesizing and designing biorefinery process is characterized mainly by limited parameters that can be taken into account, they do however provide a highly effective means for the analysis and evaluation of such processes.

2.9. C-H-O TERNARY DIAGRAMS AS A PROCESS SYNTHESIS TOOL

One of the insight-based frameworks for designing and analyzing integrated biorefineries systematically involves the utilization of the C-H-O ternary diagrams. C-H-O ternary diagrams are a method of representing chemical process with streams whose constituent molar compositions can ultimately be split into only carbon (C), hydrogen (H) and oxygen (O). C-H-O ternary diagrams can be used to illustrate and evaluate performance parameters of chemical processes as well as compare various technologies and process conditions. Cairns et al. (1963) applied C-H-O ternary diagrams to investigate conditions at which fuel cells should be operated without carbon deposition at 500 K. Cairns and Tevebaugh (1964) used the C-H-O ternary diagram to represent the equilibrium composition and the carbon deposition boundaries at atmospheric pressure and temperatures ranging from 298 to 1500 K.

Work on carbon deposition boundaries for C-H-O systems was further extended by investigating carbon deposition as a function of both temperature and pressure (Tevebaugh and Cairns, 1965). The temperature range of 298 – 1300 K at 1, 1.2, 5, 10 and 20 atm. were considered in the study and it was shown that carbon deposition boundaries are determined by temperature, pressure and O/H ratio. Mohnot and Kyle (1978) showed that carbon deposition boundaries are not only dependent on temperature and pressure but also on the amount of inert in the system. Thus, the study extended the C-H-O system into C-H-O-N system in which nitrogen was considered as an inert gas. When the carbon deposition boundaries from the C-H-O-N system were superimposed on the C-H-O system results, a maximum deviation of around 20 % was found.

Battaerd and Evans (1979) first explored the potential of C-H-O diagrams as an alternative representation of coal composition data after identifying the limitations of the Seyler's plot and the Van Kravelen's charts which were then the best-known coal composition charts. Some of the highlighted limitations included that in coal processing, water cannot be located on the Van Kravelen's diagram, whereas the Seyler's chart application was limited mainly to classifying coals rather than interpreting the processes of coalification because it provided little insight into the possible process occurring during coalification. In their study, Battaerd and Evans (*ibid.*) used the C-H-O ternary diagram to investigate the conversion of brown coal into liquid fuel by hydrogen and advocated the use of the C-H-O ternary diagram in coal technology. Stephens (1979) also used the C-H-O ternary plots to review the chemistry of the formation and maturation of coals and macerals. In this study, compositions were plotted as atomic percentages as opposed to bond equivalent percent as it was the case by Battaerd and Evans (1979).

Sasaki and Teraoka (2003) applied C-H-O ternary diagrams to represent and study operational conditions of fuel cells. Carbon deposition boundaries, partial pressures of different gaseous species including O_2, H_2 and CO, fuel gas regions and theoretical carbon electromotive force (EMF) were described. Another important use of C-H-O ternary diagrams is in chemical vapor deposition (CVD), particularly for synthetic diamond production. Bachmann et al. (1991) and Eaton and Sunkara (2000) studied diamond CVD by means of C-H-O ternary diagrams to determine the conditions necessary for carbon atoms to settle in a crystalline form as diamond. C-H-O ternary diagrams are used to locate diamond deposition, non-diamond deposition as well as no-carbon deposition regions and also to account for the differences in the quality of diamonds deposited when using various feed gas mixtures and/or composition.

Lately, the use of C-H-O ternary diagram has been employed in representing and analyzing various energy conversion processes such as gasification, combustion and other fossil and renewable fuels reforming processes at different operating conditions (Prins et al., 2003; Prins and Ptasinski, 2005; Ptasinski et al., 2007). The improvement of the efficiency of biomass gasification through torrefaction has also been analyzed based on the C-H-O ternary diagram by Prins et al. (2006).

As it can be seen from the critical review of available literature, C-H-O ternary plots have great potential for providing useful guidelines regarding biorefinery process performance parameters, technology comparison as well as identifying optimum conditions. However, Gräbner (2015) laments that despite the massive potential offered by this technique in analyzing chemical processes, it is seldom used. Even previous studies based on C-H-O ternary diagrams have not exploited the potential of the framework as a useful tool for systematic quantitative design. Moreover, in spite of the significant contribution of the previous research efforts related to C-H-O ternary systems, an underlying limitation that characterizes these studies has to do with the fact that they seem to only concentrate on the representation and modelling of a single process.

As Fernando et al. (2006) point out, the interaction of various parts of processes should be considered in order to ensure the efficient and optimum overall performance of an integrated biorefinery. Tay et al. (2010) effectively employed the C-H-O ternary diagram to evaluate the composition of syngas at equilibrium and also synthesized an integrated biorefinery even though not much detail on the synthesis and targeting steps were demonstrated. The same study on the systematic synthesis of integrated biorefinery using the C-H-O ternary diagram was explored more elaborately by Tay et al. (2011).

REFERENCES

1. Abuadala, A., Dincer, I. & Naterer, G.F. 2010. Exergy analysis of hydrogen production from biomass gasification. *International Journal of Hydrogen Energy*, 35(10): 4981–4990.

2. Adhikari, S., Thangalazhy-Gopakumar, S. & Taylor, S. 2012. CHAPTER 9. Integrated Forest Biorefineries: Gasification and Pyrolysis for Fuel and Power Production. In *RSC Green Chemistry*. Cambridge: Royal Society of Chemistry: 211–255.

3. Agrawal, R. & Singh, N.R. 2010. Solar Energy to Biofuels. *Annual Review of Chemical and Biomolecular Engineering*, 1(1): 343–364.

4. Aguayo, A.T., Ereña, J., Mier, D., Arandes, J.M., Olazar, M. & Bilbao, J. 2007. Kinetic Modeling of Dimethyl Ether Synthesis in a Single Step on a CuO−ZnO−Al2O3/γ-Al2O3 Catalyst. *Industrial & Engineering Chemistry Research*, 46(17): 5522–5530.

5. Aliyu, A.K., Modu, B. & Tan, C.W. 2018. A review of renewable energy development in Africa: A focus in South Africa, Egypt and Nigeria. Renewable and Sustainable Energy Reviews, 81: 2502–2518.

6. Altafini, C.R., Wander, P.R. & Barreto, R.M. 2003. Prediction of the working parameters of a wood waste gasifier through an equilibrium model. *Energy Conversion and Management*, 44(17): 2763–2777.

7. Andiappan, V., Ko, A.S.Y., Lau, V.W.S., Ng, L.Y., Ng, R.T.L., Chemmangattuvalappil, N.G. & Ng, D.K.S. 2015. Synthesis of sustainable integrated biorefinery via reaction pathway synthesis: Economic, incremental environmental burden and energy assessment with multiobjective optimization. *AIChE Journal*, 61(1): 132–146.

8. Arcoumanis, C., Bae, C., Crookes, R. & Kinoshita, E. 2008. The potential of di-methyl ether (DME) as an alternative fuel for compression-ignition engines: A review. *Fuel*, 87(7): 1014–1030.

9. Aresta, M. ed. 2012. *Biorefinery: from biomass to chemicals and fuels*. Berlin: de Gruyter.

10. Aznar, M.P., Corella, J., Gil, J., Martín, J.A., Caballero, M.A., Olivares, A., Pérez, P. & Francés, E. 1997. Biomass Gasification with Steam and Oxygen Mixtures at Pilot Scale and with Catalytic Gas Upgrading. Part I: Performance of the Gasifier. In A. V. Bridgwater & D. G. B. Boocock, eds. *Developments in Thermochemical Biomass Conversion*. Dordrecht: Springer Netherlands: 1194–1208.

11. Babu, B.V. & Sheth, P.N. 2006. Modeling and simulation of reduction zone of downdraft biomass gasifier: Effect of char reactivity factor. *Energy Conversion and Management*, 47(15–16): 2602–2611.

12. Bachmann, P.K., Leers, D. & Lydtin, H. 1991. Towards a general concept of diamond chemical vapour deposition. *Diamond and Related Materials*, 1(1): 1–12.

13. Baldwin S. 2007. Houses of Parliament, Parliamentary Office of Science and Technology. Transport fuels. *Postnote 293:1-4*.

14. Barnicki, S.D. & Siirola, J.J. 2004. Process synthesis prospective. *Computers & Chemical Engineering*, 28(4): 441–446.

15. Baruah, D. & Baruah, D.C. 2014. Modeling of biomass gasification: A review. *Renewable and Sustainable Energy Reviews*, 39: 806–815.

16. Basu, P. 2010. *Biomass gasification and pyrolysis: practical design and theory*. Burlington, MA: Academic Press.

17. Battaerd, H.A.J. & Evans, D.G. 1979. An alternative representation of coal composition data. *Fuel*, 58(2): 105–108.

18. Biegler, L.T., Grossmann, I.E. & Westerberg, A.W. 1997. *Systematic methods of chemical process design*. Upper Saddle River, N.J: Prentice Hall PTR.

19. Bonomi, A., Cavalett, O., Cunha, M.P. da & Lima, M.A.P. 2016. *Virtual biorefinery: an optimization strategy for renewable carbon valorization*.

http://www.search.ebscohost.com/login.aspx?direct=true&scope=site&db=nlebk&db=nlabk&AN=1108374 14 January 2017.

20. Bozell, J.J. & Petersen, G.R. 2010. Technology development for the production of biobased products from biorefinery carbohydrates—the US Department of Energy's "Top 10" revisited. *Green Chemistry*, 12(4): 539.

21. BP. 2015. *BP Statistical Review of World Energy June 2015*. http://www.bp.com/statisticalreview 15 July 2015.

22. Cairns, E.J. & Tevebaugh, A.D. 1964. CHO Gas Phase Compositions in Equilibrium with Carbon, and Carbon Deposition Boundaries at One Atmosphere. *Journal of Chemical & Engineering Data*, 9(3): 453–462.

23. Cairns, E.J., Tevebaugh, A.D. & Holm, G.J. 1963. Thermodynamics of Hydrocarbon Fuel Cells. *Journal of the Electrochemical Society*, 110(10): 1025.

24. Cano-Ruiz, J.A. & McRae, G.J. 1998. Environmentally conscious chemical process design. *Annual Review of Energy and the Environment*, 23(1): 499–536.

25. Cherubini, F., Jungmeier, G., Wellisch, M., Willke, T., Skiadas, I., Van Ree, R. & de Jong, E. 2009. Toward a common classification approach for biorefinery systems. *Biofuels, Bioproducts and Biorefining*, 3(5): 534–546.

26. Christopher, L. 2013. *Integrated forest biorefineries: challenges and opportunities*. Cambridge: Royal Society of Chemistry. http://site.ebrary.com/id/10640417 8 January 2017.

27. Ciferno, J.P. & Marano, J.J. 2002. *Benchmarking biomass gasification technologies for fuels, chemicals and hydrogen production*. Pittsburgh, PA, USA: U.S. Department of Energy National Energy Technology Laboratory.

28. Clark, J.H. & Deswarte, F.E.I. eds. 2015. *Introduction to chemicals from biomass*. Second edition. Chichester, West Sussex: John Wiley & Sons, Inc.

29. Clark, J.H., Luque, R. & Matharu, A.S. 2012. Green Chemistry, Biofuels, and Biorefinery. *Annual Review of Chemical and Biomolecular Engineering*, 3(1): 183–207.

30. Cohen, J., Janssen, M., Chambost, V. & Stuart, P. 2010. Critical Analysis of Emerging Forest Biorefinery (FBR) Technologies for Ethanol Production. *Pulp & Paper Canada*, 111: 24–30.

31. Damartzis, T., Michailos, S. & Zabaniotou, A. 2012. Energetic assessment of a combined heat and power integrated biomass gasification–internal combustion engine system by using Aspen Plus®. *Fuel Processing Technology*, 95: 37–44.

32. Damartzis, T. & Zabaniotou, A. 2011. Thermochemical conversion of biomass to second generation biofuels through integrated process design - A review. *Renewable and Sustainable Energy Reviews*, 15(1): 366–378.

33. Devi, L., Ptasinski, K.J. & Janssen, F.J.J. 2003. A review of the primary measures for tar elimination in biomass gasification processes. *Biomass and Bioenergy*, 24(2): 125–140.

34. Dimian, A.C. 2007. Renewable raw materials: chance and challenge for computer-aided process engineering. In *Computer Aided Chemical Engineering*. Elsevier: 309–318. http://linkinghub.elsevier.com/retrieve/pii/S1570794607800757 15 January 2017.

35. Dry, M.E. 2002. The Fischer–Tropsch process: 1950–2000. *Catalysis Today*, 71(3–4): 227–241.

36. Eaton, S.C. & Sunkara, M.K. 2000. Construction of a new C–H–O ternary diagram for diamond deposition from the vapor phase. *Diamond and Related Materials*, 9(7): 1320–1326.

37. Eberhard, A., Kolker, J. & Leigland, J. 2014. South Africa's Renewable Energy IPP Procurement Program: Success Factors and Lessons. Washington, DC: Public-Private Infrastructure Advisory Facility (PPIAF).

38. Edenhofer, O., Seyboth, K., Creutzig, F. & Schlömer, S. 2013. On the Sustainability of Renewable Energy Sources. *Annual Review of Environment and Resources*, 38(1): 169–200.

39. Edenhofer, O., Madruga R.P. & Sokona. Y. 2012. Renewable Energy Sources and Climate Change Mitigation - Special Report of the Intergovernmental Panel on Climate Change. Cambridge: Cambridge University Press.

40. El-Halwagi, M.M. 2012. *Sustainable design through process integration: fundamentals and applications to industrial pollution prevention, resource conservation, and profitability enhancement*. Boston, MA: Butterworth-Heinemann.

41. Elliott, D.C. 1994. Water, alkali and char in flash pyrolysis oils. *Biomass and Bioenergy*, 7(1–6): 179–185.

42. Fatih Demirbas, M. 2009. Biorefineries for biofuel upgrading: A critical review. *Applied Energy*, 86: S151–S161.

43. Fernando, S., Adhikari, S., Chandrapal, C. & Murali, N. 2006. Biorefineries: Current Status, Challenges, and Future Direction. *Energy & Fuels*, 20(4): 1727–1737.

44. Fiaschi, D. & Michelini, M. 2001. A two-phase one-dimensional biomass gasification kinetics model. *Biomass and Bioenergy*, 21(2): 121–132.

45. Fremaux, S., Beheshti, S.-M., Ghassemi, H. & Shahsavan-Markadeh, R. 2015. An experimental study on hydrogen-rich gas production via steam gasification of biomass in a research-scale fluidized bed. *Energy Conversion and Management*, 91: 427–432.

46. Garcia, L., Salvador, M., Arauzo, J. & Bilbao, R. 2001. CO_2 as a gasifying agent for gas production from pine sawdust at low temperatures using a Ni/Al coprecipitated catalyst. *Fuel Processing Technology*, 69(2): 157–174.

47. Gil, J., Corella, J., Aznar, M.P. & Caballero, M.A. 1999. Biomass gasification in atmospheric and bubbling fluidized bed: Effect of the type of gasifying agent on the product distribution. *Biomass and Bioenergy*, 17(5): 389–403.

48. Giltrap, D.L., McKibbin, R. & Barnes, G.R.G. 2003. A steady state model of gas-char reactions in a downdraft biomass gasifier. *Solar Energy*, 74(1): 85–91.

49. Gomez, L.D., Steele-King, C.G. & McQueen-Mason, S.J. 2008. Sustainable liquid biofuels from biomass: the writing's on the walls. *New Phytologist*, 178(3): 473–485.

50. González, J.F., Román, S., Bragado, D. & Calderón, M. 2008. Investigation on the reactions influencing biomass air and air/steam gasification for hydrogen production. *Fuel Processing Technology*, 89(8): 764–772.

51. Gordillo, G., Annamalai, K. & Carlin, N. 2009. Adiabatic fixed-bed gasification of coal, dairy biomass, and feedlot biomass using an air–steam mixture as an oxidizing agent. *Renewable Energy*, 34(12): 2789–2797.

52. Gräbner, M. 2015. *Industrial coal gasification technologies covering baseline and high-ash coal*. Weinheim: Wiley-VCH-Verl.

53. Graham-Rowe, D. 2011. Agriculture: Beyond food versus fuel. *Nature*, 474(7352): S6–S8.

54. Hugo, W. 2016. BioEnergy Atlas for South Africa – Synopsis Report. Pretoria: Department of Science and Technology.

55. International Energy Agency (IEA). 2017. Renewables Information: Overview. http://www.iea.org/publications/freepublications/publication/RenewablesInformation2017Overview.pdf 20 February 2018.

56. International Energy Agency (IEA). 2009. *Annual Report 2009*. Wageningen, The Netherlands: IEA.

57. International Energy Agency (IEA). 2008. *World Energy Outlook 2008*. Paris Cedex. http://www.worldenergyoutlook.org/media/weowebsite/2008-1994/weo2008.pdf.

58. Jarungthammachote, S. & Dutta, A. 2007. Thermodynamic equilibrium model and second law analysis of a downdraft waste gasifier. *Energy*, 32(9): 1660–1669.

59. Johansson, T.B., Patwardhan, A., Nakićenović, N., Gomez-Echeverri, L. & International Institute for Applied Systems Analysis eds. 2012. *Global Energy Assessment (GEA)*. Cambridge: Laxenburg, Austria: Cambridge University Press ; International Institute for Applied Systems Analysis.

60. Juan Carlos Serrano-Ruiz, Ryan M.West & James A. Dumesic. 2010. Catalytic Conversion of Renewable Biomass Resources to Fuels and Chemicals. *Annual Review* of Chemical and Biomolecular Engineering, 1: 79–100.

61. Kelloway, A. & Daoutidis, P. 2014. Process Synthesis of Biorefineries: Optimization of Biomass Conversion to Fuels and Chemicals. *Industrial & Engineering Chemistry Research*, 53(13): 5261–5273.

62. Khan, N., le Roes-Hill, M., Welz, P., Grandin, K., Kudanga, T., van Dyk, S., Ohlhoff, C., van Zyl, W.H. (Emile) & Pletschke, B. 2015. Fruit waste streams in South Africa and their potential role in developing a bio-economy. South African Journal of Science, 111(5/6). http://sajs.co.za/article/view/3627 26 February 2018.

63. Klass, D.L. 1998. *Biomass for renewable energy, fuels, and chemicals*. San Diego: Academic Press.

64. Kokossis, A.C. & Yang, A. 2010. On the use of systems technologies and a systematic approach for the synthesis and the design of future biorefineries. *Computers & Chemical Engineering*, 34(9): 1397–1405.

65. Kumar, A., Eskridge, K., Jones, D.D. & Hanna, M.A. 2009. Steam–air fluidized bed gasification of distillers grains: Effects of steam to biomass ratio, equivalence ratio and gasification temperature. *Bioresource Technology*, 100(6): 2062–2068.

66. Lange, J.-P. 2007. Lignocellulose conversion: an introduction to chemistry, process and economics. *Biofuels, Bioproducts and Biorefining*, 1(1): 39–48.

67. Lehman Brothers. 2008. *Global Oil choke Points: How Vulnerable is the Global Oil Market?* New York: Lehman Brothers Inc.

68. Li, X., Grace, J., Watkinson, A., Lim, C. & Ergüdenler, A. 2001. Equilibrium modeling of gasification: a free energy minimization approach and its application to a circulating fluidized bed coal gasifier. *Fuel*, 80(2): 195–207.

69. Li, X. & Kraslawski, A. 2004. Conceptual process synthesis: past and current trends. *Chemical Engineering and Processing: Process Intensification*, 43(5): 583–594.

70. Li, X.T., Grace, J.R., Lim, C.J., Watkinson, A.P., Chen, H.P. & Kim, J.R. 2004. Biomass gasification in a circulating fluidized bed. *Biomass and Bioenergy*, 26(2): 171–193.

71. Liu, S., Zhu, J., Chen, M., Xin, W., Yang, Z. & Kong, L. 2014. Hydrogen production via catalytic pyrolysis of biomass in a two-stage fixed bed reactor system. *International Journal of Hydrogen Energy*, 39(25): 13128–13135.

72. Luque, R., Campelo, J. & Clark, J.H. eds. 2011. *Handbook of biofuels production: processes and technologie*s. Oxford; Philadelphia: Woodhead Publishing.

73. Luu, M.T., Milani, D., Wake, M. & Abbas, A. 2016. Analysis of di-methyl ether production routes: Process performance evaluations at various syngas compositions. *Chemical Engineering Science*, 149: 143–155.

74. Lv, P., Xiong, Z., Chang, J., Wu, C.., Chen, Y. & Zhu, J.. 2004. An experimental study on biomass air–steam gasification in a fluidized bed. *Bioresource Technology*, 95(1): 95–101.

75. Lynd, L.R., von Blottnitz, H., Tait, B., de Boer, J., Pretorius, I.S., Rumbold, K. & van Zyl, W.H. 2003. Converting plant biomass to fuels and commodity chemicals in South Africa: a third chapter? South African Journal of Science, 99(11-12): 499–507.

76. Machado, G., Leon, S., Santos, F., Lourega, R., Dullius, J., Mollmann, M.E. & Eichler, P. 2016. Literature Review on Furfural Production from Lignocellulosic Biomass. Natural Resources, 07(03): 115–129.

77. Mansoornejad, B., Chambost, V. & Stuart, P. 2010. Integrating product portfolio design and supply chain design for the forest biorefinery. *Computers & Chemical Engineering*, 34(9): 1497–1506.

78. Marquardt W., Harwardt A., Hechinger M., Kraemer K., Viell J. & Voll A. 2010. The biorenewables opportunity - Toward next generation process and product systems. *AIChE Journals*, 56: 2228–2235.

79. Marsh, R., Hewlett, S., Griffiths, T. & Williams, K. 2007. Advanced Thermal Treatments for solid waste - a waste manager's guide. In *Proceedings of the 22nd International Conference on Solid Waste Management and Technology*. Philadelphia (USA).

80. Mizsey, P. & Fonyo, Z. 1990. Toward a more realistic overall process synthesis—the combined approach. *Computers & Chemical Engineering*, 14(11): 1213–1236.

81. Mohnot, S. & Kyle, B.G. 1978. Equilibrium Gas-Phase Compositions and Carbon Deposition Boundaries in the CHO-Inert System. *Industrial & Engineering Chemistry Process Design and Development*, 17(3): 270–272.

82. Namasivayam, A.M., Korakianitis, T., Crookes, R.J., Bob-Manuel, K.D.H. & Olsen, J. 2010. Biodiesel, emulsified biodiesel and dimethyl ether as pilot fuels for natural gas fuelled engines. *Applied Energy*, 87(3): 769–778.

83. Neathery, J.K. 2010. Chapter 4. Biomass Gasification. In M. Crocker, ed. *RSC Energy and Environment Series*. Cambridge: Royal Society of Chemistry: 67–94. http://ebook.rsc.org/?DOI=10.1039/9781849732260-00067 14 September 2017.

84. New Energy and Industrial Technology Development Organization (NEDO). 2015. *Clean Coal Technologies in Japan: Technological Innovation in the Coal Industry*. 2nd ed. Japan: NEDO. http://www.nedo.go.jp/content/100861237.pdf 5 May 2017.

85. Ng, D.K.S. 2010. Automated targeting for the synthesis of an integrated biorefinery. *Chemical Engineering Journal*, 162(1): 67–74.

86. Ng, D.K.S., Pham, V., El-Halwagi, M., Jiménez-Gutiérrez, A. & Spriggs, H.D. 2009. *A Hierarchical Approach to the Synthesis and Analysis of Integrated Biorefineries*.

87. Nikoo, M.B. & Mahinpey, N. 2008. Simulation of biomass gasification in fluidized bed reactor using ASPEN PLUS. *Biomass and Bioenergy*, 32(12): 1245–1254.

88. Nishida, N., Stephanopoulos, G. & Westerberg, A.W. 1981. A review of process synthesis. *AIChE Journal*, 27(3): 321–351.

89. Ogawa, T., Inoue, N., Shikada, T. & Ohno, Y. 2003. Direct dimethyl ether synthesis. *Journal of natural gas chemistry*, 12(4): 219–227.

90. Pandey, A. ed. 2009. *Handbook of plant-based biofuels*. Boca Raton: CRC Press.

91. Patel, B. 2015. A Thermodynamic Targeting Approach for the Synthesis of Sustainable Biorefineries. In *Computer Aided Chemical Engineering*. Elsevier: 1283–1288. http://linkinghub.elsevier.com/retrieve/pii/B9780444635778500590 28 April 2017.

92. Patra, T.K. & Sheth, P.N. 2015. Biomass gasification models for downdraft gasifier: A state-of-the-art review. *Renewable and Sustainable Energy Reviews*, 50: 583–593.

93. Pradhan, A. & Mbohwa, C. 2014. Development of biofuels in South Africa: Challenges and opportunities. *Renewable and Sustainable Energy Reviews*, 39: 1089–1100.

94. Prins, M., Ptasinski, K. & Janssen, F. 2007. From coal to biomass gasification: Comparison of thermodynamic efficiency. *Energy*, 32(7): 1248–1259.

95. Prins, M.J. & Ptasinski, K.J. 2005. Energy and exergy analyses of the oxidation and gasification of carbon. *Energy*, 30(7): 982–1002.

96. Prins, M.J., Ptasinski, K.J. & Janssen, F.J.J.G. 2006. More efficient biomass gasification via torrefaction. *Energy*, 31(15): 3458–3470.

97. Prins, M.J., Ptasinski, K.J. & Janssen, F.J.J.G. 2003. Thermodynamics of gas-char reactions: first and second law analysis. *Chemical Engineering Science*, 58(3-6): 1003–1011.

98. Ptasinski, K.J. 2016. *Efficiency of biomass energy: an exergy approach to biofuels, power, and biorefineries*. Hoboken, New Jersey: Wiley.

99. Ptasinski, K.J., Prins, M.J. & Pierik, A. 2007. Exergetic evaluation of biomass gasification. *Energy*, 32(4): 568–574.

100. Puig-Arnavat, M., Bruno, J.C. & Coronas, A. 2010. Review and analysis of biomass gasification models. *Renewable and Sustainable Energy Reviews*, 14(9): 2841–2851.

101. Qin, K., Lin, W., Jensen, P.A. & Jensen, A.D. 2012. High-temperature entrained flow gasification of biomass. *Fuel*, 93: 589–600.

102. Ragauskas, A.J. 2006. The Path Forward for Biofuels and Biomaterials. *Science*, 311(5760): 484–489.

103. Rapagnà, S. 2000. Steam-gasification of biomass in a fluidised-bed of olivine particles. *Biomass and Bioenergy*, 19(3): 187–197.

104. Rauch, R., Hrbek, J. & Hofbauer, H. 2014. Biomass gasification for synthesis gas production and applications of the syngas: Biomass gasification for synthesis gas production. *Wiley Interdisciplinary Reviews: Energy and Environment*, 3(4): 343–362.

105. Ronert Evans. 2015. *Fueling Our Future: An Introduction to Sustainable Energy*. Cambridge, UK: Cambridge University Press. http://ebooks.cambridge.org/ebook.jsf?bid=CBO9780511807015.

106. Ruoppolo, G., Ammendola, P., Chirone, R. & Miccio, F. 2012. H2-rich syngas production by fluidized bed gasification of biomass and plastic fuel. *Waste Management*, 32(4): 724–732.

107. Sammons, N.E., Yuan, W., Eden, M.R., Aksoy, B. & Cullinan, H.T. 2008. Optimal biorefinery product allocation by combining process and economic modeling. *Chemical Engineering Research and Design*, 86(7): 800–808.

108. Sasaki, K. & Teraoka, Y. 2003. Equilibria in Fuel Cell Gases. *Journal of The Electrochemical Society*, 150(7): A885.

109. Shaddix, C.R. 2011. Chapter 7. Advances in Gasification for Biofuel Production. In B. A. Simmons, ed. *RSC Energy and Environment Series*. Cambridge: Royal Society of Chemistry: 136–155. http://ebook.rsc.org/?DOI=10.1039/9781849732857-00136 15 January 2017.

110. Sikarwar, V.S., Zhao, M., Clough, P., Yao, J., Zhong, X., Memon, M.Z., Shah, N., Anthony, E.J. & Fennell, P.S. 2016. An overview of advances in biomass gasification. *Energy Environ. Sci.*, 9(10): 2939–2977.

111. Sims, R.E.H. ed. 2004. *Bioenergy options for a cleaner environment in developed and developing countries*. 1st ed. Amsterdam; Boston: Elsevier.

112. Spellman, F.R. 2012. *Forest-based biomass energy: concepts and applications*. Boca Raton, FL: CRC Press.

113. Stephanopoulos, G. & Reklaitis, G.V. 2011. Process systems engineering: From Solvay to modern bio- and nanotechnology. *Chemical Engineering Science*, 66(19): 4272–4306.

114. Stephens, J.F. 1979. Coal as a C-H-O ternary system. 1. Geochemistry. *Fuel*, 58(7): 489–494.

115. Strezov, V. & Evans, T.J. eds. 2015. *Biomass processing technologies*. Boca Raton: CRC Press, Taylor & Francis Group.

116. Stuart, P.R. & El-Halwagi, M.M. eds. 2013. *Integrated biorefineries: design, analysis, and optimization*. Boca Raton, FL: CRC Press.

117. Sun, K., Lu, W., Qiu, F., Liu, S. & Xu, X. 2003. Direct synthesis of DME over bifunctional catalyst: surface properties and catalytic performance. *Applied Catalysis A: General*, 252(2): 243–249.

118. Tang, M.C., Chin, M.W.S., Lim, K.M., Mun, Y.S., Ng, R.T.L., Tay, D.H.S. & Ng, D.K.S. 2013. Systematic approach for conceptual design of an integrated biorefinery with uncertainties. *Clean Technologies and Environmental Policy*, 15(5): 783–799.

119. Tay, D.H.S. & Ng, D.K.S. 2012. Multiple-cascade automated targeting for synthesis of a gasification-based integrated biorefinery. *Journal of Cleaner Production*, 34: 38–48.

120. Tay, D.H.S., Ng, D.K.S., Kheireddine, H. & El-Halwagi, M.M. 2011. Synthesis of an integrated biorefinery via the C–H–O ternary diagram. *Clean Technologies and Environmental Policy*, 13(4): 567–579.

121. Tay, D.H.S., Kheireddine, H., Ng, D.K.S., El-Halwagi, M.M., 2010. Synthesis of an integrated biorefinery via the C-H-O ternary diagram. *Chemical Engineering Transactions*: 1411–1416.

122. Tevebaugh, A.D. & Cairns, E.J. 1965. Carbon Deposition Boundaries in the CHO System at Several Pressures. *Journal of Chemical & Engineering Data*, 10(4): 359–362.

123. Waldron, K.W. ed. 2014. *Advances in biorefineries: biomass and waste supply chain exploitation*. Amsterdam: Elsevier/Woodhead Publishing.

124. Wang, Y. & Kinoshita, C.M. 1993. Kinetic model of biomass gasification. *Solar Energy*, 51(1): 19–25.

125. Xianwen, D., Chuangzhi, W., Haibin, L. & Yong, C. 2000. The Fast Pyrolysis of Biomass in CFB Reactor. *Energy & Fuels*, 14(3): 552–557.

126. Xu, Y., Hanna, M.A. & Isom, L. 2008. “Green” Chemicals from Renewable Agricultural Biomass - A Mini Review. *The Open Agriculture Journal*, 2(1): 54–61.

127. Yergin Daniel. 2006. Ensuring Energy Security. *Foreign Affairs*, 85(2): 69–82.

128. Yuan, Z., Chen, B. & Gani, R. 2013. Applications of process synthesis: Moving from conventional chemical processes towards biorefinery processes. *Computers & Chemical Engineering*, 49: 217–229.

129. Zainal, Z., Rifau, A., Quadir, G. & Seetharamu, K. 2002. Experimental investigation of a downdraft biomass gasifier. *Biomass and Bioenergy*, 23(4): 283–289.

130. Zainal, Z.A., Ali, R., Lean, C.H. & Seetharamu, K.N. 2001. Prediction of performance of a downdraft gasifier using equilibrium modeling for different biomass materials. *Energy Conversion and Management*, 42(12): 1499–1515.

131. Zhang, M. ed. 2012. Artificial higher order neural networks for modeling and simulation for computer science and engineering: trends for emerging applications. Hershey, PA: Information Science Reference.

132. Zhu, Y., Wang, S., Ge, X., Liu, Q., Luo, Z. & Cen, K. 2010. Experimental study of improved two step synthesis for DME production. *Fuel Processing Technology*, 91(4): 424–429.

CHAPTER 3

METHODOLOGY

3.1. INTRODUCTION

Since biorefinery systems consist of raw materials and chemical products that are predominantly made up of carbon (C), hydrogen (H) and oxygen (O), biorefineries can be considered as C-H-O ternary systems. For example, lignocellulosic biomass feedstock is expressed generically as $C_nH_mO_pN_q$, where n-q represent the respective atomic number of carbon (C), hydrogen (H), oxygen (O) and nitrogen (N) determined from the ultimate analysis of the biomass. The minor components of biomass such as nitrogen and sulphur are not considered in the C-H-O representation because they act as inert and do not take part in the reactions. Other biorefinery chemical compounds include, amongst others hydrocarbons, alcohols (such as methanol and ethanol), CO_2, synthesis gas (CO and H_2), CH_4, H_2O, etc. and all these compounds are composed of C, H, and O as well.

This chapter therefore presents an overview of the fundamental concepts that will be used in this dissertation. In particular, how the C-H-O ternary diagram will be used to represent material balance and thermodynamic equilibrium to gain insight into the efficient utilization of raw materials (i.e. biomass) as well as optimum process conditions for the biorefinery processes. This framework allows us to use these fundamental concepts for the purpose of setting process targets as well as synthesizing biorefinery processes with focus on sustainability. Points and lines series of C-H-O ternary diagrams are traced and plotted using the Prosim ternary diagram program. A summary of the overall methods that will be used in the study is presented diagrammatically in Figure 3.1.

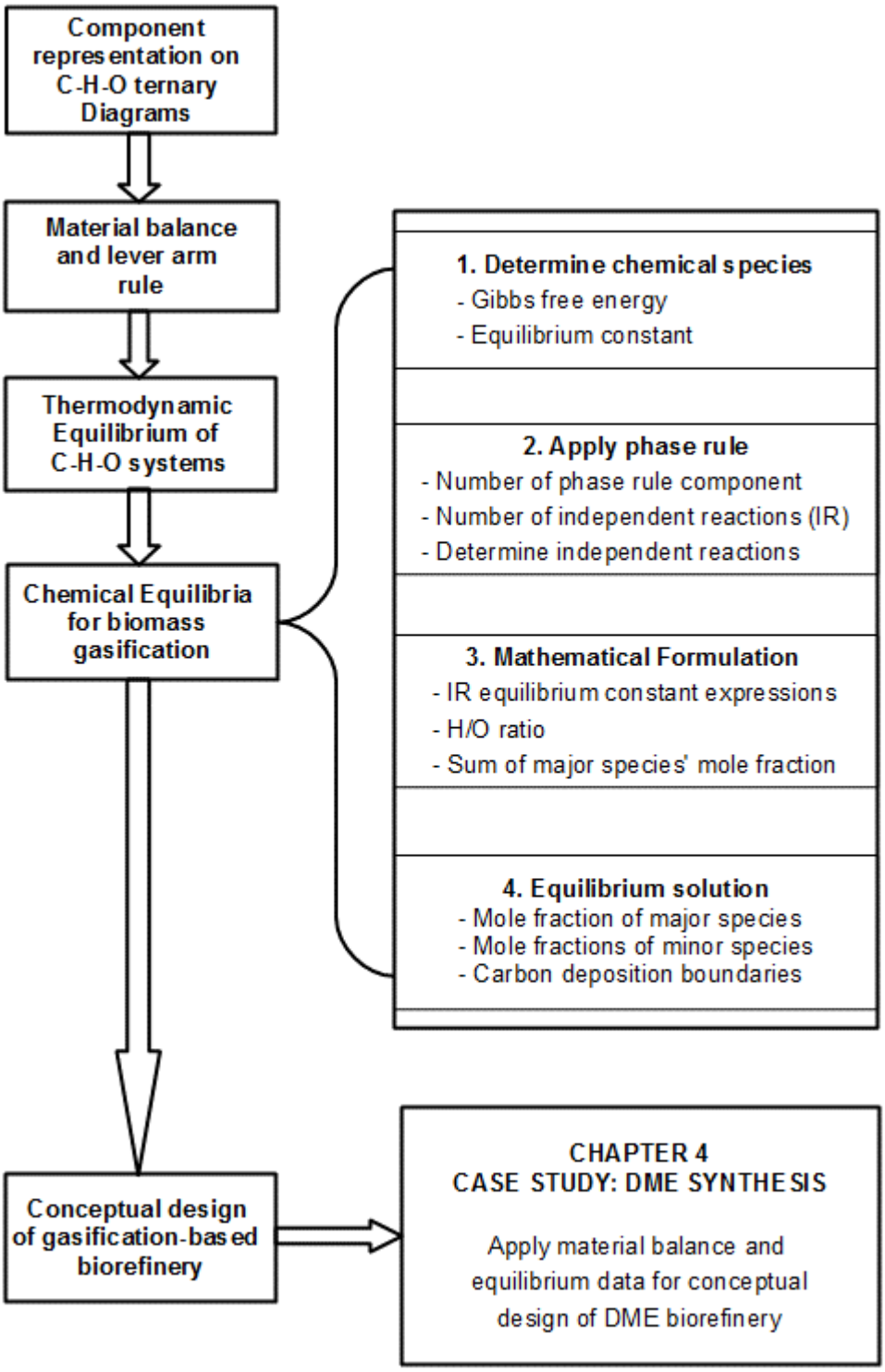

Figure 3.1. Summary of the proposed methods for the study

3.2. REPRESENTING COMPONENTS AND COMPOSITIONS ON THE C-H-O TERNARY DIAGRAM

We begin by first illustrating how biorefinery systems are represented diagrammatically using the C-H-O ternary diagram. When representing biorefineries on the C-H-O ternary diagram, the composition of the three atomic species (C,H and O) are plotted on an equilateral triangular grid that is subdivided into equidistant lines parallel to the three sides (Cahn and Haasen, 1996). Every point on the ternary plot represents a stream with different compositions of the three atomic species in terms of mole fraction or weight percent. Figure 3.2 illustrates a triangular grid used to represent the composition of a C-H-O system. The following key points can be observed from Figure 3.2:

- The vertices C, H and O represent pure components. For example, H_2 is represented at the H vertex
- Binary mixtures of the atomic species are represented along the edges: for example, any point along the line C-H is composed entirely of components C and H without O.
- Mixtures of the three atomic species are represented by points inside the triangle with each point representing a different composition.

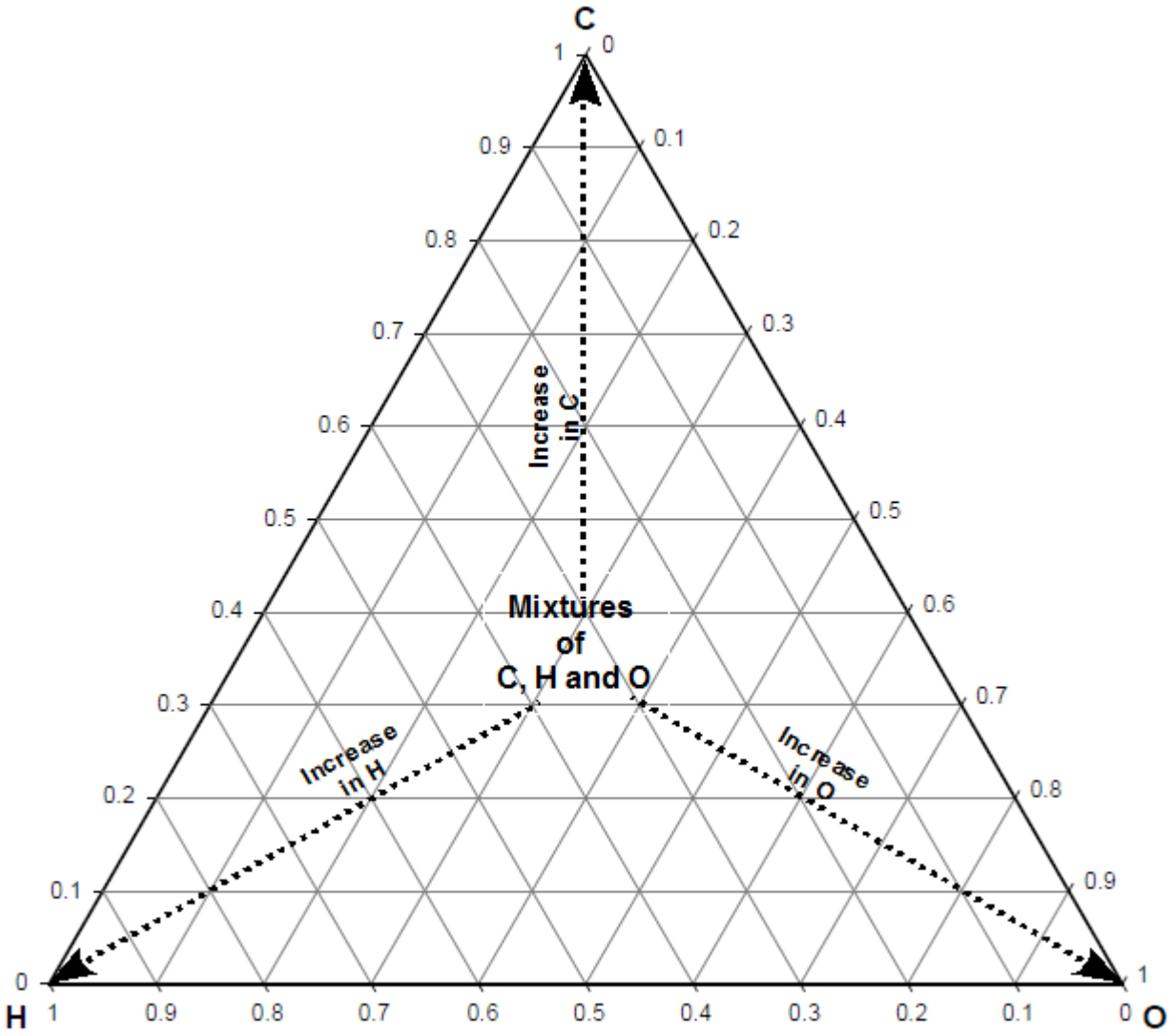

Figure 3.2. Triangular grid for representing composition in a C-H-O ternary system

There are three common ways to determine the ratios of the three atomic species (C, H and O) represented by a point on a ternary diagram. These three methods are illustrated in the following section using an arbitrary point P (Lee, 2012)

Method 1 - A line is drawn through the point P parallel to each of the sides of the triangle.

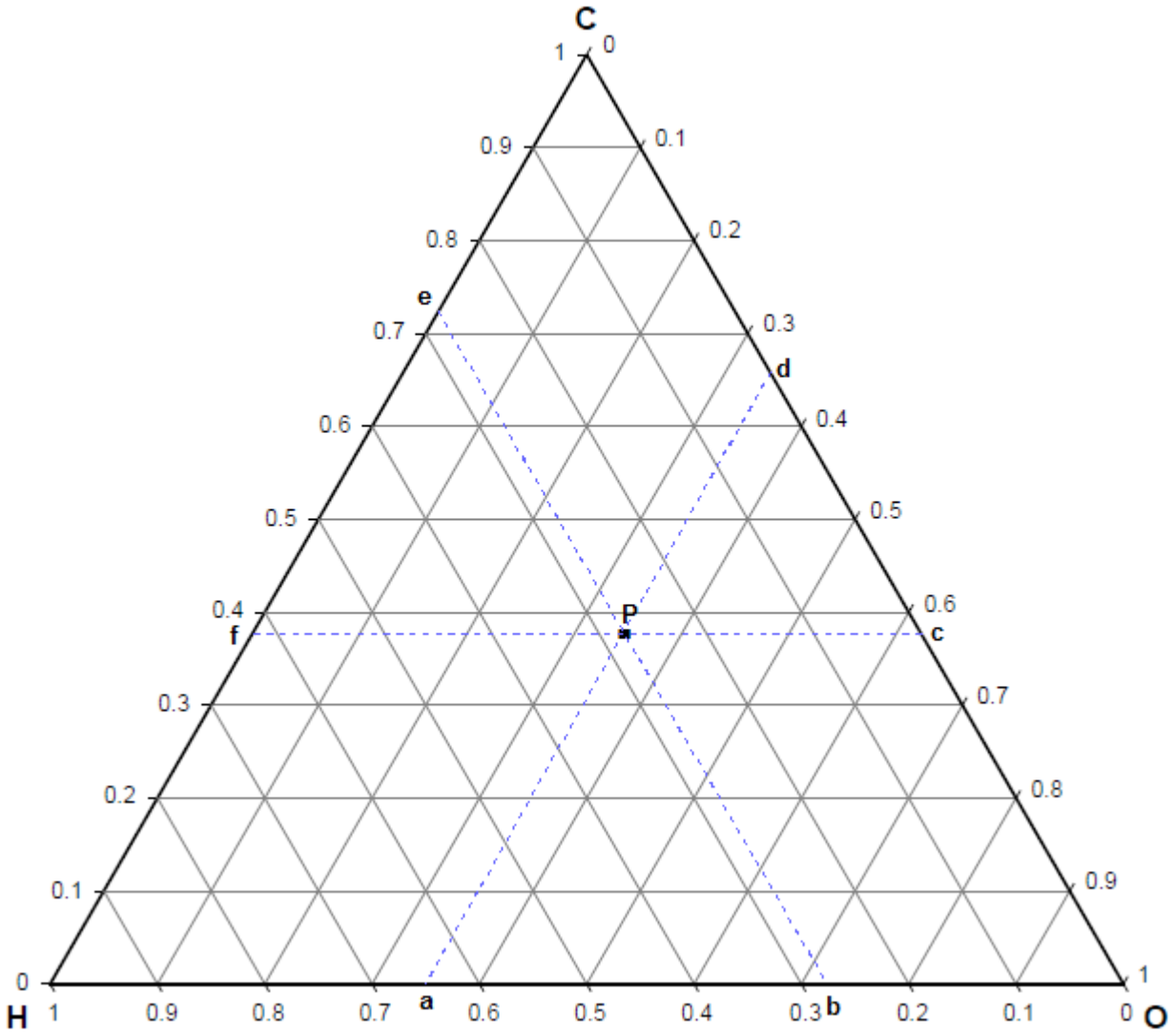

Figure 3.3. Determining the composition of a point/stream in a C-H-O ternary diagram

In this case,

$$\text{Proportion of H} = \frac{Ob}{HO} = \frac{eC}{CH}$$

$$\text{Proportion of O} = \frac{Ha}{OH} = \frac{cD}{OC}$$

$$\text{Proportion of C} = \frac{Hf}{CH} = \frac{Oc}{CO}$$

Method 2 - A line is drawn through P parallel to each side of the triangle such that each side is divided into three parts/segments.

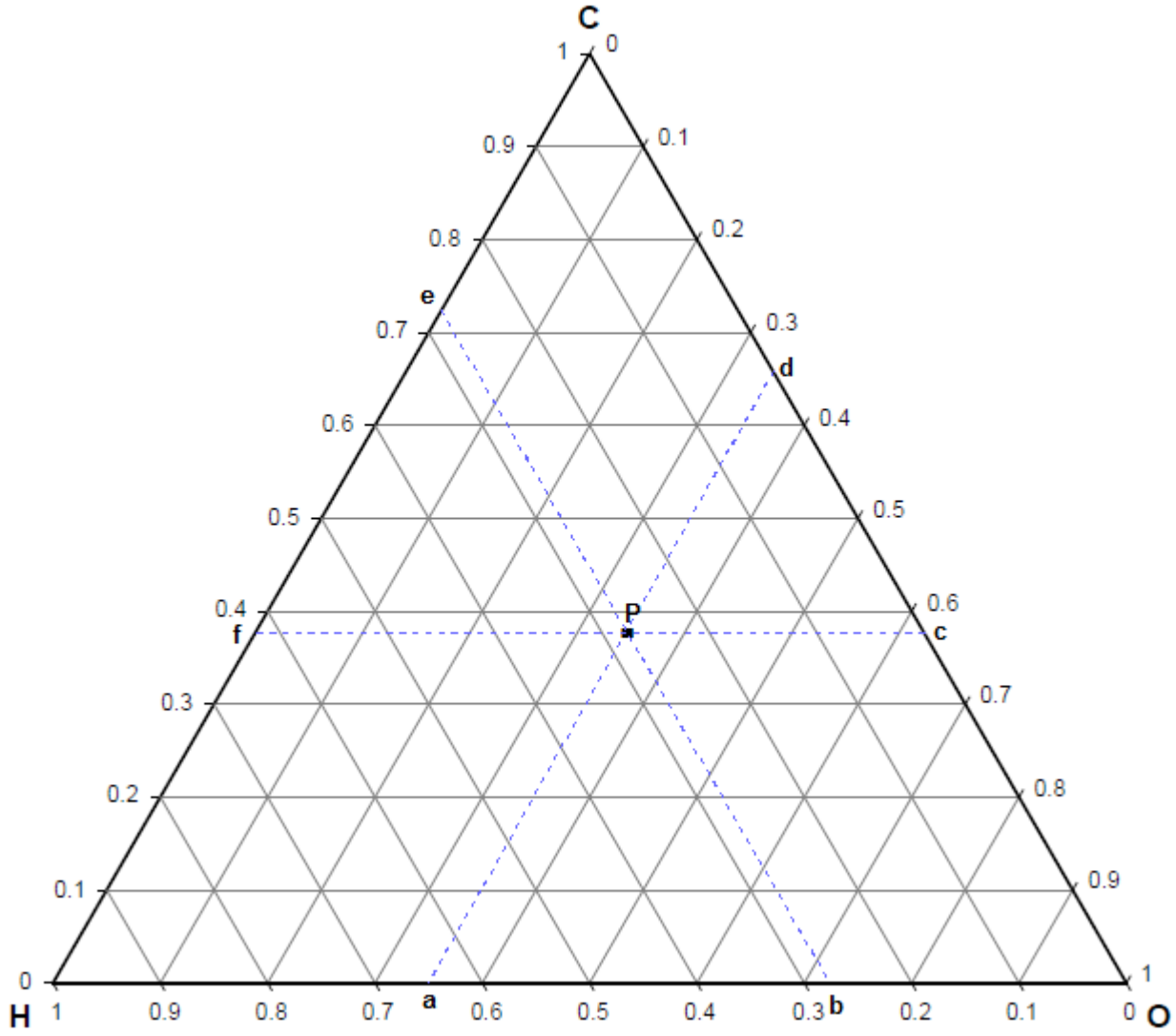

Figure 3.4. Determining the composition of a point/stream in a C-H-O ternary diagram

Considering side O-C for example, we get

$$\text{Proportion of H} = \frac{cd}{OC}$$

$$\text{Proportion O} = \frac{Cd}{OC}$$

$$\text{Proportion of C} = \frac{cO}{OC}$$

The composition of each constituent element can also be determined from the sides H-O and H-C. Since the edge is divided into three parts, the two segments at each end represent the proportions of the species at the opposite ends and the middle part represents the proportion of the third species.

Method 3 - A line is drawn through the point P from the vertices to the opposite sides of the triangle.

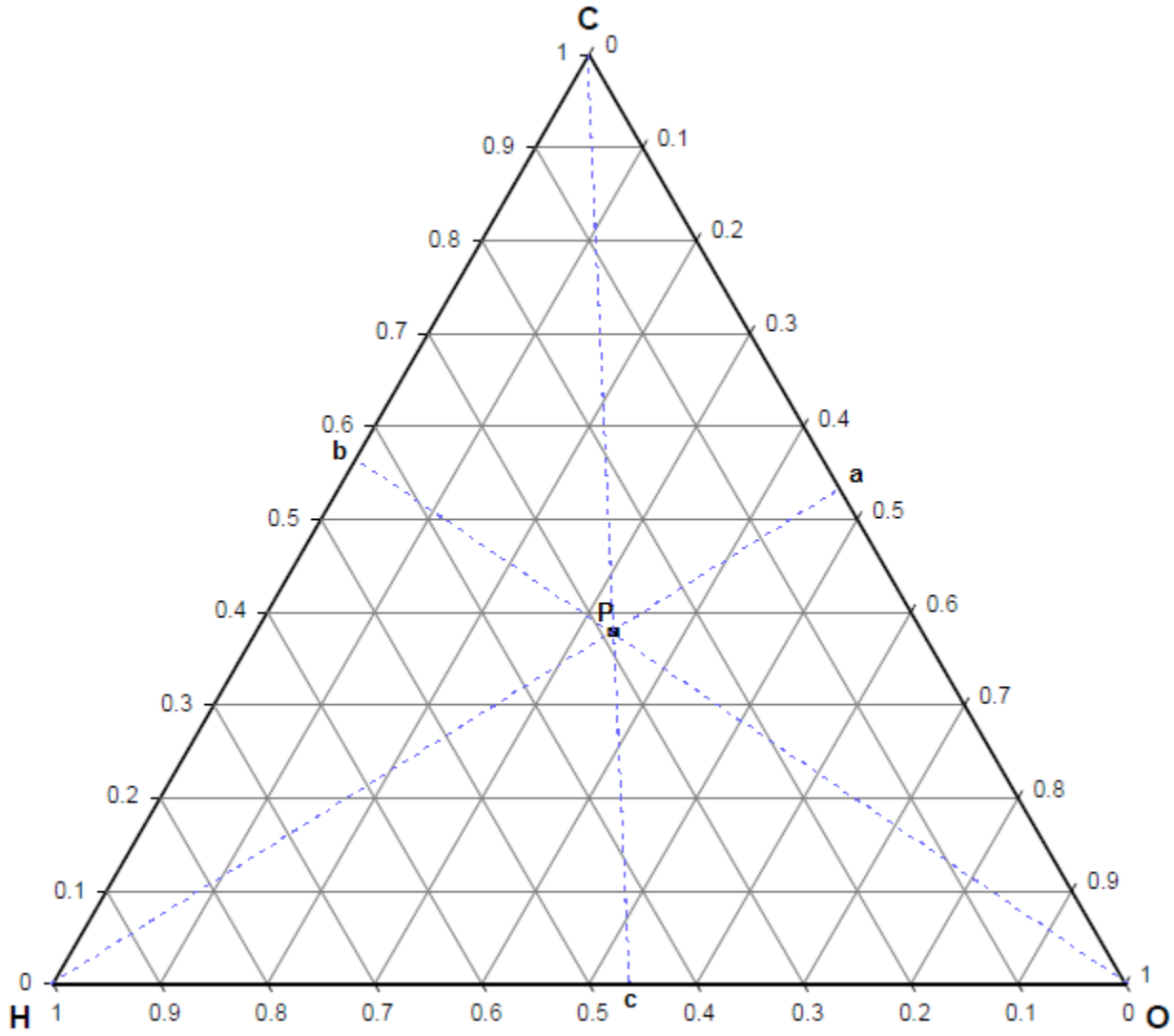

Figure 3.5. Determining the composition of a point/stream in a C-H-O ternary diagram

In this case,

$$\frac{\text{proportion of H}}{\text{proportion of O}} = \frac{\text{cO}}{\text{Hc}}$$

$$\frac{\text{proportion of O}}{\text{proportion of C}} = \frac{\text{aC}}{\text{Oa}}$$

$$\frac{\text{proportion of C}}{\text{proportion of H}} = \frac{\text{Hb}}{\text{bC}}$$

As we can see, every component in biorefineries can be represented as a unique point on the C-H-O ternary diagram based on their molar compositions. In addition, the C-H-O ternary diagram can also be applied to track chemical reaction pathways by reallocation of the products and reactants. When the lever rule is incorporated in the C-H-O ternary diagram, the material balance and process targets of the chemical reaction pathways in the biorefinery can be determined as illustrated in the following section.

3.3. MATERIAL BALANCE

Material balance basically refers to the application of the law of conservation of mass usually in the analysis and modelling of chemical processes. The law of mass conservation essentially states that the mass of an isolated system remains constant irrespective of the changes that are occurring within the system. Therefore, the material balance accounts and quantifies the flow of materials that enter and exit individual operation units and/or processes. It can be applied either to individual units, e.g. reactors, flash column, etc. or to an entire process flowsheet.

3.3.1. Material balance for synthesizing processes

In addition to its routine/typical application in analysis and modelling of processes, material balances can also be used in synthesis of processes (Patel et al., 2007). Chemical processes usually have complex flowsheets as a result of numerous reactions, unit operations, recycles, by-passes, etc. This, in turn, makes the material balance of chemical processes extremely complex as well. But, the dimensionality and complexity of such process can be overcome by atomic species balance, thereby, reducing the material balance of the entire process into “input = output” at steady state. This makes the atomic species balance a useful process synthesis tool that enables one to carry out material balance without the need to consider

every individual process unit and stream. Instead, the entire process is considered in terms of only its inputs and outputs.

To illustrate this approach, consider a biorefinery synthesis problem in which it is required to produce 200 mol/day of methanol (CH_3OH) given biomass, H_2O and CO_2 as inputs and/or outputs of the process. Based on the work by Prins et al. (2003), biomass can generally be represented with the formula $CH_{1.4}O_{0.59}N_{0.0017}$. It is assumed that N_2 acts as an inert gas and therefore does not take part in the reaction process (Tay et al., 2011). Therefore, biomass can be thought of as consisting of only C, H, and O and its formula becomes $CH_{1.4}O_{0.59}$.

Assuming production of 1 mol of CH_3OH, the overall material balance can be expressed as

$$aCH_{1.4}O_{0.59} + bH_2O + cCO_2 - CH_3OH = 0 \quad (3.1)$$

where *a*, *b* and *c* are respective amounts (in moles) of biomass, water and carbon dioxide required to produce 1 mol of methanol.

The atomic species balance for the process becomes:

$$\text{C balance: } a + c = 1 \quad (3.2i)$$
$$\text{H balance: } 1.4a + 2b = 4 \quad (3.2ii)$$
$$\text{O balance: } 0.59a + b + 2c = 1 \quad (3.2iii)$$

Therefore, the overall material balance for the process corresponds to

$$1.422CH_{1.4}O_{0.59} + 1.005H_2O - 0.422CO_2 - 1CH_3OH = 0 \quad (3.3)$$

Since all components were initially specified as input, then the negative value of *c* means that CO_2 occurs as a product in the process. The material balance can then be scaled up to determine the amounts of biomass, CO_2 and H_2O required to produce 200 mol of methanol. Based on Equation 3.3, 284.4 mol $CH_{1.4}O_{0.59}$, 201 mol H_2O are required to produce 200 mol CH_3OH and 84.4 mol CO_2. Therefore, we see from this example how material balance in terms

of atomic species can be utilized in synthesizing biorefinery processes without requiring information about the various unit operations and streams involved.

3.3.2. Material balance as a target for processes

Material balance can also be applied to set process targets (Patel et al., 2007). In this case, the material balance of a process represents the minimum amount of inputs required for the production of a specific product. When employed for setting targets for a process, material balances can also provide insights into by-products and waste that may be generated in the process. Consider for instance the production of 1 mole of methanol from methane and oxygen. The material balance can be given as follows

$$aCH_4 + bO_2 - 1CH_3OH = 0 \quad (3.4)$$

The minimum amount of methane and oxygen required for the process can be determined by applying the atom balance for each species. That is,

$$\text{C Balance: } a = 1 \quad (3.5i)$$

$$\text{H Balance: } 4a = 4 \text{ or } a = 1 \quad (3.5ii)$$

$$\text{O balance: } 2b = 1 \text{ or } b = 0.5 \quad (3.5iii)$$

Therefore, the material balance corresponds to

$$1CH_4 + 0.5O_2 - CH_3OH = 0 \quad (3.6)$$

That is, to produce 1 mole of methanol, a minimum of 1 mole of CH_4 and 0.5 mole of O_2 is required. These being the minimum quantities of each component, the material balance represents a *target* for the process.

Suppose that one fed excess oxygen, say 1 mole instead of 0.5 moles. The material balance of the process will be different as a result of the formation of by-product or waste. Water and

carbon dioxide are possible by-products/waste in this instance and the material balance can be written as follows.

$$aCH_4 + 1\ O_2 + b\ CO_2 + c\ H_2O - 1\ CH_3OH = 0 \qquad (3.7)$$

Applying the atomic species balance,

$$\text{C balance: } a + b = 1 \qquad (3.8i)$$

$$\text{H balance: } 4a + 2c = 4 \qquad (3.8ii)$$

$$\text{O balance: } 2 + 2b + c = 1 \qquad (3.8iii)$$

The resulting material balance becomes,

$$1.25CH_4 + 1\ O_2 - 0.25\ CO_2 - 0.5\ H_2O - 1\ CH_3OH = 0 \qquad (3.9)$$

It is important to note that the negative values for *b* and *c* indicates that the components occur as product because we had initially specified all the components as feed material. By feeding more oxygen than required, more CH_4 needs to be added to the process and CO_2 and H_2O get produced as undesirable by-products/waste. This results in wastage of raw materials, which implies more processing, i.e. larger equipment and more separation steps.

3.3.3. Inverse lever arm rule

One of the principles that enable the use of ternary diagrams in representing material balances of chemical processes is the inverse lever arm rule (or simply the lever rule). The inverse lever arm rule is a mathematical expression that is based on the principle of material balance or conservation of matter (Campbell, 2008). It essentially makes use of the linear relationship that exists between composition and mass (or moles) to determine relative amounts in a system (Dahm and Visco, 2013).

Consider arbitrary points A and B in a C-H-O ternary diagram, representing components of streams A and B respectively (Figure 3.6). To define each stream, only two compositions of the constituent elements (i.e. C, H and O) are required. For example, we can specify the composition of the streams in terms of only carbon and hydrogen atoms. In this case, the composition of steam A is denoted by x_{CA} and x_{HA} and the composition of stream B is denoted by x_{CB} and x_{HB}

where

x_{CA} and x_{HA} are the respective atomic ratios of carbon and hydrogen at stream A, and
x_{CB} and x_{HB} are the respective atomic ratios of carbon and hydrogen at stream B

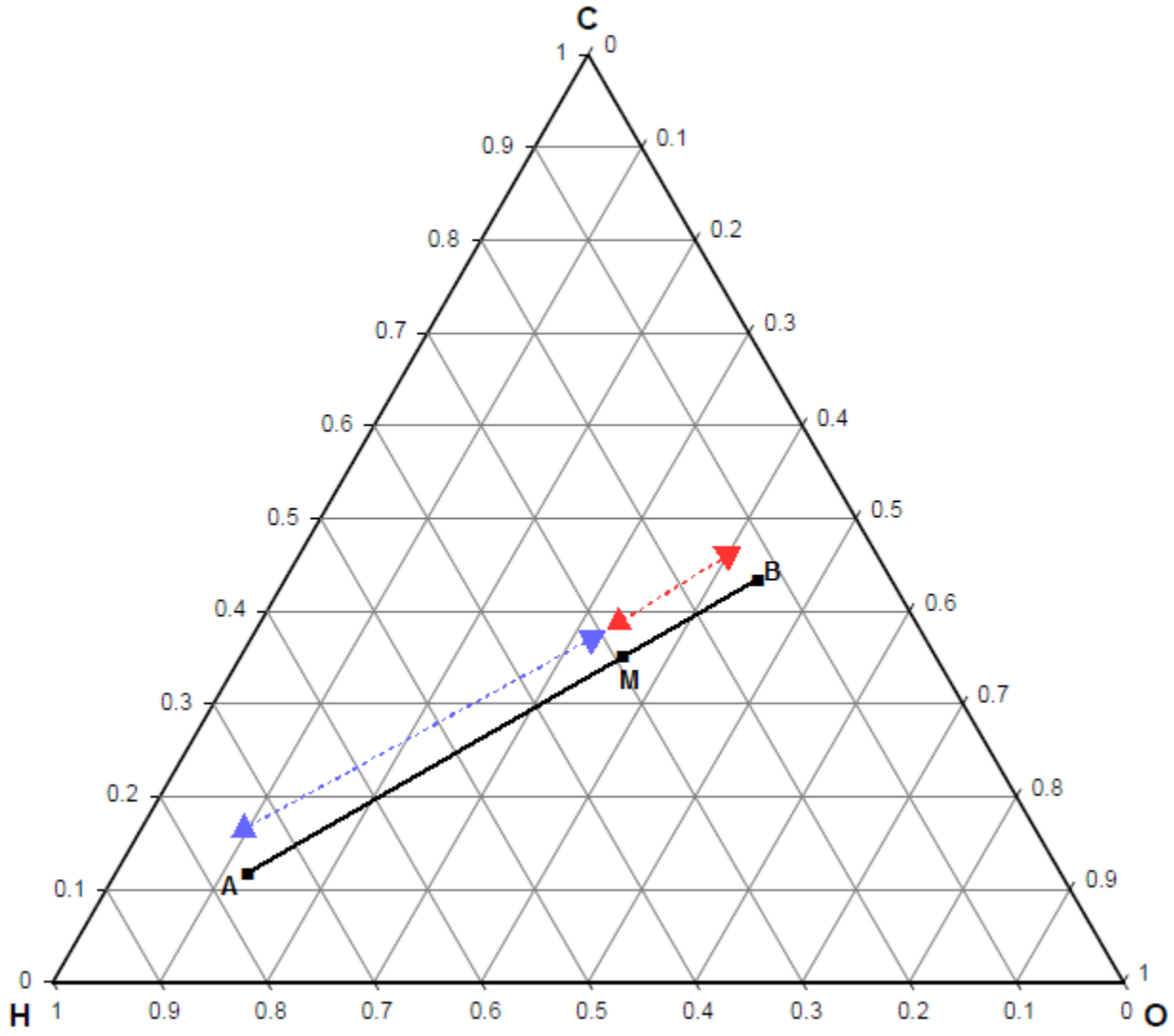

Figure 3.6. Lever arm rule and ternary mixing rule

The ternary mixing rule states that when the two streams (A and B) mix, a resultant product stream represented by point M lies on a straight line joining the two streams (Kiss, 2013). The composition of point M on the C-H-O ternary diagram is also given in terms of carbon and hydrogen atomic ratio as x_{CM} and x_{HM} respectively. The mixing process is represented graphically by joining the two points (A and B) using a straight line that passes through point M. The straight line is called the tie-line and it is used to perform the material balance for the process.

Using the geometric relationship derived from the overall molar balance and the two component balance around point M, we get

$$\text{Overall balance: } M = A + B \tag{3.10i}$$

$$\text{Carbon balance: } Mx_{CM} = Ax_{CA} + Bx_{CB} \tag{3.10ii}$$

$$\text{Hydrogen balance: } Mx_{HM} = Ax_{HA} + Bx_{HB} \tag{3.10iii}$$

Substituting Equation 3.10i into Equation 3.10ii and 3.10iii, we get

$$A(x_{CM} - x_{CA}) = B(x_{CB} - x_{CM}) \tag{3.11}$$

$$A(x_{HM} - x_{HA}) = B(x_{HB} - x_{HM}) \tag{3.12}$$

The two equations can be rearranged and solved for the ratio of A/B such that

$$\frac{A}{B} = \frac{x_{CB}-x_{CM}}{x_{CM}-x_{CA}} = \frac{x_{HB}-x_{HM}}{x_{HM}-x_{HA}} = \frac{\overline{BM}}{\overline{AM}} \tag{3.13}$$

where $\overline{BM}$ is the distance between point M and B and $\overline{AM}$ is the distance between point M and A in Figure 3.6

It can also be shown from the material balance that

$$\frac{A}{M} = \frac{x_{CM}-x_{CB}}{x_{CA}-x_{CB}} = \frac{x_{HM}-x_{HB}}{x_{HA}-x_{HB}} = \frac{\overline{BM}}{\overline{AB}} \tag{3.14}$$

$$\frac{B}{M} = \frac{x_{CM}-x_{CA}}{x_{CB}-x_{CA}} = \frac{x_{HM}-x_{HA}}{x_{HB}-x_{HA}} = \frac{\overline{AM}}{\overline{AB}} \tag{3.15}$$

As we can see, the amount of each stream is determined by taking the length of the tie line from the opposite side of M and dividing it by the total length of the tie line. For example, the fraction of B is determined by taking the length of the tie line from A to M and dividing it by the total length of the tie line. When the composition axis of the ternary diagram is scaled in

weight percent, the fraction determined from the inverse lever rule will be a mass fraction. Likewise, when the composition axis is scaled in mole percent, the fraction will be a mole fraction.

We will now illustrate the application of the lever arm rule in the C-H-O ternary diagram and the use of material balance to set process targets in a biorefinery process that involves the complete combustion of biomass. As indicated before, lignocellulosic biomass is represented using a general formula $CH_{1.4}O_{0.59}$. Considering the complete combustion of 1 mol of biomass, the material balance for the process can be expressed as

$$1CH_{1.4}O_{0.59} + a\ O_2 + b\ H_2O + c\ CO_2 = 0 \tag{3.16}$$

where *a*, *b* and *c* are the respective amounts (in moles) of oxygen, water and carbon dioxide required for combustion of 1 mol of biomass.

The atomic species balance for the process becomes

$$\text{C balance: } c = -1 \tag{3.17i}$$

$$\text{H balance: } 2b = -1.4 \tag{3.17ii}$$

$$\text{O balance: } 2a + b + 2c = -0.59 \tag{3.18}$$

Therefore, the overall material balance for the combustion process corresponds to

$$1CH_{1.4}O_{0.59} + 1.055O_2 - 0.7H_2O - 1CO_2 = 0 \tag{3.19}$$

From the material balance, the complete combustion of 1 mol of biomass requires a minimum of 1.055 mol of O_2. In this process, a minimum of 0.7 mol H_2O and 1 mol CO_2 are also produced. The material balance of the process can also be written as

$$CH_{1.4}O_{0.59} + 1.055O_2 \Longrightarrow CO_2 + 0.7\ H_2O \tag{3.20}$$

To depict the process in the C-H-O ternary diagram, we first need to determine the molar ratios of C, H and O for every component involved in the process. The molar ratio of carbon, hydrogen and oxygen in the lignocellulosic biomass feedstock is calculated as 0.333, 0.468, and 0.197 respectively (See Appendix A). The molar ratios are also calculated in the same manner for CO_2 and H_2O, with C/O = 0.33 and H/O = 0.67 respectively. The oxidant (O_2) is assumed to be pure and therefore has molar ratio of 1. These compounds are plotted on a C-H-O ternary diagram according to the methods discussed earlier in Figure 3.7.

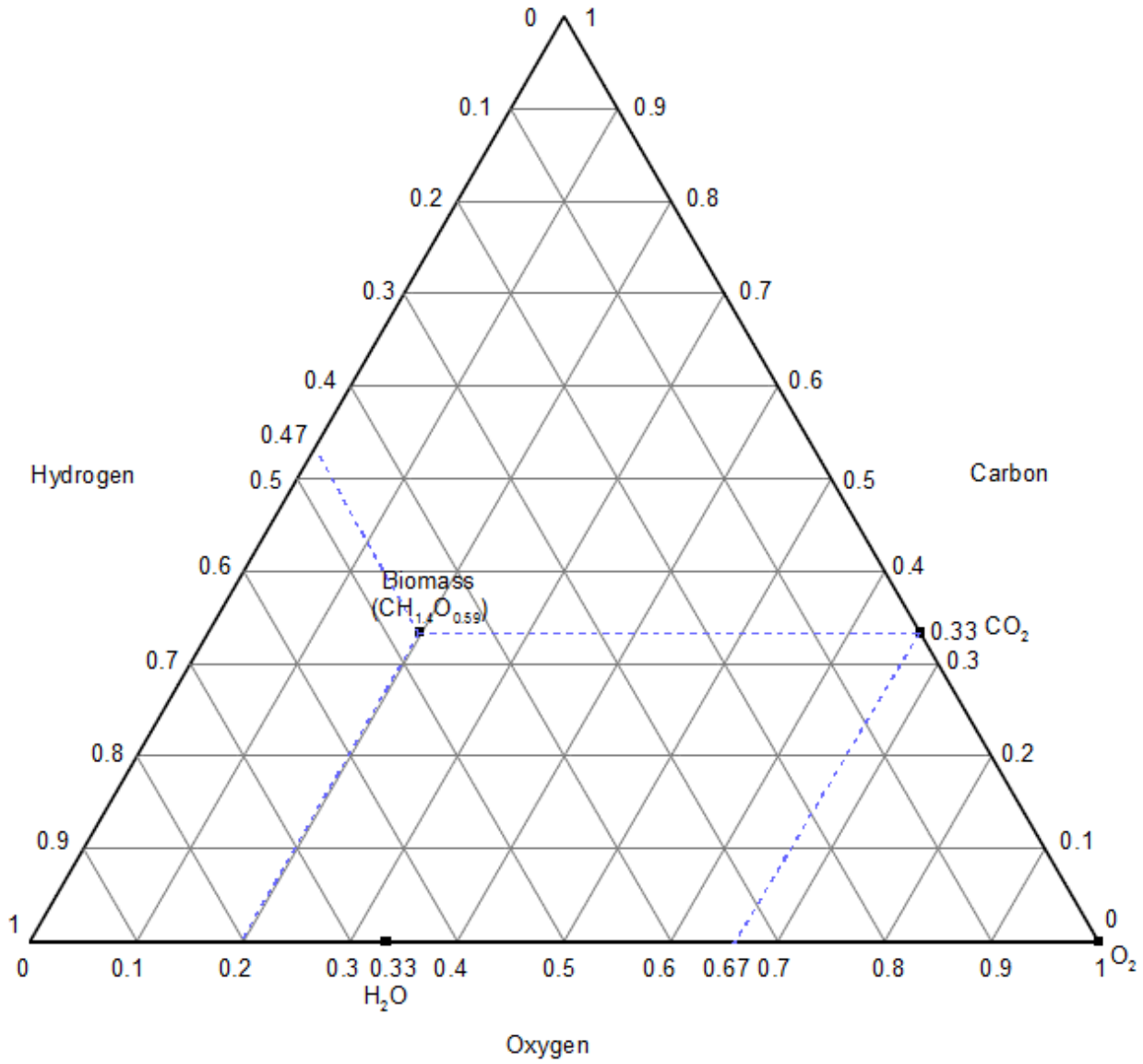

Figure 3.7. Representation of biorefinery compounds on a C-H-O ternary diagram

After plotting the points, the above material balance is represented on the C-H-O ternary diagram by first joining the reactants (i.e. biomass and O_2) with a straight line called a reactant line. Another line called the product line connects the product, CO_2 and H_2O. The two lines, namely the product and reactant lines cross one another at a point that Tay et al. (2011) refers to as the equilibrium point (Point M). Point M is unique in that it designates the stage where the equilibrium state of the mixture of products and reactants is achieved. For a complete conversion of the biomass, the equilibrium point (Point M) will only consist of the products (i.e. CO_2 and H_2O) in stoichiometric proportions. Figure 3.8 depicts the combustion reaction pathway on a C-H-O ternary diagram.

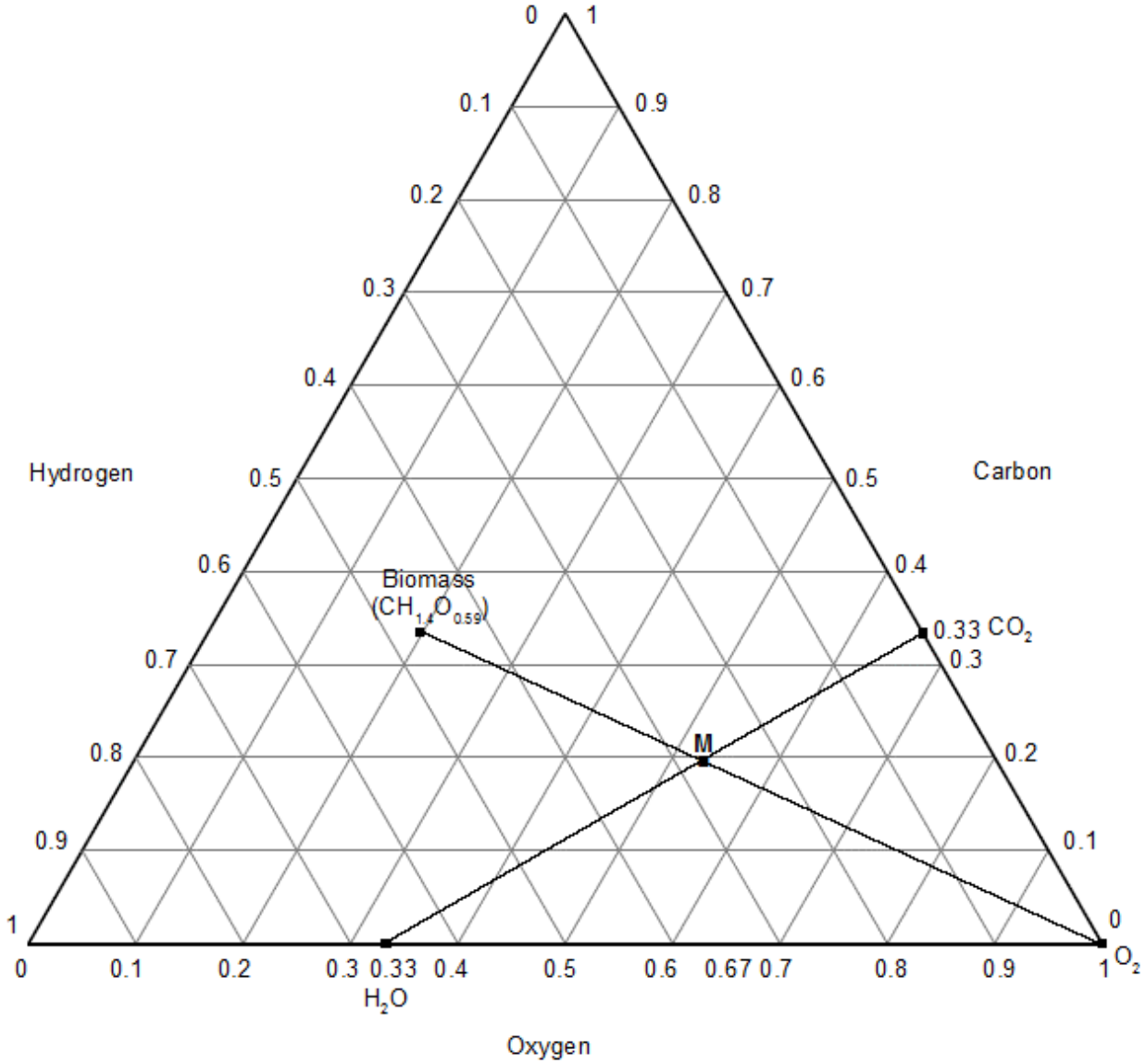

Figure 3.8. Representation of biomass combustion process on a C-H-O ternary diagram

The next step is to determine the amount of the gas phase and eventually the stoichiometric coefficients for the reaction. This is achieved using the inverse lever arm rule. First, the total lengths as well as the segments of the total length with respect to the mixture point M are measured for both the reactant and product line using an Acrobat reader DC measuring tool. The Acrobat reader DC measuring tool does not require calibration since the measurements will be expressed as relative distances/lengths. The measurements for the reactant and product lines are shown in Figures 3.9 and 3.10 respectively.

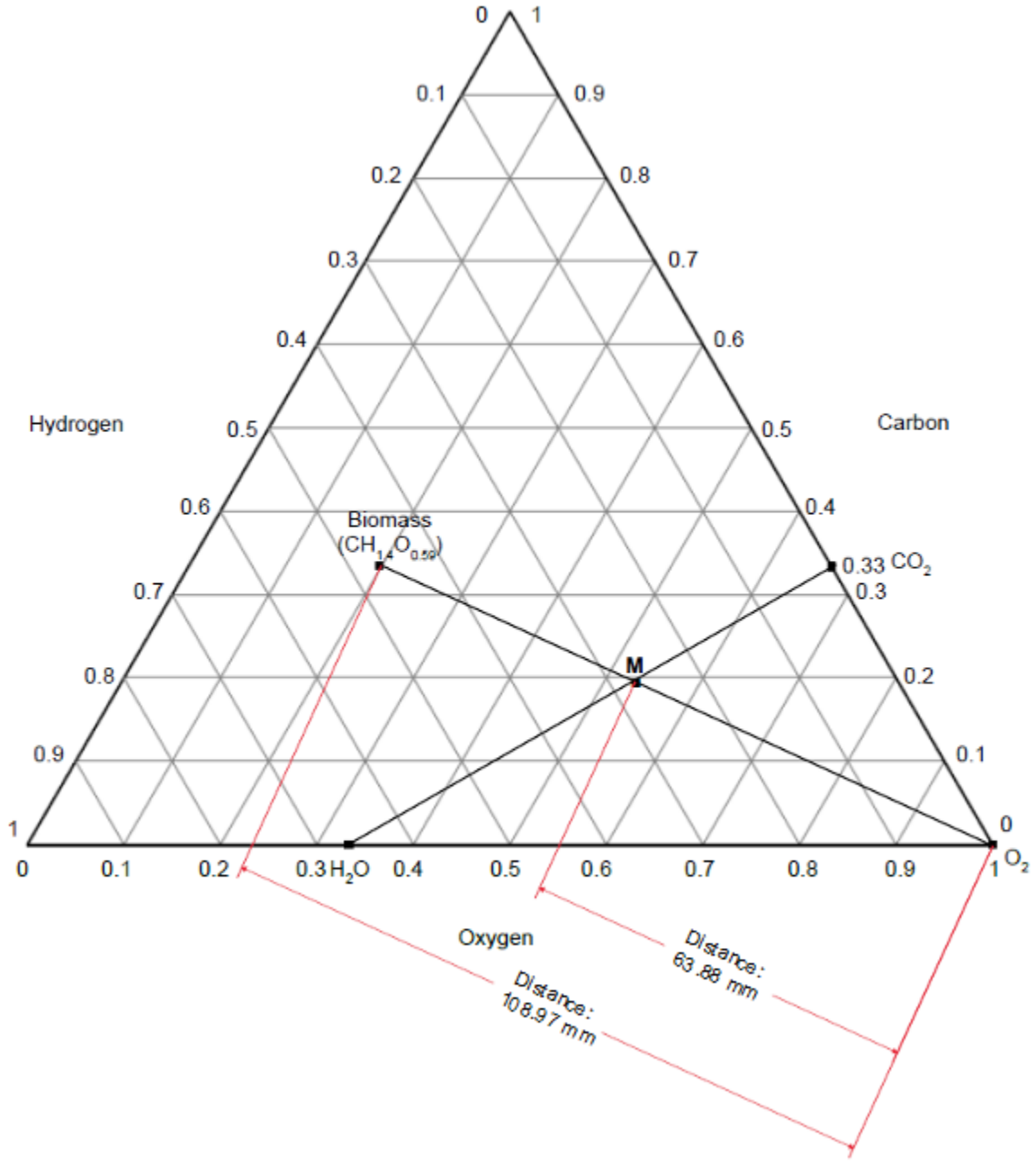

Figure 3.9. Distance measurement of reactant line

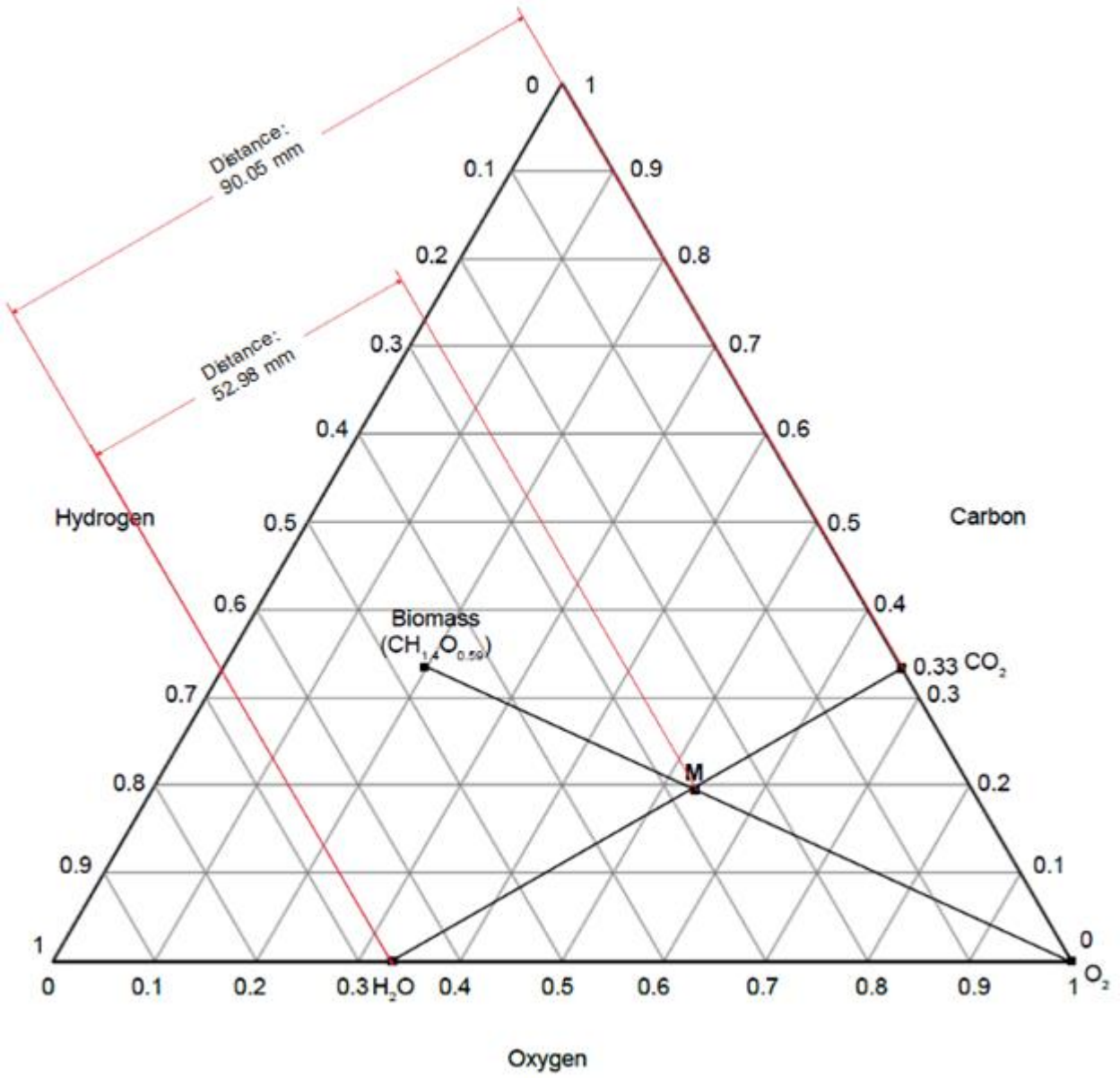

Figure 3.10. Distance measurement of product line

The measurements of both the reactant and product lines are expressed as relative distance with respect to point M. That is, the segment of the total distance from one end to point M is divided by the total length. This gives the relative distance of the lever with respect to point M. The distance between point M and the opposite segments of the lines is calculated by subtracting the previously determined segment from one. The relative distances (lever arms) of biomass and oxygen on the reactant line are $D_{BIO} = 0.586$ and $D_{O2} = 0.414$. Similarly, the

lever arms of H_2O and CO_2 on the product line are D_{H_2O}= 0.588 and D_{CO_2}= 0.412. The calculations for the relative distance are shown in Appendix A. Figure 3.11 shows the representation of the material balance of the combustion process using the inverse lever rule on the C-H-O ternary diagram.

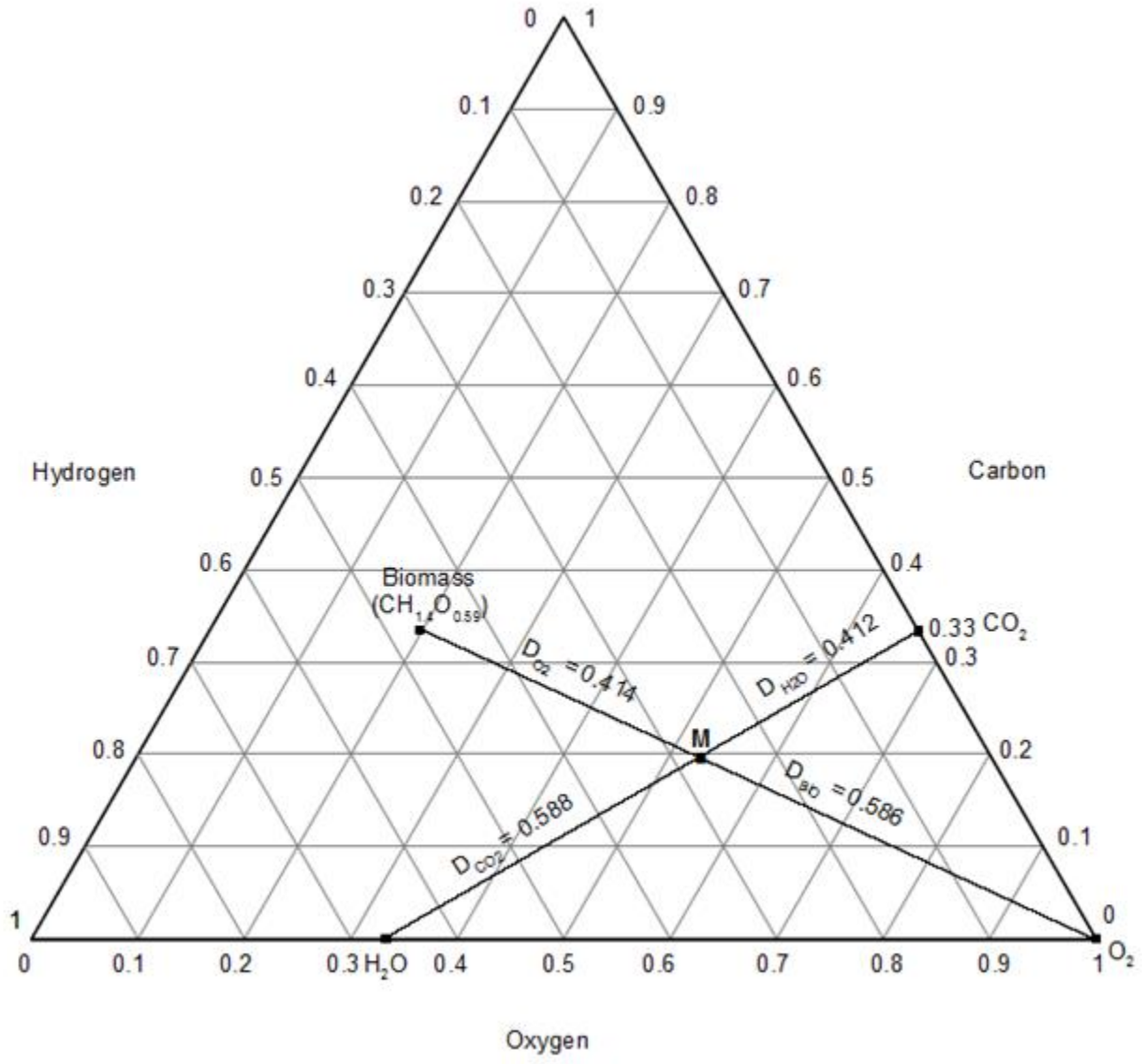

Figure 3.11. Complete representation of material balance for the biomass combustion process using the lever rule

Since molar fractions of the constituent atoms are plotted on the C-H-O ternary diagram, the lever arms in the diagram do not reflect the stoichiometry of the reaction directly. So, in order to account for the stoichiometric coefficients of the reactants and products, the atomic number in the reactant and product molecules has to be considered. An equation for determining the stoichiometric coefficients of the process by accounting for the ratios of different atoms involved is given by Tay et al. (2011) as

$$\frac{\text{Length, } D_{CH}}{\text{Total length between reactant or product}} = \frac{(\text{Stoichiometric coefficient, SC}) \times (\text{Number of atoms in CH})}{\text{Total number of atoms for all reactants or products}} \tag{3.21}$$

where

CH denotes a compound under consideration in the product or reactant stream, and

SC is the stoichiometric coefficient

Equation 3.21, in conjunction with the inverse lever arm rule can be applied to determine the stoichiometric coefficients for the complete oxidation of one mole of biomass into products (H_2O and CO_2). By solving Equation 3.21, the stoichiometric coefficients for O_2, CO_2 and H_2O are determined to be 1.055, 1.0 and 0.7 respectively (Appendix A). Incidentally, the values which are determined from the C-H-O ternary diagram by using the inverse lever arm rule are identical to those obtained from the material balance of the combustion process as given by Equation 3.20. These methods are explored further in Chapter 4 where they are applied for the conceptual design of an integrated biorefinery.

3.4. THERMODYNAMIC EQUILIBRIUM OF C-H-O SYSTEMS

In the previous section, we looked at how process targets and limits imposed by the material balance of the process could be applied in the synthesis of biorefinery processes. The equilibrium state of processes also sets thermodynamic limits to the performance of processes. This implies that we can also use chemical equilibrium of systems in the design, evaluation as well as improvement of biorefineries processes (Li et al., 2001). Even though

chemical equilibrium is seldom attained in processes, it does however provide an indication of important benchmarks and insights which can be helpful for chemical engineers during the conceptual design of processes. That is, by determining the equilibrium state of a process, theoretical performance limits or targets of the process are also determined.

This study focuses on biorefineries which are based on the syngas platform. Therefore, we will look at the calculations of equilibrium composition for the C-H-O system. The calculation of the chemical equilibrium of the C-H-O system allows us to represent the biomass gasification process and can be used to determine the limits on the production and composition of bio-syngas. Thermodynamic equilibria also provide valuable insights into the theoretical limits of the desired syngas platform when biomass is gasified under a given set of conditions (Gunawardena and Fernando, 2014). A quick estimation of the equilibrium composition of the gas-phase in the biomass gasification process can be made under a variety of reaction conditions. This way, process parameters that would result in optimum conversion of the biomass feedstock into syngas can be determined.

In the following section, we introduce some of the thermodynamic principles and considerations we will use in analysing and calculating chemical equilibria for the C-H-O system.

3.4.1. Gibbs energy and equilibrium

The Gibbs energy is the thermodynamic potential of a reaction and it is minimized when a reaction reaches equilibrium. Thus, the Gibbs energy change of a process, ΔG, can be considered as a measure of its net 'driving force" (Smallman and Bishop, 2006). A negative value of ΔG represents a finite driving force for the process in the forward direction, whereas a positive value represents a driving force in the reverse direction. When $\Delta G = 0$, the forward and reverse driving forces are equal, and thus the process occurs in both directions at the same rate. This is indicative of a system at equilibrium.

For a process that occurs with reactants and products at nonstandard conditions, the change in the Gibbs energy, ΔG, is related to the standard Gibbs energy change (ΔG^o) by

$$\Delta G = \Delta G^o + RT\ln Q \qquad (3.22)$$

Where,

R is the gas constant (8.314 J/K·mol)

T is absolute temperature, and

Q is the reaction quotient

For a system at equilibrium, $\Delta G = 0$ and $K = Q$ and Equation 3.22 becomes

$$0 = \Delta G^o + RT\ln K \text{ or } K = \exp\left(-\frac{\Delta G^o}{RT}\right) \quad \text{(at equilibrium)} \qquad (3.23)$$

This equation offers a useful relationship for deriving equilibrium constant from the standard Gibbs energy change and vice versa. Table 3.1 gives a summary of the relationship between the two thermodynamic properties.

Table 3.1. Relations between Standard Gibbs Energy Changes and Equilibrium Constants

K	$\Delta G°$	Comments
> 1	< 0	Products are more abundant at equilibrium.
< 1	> 0	Reactants are more abundant at equilibrium.
= 1	= 0	Reactants and products are equally abundant at equilibrium.

In the same manner that the magnitude of ΔG provides us with valuable information regarding a process, the size of the equilibrium constant value can enable us to make certain judgments about the extent of the chemical reaction. Generally, a small value of the equilibrium constant means that the reaction will not proceed to any appreciable degree and will predominantly be

reactants at equilibrium. A reaction with an equilibrium constant value less than 0.001 is assumed not to occur at all (Natarajan, 2014). On the other hand, reactions with numerical values of K larger than 1 have more products than reactants. While an equilibrium constant value greater than 1000 is generally assumed to proceed to completion (*ibid.*).

Equation 3.23 provides the temperature effect on the equilibrium constant. Baron et al. (1976) expresses Equation 3.23 at non-standard conditions in terms of Gibbs energy polynomial function as

$$-\frac{\Delta G}{RT} = \ln K_i = b_1 T^{-1} + b_2 \ln T + b_3 T + b_4 T^2 + b_5 T^3 \qquad (3.24)$$

where K_i is the thermodynamic equilibrium constant for the formation reaction of the given component at temperature T (K).

The values for the coefficients in the Gibbs energy expression for components of interest in this study are given in Table 3.2

Table 3.2. Coefficients used in the Gibbs energy expression

Component	b_1	b_2	b_3 ($\times 10^{-3}$)	b_4 ($\times 10^{-9}$)	b_5 ($\times 10^{-10}$)
H_2	0	0	0	0	0
H_2O	28 780	-0.69477	-1.4283	0.74925	-1.3785
CH_4	8 372.2	-1.0769	-5.6435	2.9046	-5.2351
CO	13 612	1.8317	-2.7584	0.6536	-0.78772
CO_2	47 280	0.1322	-0.94025	0.45112	-0.91901
N_2	0	0	0	0	0
O_2	0	0	0	0	0
C	0	0	0	0	0

When equilibrium constant is expressed in terms of activity (fugacity), it is given as

$$K = \prod_j a_j^{v_j} \tag{3.25}$$

where a_j is the activity and v_j is the stoichiometric coefficient.

The fugacity and activity of a component j are related by

$$a_j = \frac{f_j}{f_j^o} \tag{3.26}$$

with f_j being the fugacity of component j, and

f_j^o the fugacity of component j in the standard state (i.e. at 1 atm.)

For an ideal gas mixture, the fugacity of a component is equal to the partial pressure of the component. Thus,

$$f_j = P_j = x_j P \tag{3.27}$$

where x_j is the mole fraction and P_j and P are partial pressure and system pressure respectively.

Thus, Equation 3.26 becomes

$$a_j = \frac{P_j}{1\ \text{atm}} = \frac{x_j P}{1\ \text{atm}} \tag{3.28}$$

Therefore, for a generalized reaction

$$\alpha A + bB \rightleftharpoons cC + dD$$

the equilibrium constant is given from Equation 3.25 as

$$K = a_A^{-\alpha} a_B^{-b} a_C^c a_D^d = \frac{a_C^c a_D^d}{a_A^\alpha a_B^b} \tag{3.29}$$

Considering an ideal gas mixture situation,

$$K_f = \frac{\left(\frac{x_C P}{1\ \text{atm}}\right)^c \left(\frac{x_D P}{1\ \text{atm}}\right)^d}{\left(\frac{x_A P}{1\ \text{atm}}\right)^\alpha \left(\frac{x_B P}{1\ \text{atm}}\right)^b} = \frac{(x_C)^c (x_D)^d}{(x_A)^\alpha (x_B)^b} \tag{3.30}$$

The value of the equilibrium constant is calculated by using the standard Gibbs energy of formation data based on the thermodynamic relation as follows

$$K_{eqm} = \exp\left(\sum_{y=1}^{q} v_y \ln k_{prod} - \sum_{z=1}^{r} v_z \ln k_{reac}\right) \quad (3.31)$$

where

K_{eqm} is the equilibrium constant for the specific reaction,

v_z and v_y are stoichiometric coefficients for reactants and products respectively, while k_{prod} and k_{reac} denote the thermodynamic equilibrium constants for the formation reactions of product and reactant molecular specie, in the system.

3.4.2. The Gibbs phase rule

The Gibbs phase rule offers a theoretical basis that uses thermodynamics to characterize the chemical equilibrium state of a system (Weinhold, 2009). It is therefore one of most important principles for understanding chemical systems at equilibrium. It gives the number of intensive variables (e.g. parameters such as temperature, total pressure and chemical composition) that needs to be specified in order to define the condition of system at equilibrium (Ball and Baer, 2015). For a non-reactive multi-component heterogeneous system at equilibrium, the phase rule is expressed as

$$F = 2 - \pi + C \quad (3.32)$$

where

F is the number of degrees of freedom (variance),

π is the number of phases, and

C is the number of components

In the case of reactive systems, Equation 3.32 is modified slightly and it is expressed as

$$F = 2 - \pi + N - r \quad (3.33)$$

where N is number of chemicals species and

r is the number of independent reactions.

From Equations 3.32 and 3.33, it can be seen that the relationship between the number of components (C) and the number of species (N) is given as (Denbigh, 1981)

$$C = N - r \tag{3.34}$$

We will apply the Gibbs phase rule in section 3.5 when we perform the thermodynamic analysis of the biomass gasification process for the calculation of chemical equilibria.

3.4.3. Carbon deposition boundaries

Many industrial processes are faced with the challenge of undesirable formation of solid carbon deposition (coking, fouling, soot formation, etc.) (Jaworski et al., 2016). An important question for chemical engineers related to chemical equilibrium compositions is, "under what conditions will solid carbon form"? Answering this question enables engineers to design processes clear of those conditions.

Carbon deposition boundaries present a simple and insightful method to predict whether or not solid carbon will form in a given system. For a C-H-O system with a gas-phase composition in equilibrium with carbon, carbon deposition boundaries are prepared by converting the equilibrium compositions of the gaseous components to atom percentages of constituent elements and plotting them on a ternary diagram for different O/H ratios at a specific value of pressure and temperature (Mohnot and Kyle, 1978).

Figure 3.12 explains how solid carbon formation can be evaluated in C-H-O ternary diagrams using carbon deposition boundaries. Consider a carbon deposition boundary drawn for an arbitrary temperature and pressure shown in Figure 3.12. For a specific temperature, pressure and H/O ratio, any point on the diagram that lies above the deposition boundary signifies the presence of solid carbon deposits. Conversely, if a system point is located below the deposition boundary line, there is no solid carbon deposited. Taking for example point W

in Figure 3.12, it lies above the carbon deposition boundary and therefore the system has solid carbon at equilibrium with the gas-phase composition corresponding to point X. The relative amount of the gas phase atoms and the solid carbon can then be determined using the lever arm rule.

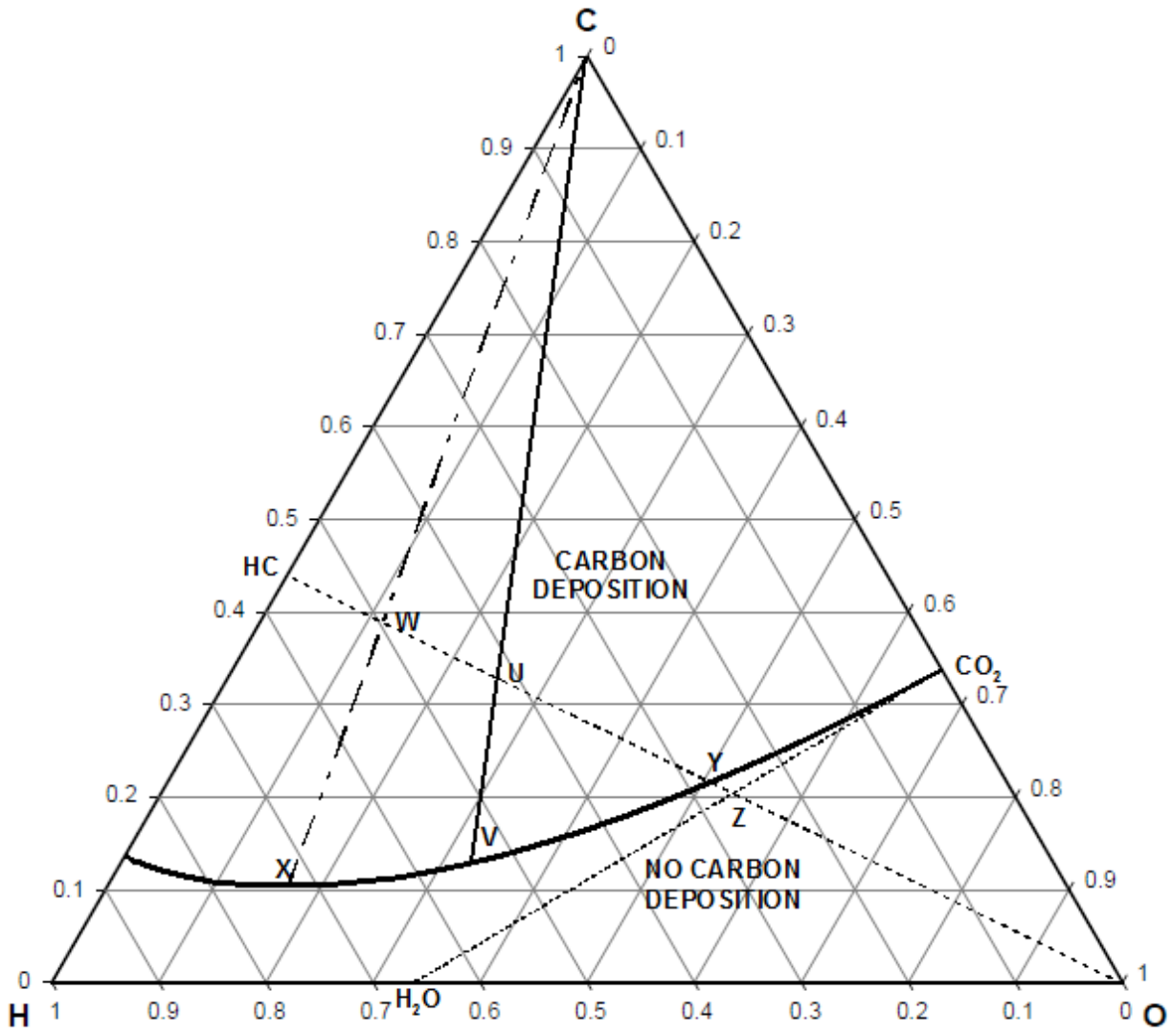

Figure 3.12. C-H-O system carbon deposition boundary

C-H-O ternary plots with carbon deposition boundaries can also provide additional information regarding process reactions. For any carbonaceous system, the effect of varying either oxygen or hydrogen can be determined using such C-H-O ternary diagrams with carbon deposition

boundaries. Consider the oxidation of a hydrocarbon with a composition represented arbitrarily by point HC in Figure 3.12. We can see that the composition of the overall reaction mixture shifts from HC towards O in proportion to the amount of oxygen or air added. At point U, the system has solid carbon in equilibrium with the gas-phase composition of carbon, hydrogen and oxygen given by point V. On the other hand, the minimum amount of the oxidant that can be supplied without the risk of forming carbon at equilibrium is represented by point Y. Point Z represents the condition where complete combustion or oxidation takes place when only H_2O and CO_2 are present at equilibrium.

3.5. CALCULATION OF CHEMICAL EQUILIBRIA FOR BIOMASS GASIFICATION

Now that we have looked at some principles pertaining to chemical equilibria, we employ these thermodynamic principles in analysing and calculating the chemical equilibrium for the C-H-O system that represents biomass gasification. The method we develop considers the basic gasification system that involves the gas-phase composition in the presence of solid carbon at 1 atm. and 800, 900, 1000, 1200 and 1500 K. The process of computing equilibrium composition of chemical systems involves an interplay of thermodynamic principles and numerical analysis (Zeleznik and Gordon, 1968). The general approach in calculating chemical equilibria is delineated in four key steps (Kyle, 1984).

- Determine the chemical species that exist in significant amounts at equilibrium
- Apply the phase rule
- Formulate the problem mathematically
- Obtain a mathematical solution for the problem

This approach is adopted to systematically analyze and calculate equilibrium gas composition of the C-H-O system that will be used to represent the biomass gasification process.

3.5.1. Determination of chemical species

Two important thermodynamic properties, namely the Gibbs energy change as well as the equilibrium constant are used to determine the species present at equilibrium in the system. However, this study will use only the Gibbs energy change for the equilibrium analysis of chemical species. The change in the Gibbs energy of formation (ΔG^f) for the species that can be formed from C, H and O are listed in Table 3.3 for the temperatures under consideration (800, 900 and 1000, 1200 and 1500 K) in the study.

Table 3.3. Gibbs energy change of formation for species in the C-H-O system (Stull et al., 1987)

Species	ΔG^f (kcal/gmol)				
	800 K	900 K	1000 K	1200 K	1500 K
CO_2	-94.54	-94.58	-94.61	-94.66	-94.72
CO	-43.68	-45.82	-47.95	-52.04	-58.23
H_2O	-48.65	-47.36	-46.04	-43.36	-39.29
CH_4	-0.56	1.99	4.58	9.90	17.86
C (solid, graphite)	0.00	0.00	0.00	0.00	0.00
H_2	0.00	0.00	0.00	0.00	0.00
CH_3OH	-21.10	-17.3	-13.46	-	-
C_2H_4	24.49	26.35	28.25	-	-
C_2H_2	43.18	41.88	40.61	-	-
C_2H_6	15.91	21.00	26.13	-	-

Chemical species that have more negative change in Gibbs energy (ΔG^f) are thermodynamically possible (i.e. spontaneous) and therefore will be predominant at

equilibrium. It is important to note however that the spontaneity or thermodynamic possibility of a chemical reaction is not related to its kinetics, hence it is possible to have a negative ΔG^f for a species formation reaction, but the reaction happens so slowly that it can be excluded in the species selection. Species whose formation reactions have a positive ΔG^f are non-spontaneous and therefore their formation is not thermodynamically possible.

Based on Table 3.3, ΔG^f for H_2O and CO_2 are extremely negative, therefore these species will be present in significant quantities. Because of the extremely negative ΔG^f for H_2O and CO_2, species with positive ΔG^f (e.g. ethane (C_2H_6), acetylene (C_2H_2), and ethylene (C_2H_4)) are considered as trace component in the system. The ΔG^f for the formation of C (graphite) and H_2 is zero at all temperatures, indicating that their formation reactions are at equilibrium at all temperatures. Their products and reactants exist in equal amounts at all temperatures. The behavior of the gas phase of the system at equilibrium can be visualized using composition regions in a C-H-O ternary diagram as shown in Figure 3.13.

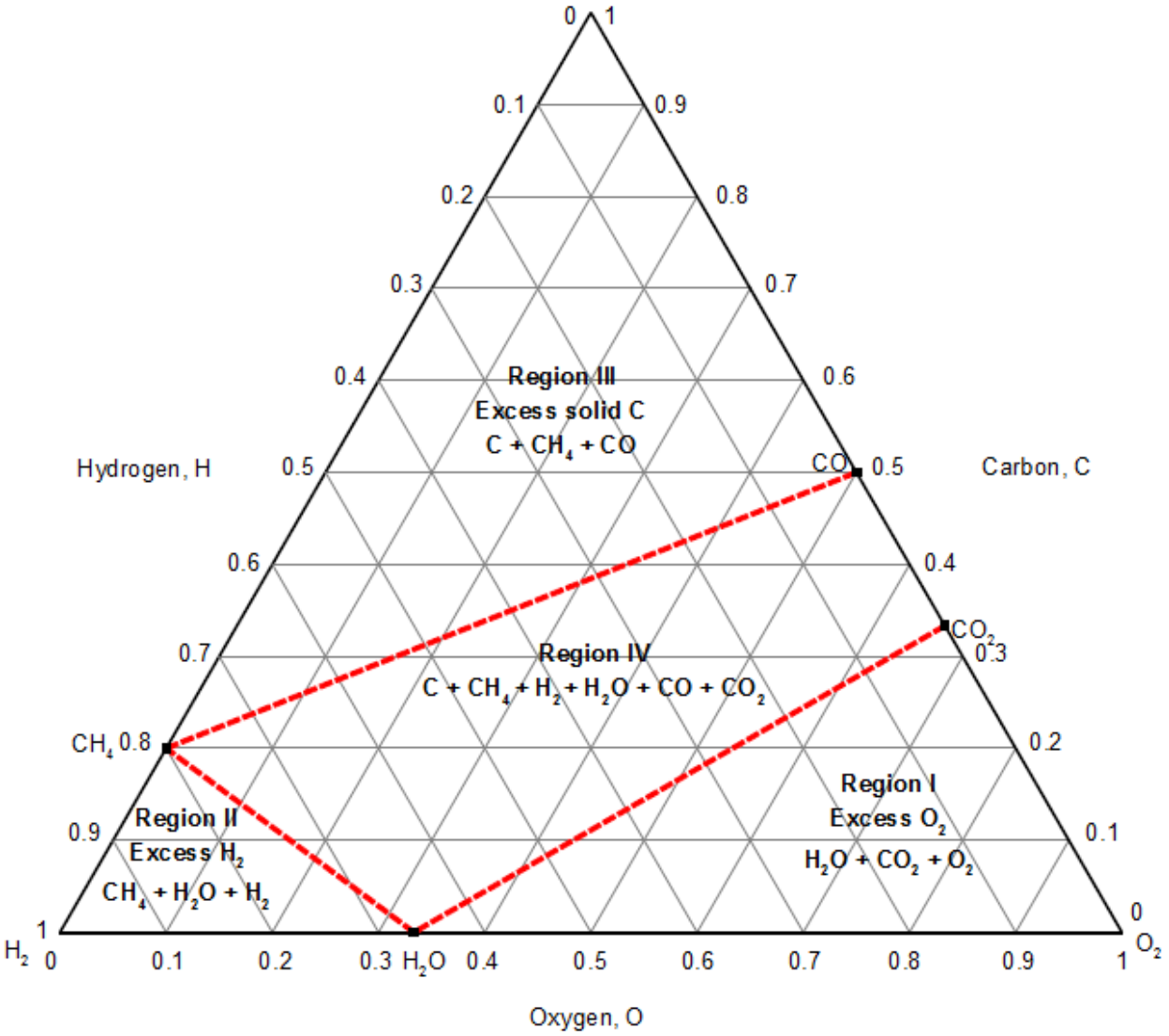

Figure 3.13. Regions of a C-H-O diagram (Kyle, 1984)

The C-H-O ternary diagram is scaled in atom percent and the overall atomic composition of the system can be represented by means of points on the diagram. Figure 3.13 shows points that represent the abundant species, i.e. CO, CO_2, H_2O and CH_4 as reflected by the Gibbs energy change of formation reactions in Table 3.3. Three regions labeled I, II, and III denote areas where oxygen, hydrogen and carbon are respectively present in excess. Region I, where there is excess oxygen, hydrogen and carbon will exist as H_2O and CO_2 respectively. Therefore, these species will be present almost exclusively because of their extremely negative ΔG^f values. Region II where hydrogen is in excess, oxygen is expected to exist as H_2O whereas

carbon exists as CH_4. In the same way, with carbon in excess (i.e. Region III), it is expected that hydrogen will exist as CH_4 whereas oxygen will exist as CO and thus, CH_4 and CO will be predominant.

Points in region IV however present a challenge since at this region, CO, C(s), CO_2, H_2O, CH_4, O_2 and H_2 could potentially exist as major species at equilibrium. Due to the extremely negative change in the Gibbs energy for the formation of H_2O and CO_2, the partial pressure of O_2 in this region becomes extremely small comparatively and therefore it does not need to be considered. The small quantity of oxygen in turn causes the amounts of other organic compounds that contain oxygen to be relatively low as well, methanol being the case in point. This is despite the fact that it has a negative ΔG^f and its formation appears favorable under thermodynamics perspective.

Therefore, from Table 3.3, the species that are considered to be important at equilibrium are CO, C(s), CO_2, H_2, H_2O and CH_4. That is, the number of chemical species (N) in the C-H-O system according to Equation 3.33 equals 6 (N = 6).

3.5.2. Applying the phase rule

We have seen that the phase rule allows us to determine the number of degrees of freedom, which are the number of independent variables the must be arbitrarily fixed to establish the intensive state of the system (Narayanan, 2013). Through the phase rule, we can predict what will happen to the system elements when they are subjected to changes in the variables that can be manipulated (i.e. temperature and pressure). For example, what happens to the composition of a certain species (e.g. CH_4) when temperature in the system increases? As shown in section 3.4.2, in order to determine the degree of freedom from the phase rule, we first need to determine the number of species (C) and the number of independent reactions (r) and this is done in the following section.

3.5.2.1. Determination of the number of components, C

The number of components, *C* is the number of constituents (elements or compounds) that are chemically independent in the system. It describes the minimum number of independent species necessary to define the composition of all phases of the system (Atkins and De Paula, 2006). The number of phase rule components (C) is determined from the matrix constructed using the atom coefficient of the six chemical species that make up the system as shown below:

Table 3.4. Construction of the atom coefficient matrix

		System atoms		
i	Species	C	H	O
1	CO_2	1	0	2
2	H_2O	0	2	1
3	CO	1	0	1
4	CH_4	1	4	0
5	H_2	0	2	0
6	C	1	0	0

The resultant coefficient matrix then becomes

$$\begin{bmatrix} 1 & 0 & 2 \\ 0 & 2 & 1 \\ 1 & 0 & 1 \\ 1 & 4 & 0 \\ 0 & 2 & 0 \\ 1 & 0 & 0 \end{bmatrix}$$

The number of phase rule components (C) equals the rank of the coefficient matrix. We use the rank function in Matlab® v.7.14 to find the rank of the matrix. The rank of the atom coefficient matrix is 3, implying that the number of phase rule components equals 3. This means that at least 3 components are required to quantitatively express the composition of all the phases when the system is at equilibrium. We can see from the system that the three components are C, H and O.

3.5.2.2. Determination of independent reactions (r)

Using the relationship between the number of phase rule components (C) and the number of chemical species (N) in Equation 3.34, the number of independent reactions (r) in the system can be calculated as shown in Appendix B. From Equation 3.34, it is found that there are three independent reactions, that is r = 3. Once the number of independent reactions is calculated, the next step is to determine the set of equations. This is done by writing the equations for the formation reactions of every species that exist as a molecule and is found in a significant amount in the system.

From the formation reaction equations, species that are not amongst the major species get eliminated by combining the formation reaction equations of the major species. This results in a set of equations that represent the number of independent chemical reactions in the system. The procedure for determining the independent reactions is shown in Appendix B and the set of three independent equations are

$$\text{Boudouard equilibrium: } 2CO \Leftrightarrow C + CO_2 \quad (2.6)$$

$$\text{Heterogeneous water gas shift reaction: } H_2 + CO \Leftrightarrow C + H_2O \quad (2.7)$$

$$\text{Hydrogenation gasification/Methanation: } C + 2H_2 \Leftrightarrow CH_4 \quad (2.8)$$

It is important to note that more than one set of independent reactions can be derived. However, the solution of the chemical equilibrium based on any pair of independent reactions would yield the same results (Mountouris et al., 2006). When applying the phase rule, there are two scenarios that need to be considered, depending on whether there is solid carbon or

not in the system. When there is no solid carbon in the system and the system exists only as a gas phase, then, $\pi = 1$. Therefore, from Equation 3.33, we get

$$F = 2 - \pi + N - r = 2 - 1 + 6 - 3 = 4$$

The system has a maximum of four degrees of freedom and therefore could be defined by specifying the temperature, pressure as well as two elemental ratios. The elemental ratios serve to provide a relationship among species mole fractions and also reducing the degrees of freedom. In this case, the H/O and C/H elemental ratio would be incorporated in the equilibrium calculations.

A more practical case that represents the gasification process well involves the gaseous phase in equilibrium with solid carbon. In this case, there are two phases (i.e. $\pi = 2$) and the phase rule expression becomes from Equation 3.33,

$$F = 2 - \pi + N - r = 2 - 2 + 6 - 3 = 3$$

The system has a degree of freedom of three and thus specifying temperature, pressure and one elemental ratio will define the system's equilibrium. The H/O ratio is chosen and used to relate the species mole fraction for the gasification system equilibrium.

3.5.3. Mathematical formulation

Complex chemical equilibria for C-H-O systems are formulated using two main approaches - the equilibrium constants approach as well as the minimization of the Gibbs energy approach (Cairns and Tevebaugh, 1964). At equilibrium, the Gibbs energy of a system is minimised at constant temperature and pressure. The same criterion provides the basis for defining the equilibrium constant, showing that the two approaches are only variants of the same principle of thermodynamics. Yongdong and Yan (2010) explain that the equilibrium constant approach is useful for relatively simple chemical reaction systems, typically with small number of

gaseous and solid species. This approach is adopted in this study for modelling the biomass gasification process.

Chemical equilibrium systems usually consist of multiple chemical reactions. Therefore, formulating equilibrium systems through the equilibrium constant method involves R number of independent equilibrium constant expressions which relates the variables of the N-species in the system. The method also incorporates additional equations from elemental balances and stoichiometric constraints.

Because the system we consider in this study operates at relatively low pressure (i.e. 1 atm.), and high temperature (800, 900, 1000, 1200 and 1500 K), all the gases are assumed to behave ideally. That is, the fugacity coefficient for all the gaseous components is taken to be one. In the same way, the activity coefficient of solid carbon (graphite) is also taken to be one. Therefore, the corresponding expressions for the equilibrium constants of the three independent reactions derived in the previous section are given as:

2.15

Boudouard equilibrium: $2CO_{(g)} \Leftrightarrow C_{(s)} + CO_{2(g)}$ (2.15)

$$K_{E\text{-}1} = \frac{x_{CO_2}}{x_{CO}^2 P} \tag{3.35}$$

Heterogeneous water gas shift reaction: $H_{2(g)} + CO_{(g)} \Leftrightarrow C_{(s)} + H_2O_{(g)}$ (2.16)

$$K_{E\text{-}2} = \frac{x_{H_2O}}{x_{H_2} x_{CO} P} \tag{3.36}$$

Hydrogenation gasification/Methanation: $C_{(s)} + 2H_{2\,(g)} \Leftrightarrow CH_{4(g)}$ (2.17)

$$K_{E\text{-}3} = \frac{x_{CH_4}}{x_{H_2}^2 P} \tag{3.37}$$

Where x_i denotes the molar fraction of component i and P is the operating pressure of the system.

From the Gibbs energy polynomial function in Equation 3.24, the natural logarithms of the equilibrium constants for the formation of CO, CO_2, CH_4 and H_2O at temperatures considered for the gasification process are presented in Table 3.5 (Baron et al., 1976).

Table 3.5. Natural logarithms of equilibrium constants for formation of H_2O, CH_4, CO and CO_2

Temp (K)	$\ln K_{H_2O}$	$\ln K_{CH_4}$	$\ln K_{CO}$	$\ln K_{CO_2}$
800	30.60	0.34	27.40	59.50
900	26.50	-1.13	25.60	52.90
1000	23.20	-2.33	24.10	47.60
1200	18.20	-4.15	21.80	39.70
1500	13.20	-5.99	19.50	31.80

The values of the equilibrium constants for the three independent reactions are determined from Equation 3.31 using the data in Table 3.5. The values at different temperatures are given in Table 3.6.

Table 3.6. Values of equilibrium constants for the system's independent reactions

T(K)	K_{E-1}	K_{E-2}	K_{E-3}
800	101.000	1.410	23.700
900	5.681	0.323	2.457
1000	0.577	0.097	0.399
1200	0.019	0.016	0.026
1500	0.001	0.003	0.002

As is clear from Table 3.6, the values of the equilibrium constants for the three independent reactions become smaller as the temperature increases from 800 K to 1500 K. This means that at higher temperatures, the three reactions are predominantly reactants at equilibrium. The three independent reactions as written will proceed to the left, resulting in increased reactant concentrations.

We can plug the values of the equilibrium constants from Table 3.6 into the equilibrium constant expressions for the three independent reactions (Equation 3.35, 3.36 and 3.37) at a specific temperature. Taking for example temperature at 800 K, Equations 3.35, 3.36 and 3.37 respectively correspond to

$$K_{E-1} = 101 = \frac{x_{CO_2}}{x_{CO}^2 P} \tag{3.35}$$

$$K_{E-2} = 1.41 = \frac{x_{CH_4}}{x_{H_2}^2 P} \tag{3.36}$$

$$K_{E\text{-}3} = 23.7 = \frac{x_{H_2O}}{x_{H_2} x_{CO} P} \tag{3.37}$$

For the material balance constraint, we consider the condition of one mole total product containing a fixed H/O ratio. That is,

$$x_{H_2} + x_{CO} + x_{CO_2} + x_{H_2O} + x_{CH_4} = 1 \tag{3.38}$$

Taking the H/O ratio of 0.01 as an example, we get

$$\frac{H}{O} = \frac{2x_{H_2} + 2x_{H_2O} + 4x_{CH_4}}{x_{CO} + x_{H_2O} + 2x_{CO_2}} = 0.01 \tag{3.39}$$

Therefore, re-arranging Equations 3.35, 3.36, 3.37, 3.38 and 3.39, we arrive at the following system of equations

$$101.0x_{CO}^2 P - x_{CO_2} = 0 \tag{3.35}$$

$$1.41x_{H_2}^2 P - x_{CH_4} = 0 \tag{3.36}$$

$$23.7x_{H_2} x_{CO} P - x_{H_2O} \tag{3.37}$$

$$2x_{H_2} + 1.99\, x_{H_2O} + 4x_{CH_4} - 0.01x_{CO} - 0.02x_{CO_2} = 0 \tag{3.38}$$

$$x_{H_2} + x_{CO} + x_{CO_2} + x_{H_2O} + x_{CH_4} = 1 \tag{3.39}$$

3.5.4. Mathematical solution

In the previous step, we have used numerical procedures to formulate the C-H-O system into a mathematical problem that involves a set of five equations in terms of the mole fractions of the gas-phase composition at 800 K and H/O = 0.01. The system of equations is solved simultaneously using a Microsoft 2013 excel solver on an ASUS digital computer. In the computation of the mole fraction of the equilibrium gas-phase composition, a nonlinear

equation method with a convergence of 0.0001 is used. Solving the system of equations at 800 K and H/O = 0.01, we get

$$x_{CO} = 0.094$$
$$x_{H_2} = 0.003$$
$$x_{CO_2} = 0.896$$
$$x_{H_2O} = 0.007$$
$$x_{CH_4} = 0.000$$

The rest of the data calculated for the equilibrium syngas composition for the parameters considered in the study is presented in Table A.2 in Appendix F.

To plot the carbon deposition boundaries, we convert the equilibrium syngas composition data into percentages of C, H and O for each temperature and different H/O ratios. First, we determine the percentage fraction of each element (i.e. C, H and O) for every species in the gas-phase as shown in Table 3.7.

Table 3.7. Percentage of C, H, and O in component species

		Number of moles in species			Total atoms in species	Percentage Atomic fraction		
i	Species	C	H	O		C	H	O
1	H_2	0	1	0	1	0.0	100.0	0.0
2	CO	1	0	1	2	50.0	0.0	50.0
3	CO_2	1	0	2	3	33.3	0.0	66.7
4	H_2O	0	2	1	3	0.0	66.7	33.3
5	CH_4	1	4	0	5	20.0	80.0	0.0

The C, H and O percentages in the equilibrium syngas composition are then calculated for each temperature and H/O ratio as the sum of the product of the gas phase compositions and the atomic percentages of each species. For instance, at 800 K and H/O = 0.01 (above), the percentages of C, H and O are calculated as follows,

Carbon: $0.094 \times 0 + 0.003 \times 0.5 + 0.896 \times 0.333 + 0.007 \times 0 + 0.00 \times 0.2 = 0.30$
Hydrogen: $0.094 \times 1 + 0.003 \times 0 + 0.896 \times 0 + 0.007 \times 0.667 + 0 \times 0.8 = 0.099$
Oxygen: $0.094 \times 0 + 0.003 \times 0.5 + 0.896 \times 0.667 + 0.007 \times 0.333 + 0.00 \times 0 = 0.601$

The atom percentages of C, H and O can then be plotted as carbon deposition boundaries on the C-H-O ternary diagram at each temperature and H/O ratio for the parameters considered in the study. Table A.3 in Appendix F presents the data for the atom percentages of C, H and O for plotting carbon deposition boundaries.

REFERENCES

1. Atkins, P.W. & De Paula, J. 2006. *Atkins' Physical chemistry*. 8th ed. Oxford ; New York: Oxford University Press.

2. Ball, D.W. & Baer, T. 2015. *Physical chemistry*. Second edition. Stamford, CT: Wadsworth Cengage Learning.

3. Baron, R.E., Porter, J.H. & Hammond, O.H. 1976. *Chemical equilibria in carbon-hydrogen-oxygen systems*. Cambridge, Mass: MIT Press.

4. Cahn, R.W. & Haasen, P. eds. 1996. *Physical metallurgy*. 4th ed. Amsterdam; New York: North-Holland.

5. Cairns, E.J. & Tevebaugh, A.D. 1964. CHO Gas Phase Compositions in Equilibrium with Carbon, and Carbon Deposition Boundaries at One Atmosphere. *Journal of Chemical & Engineering Data*, 9(3): 453–462.

6. Campbell, F.C. ed. 2008. *Elements of metallurgy and engineering alloys*. Materials Park, Ohio: ASM International.

7. Dahm, K.D. & Visco, D.P. 2013. *Fundamentals of chemical engineering thermodynamics*. 1st Ed. Mason, OH: Cengage Learning.

8. Denbigh, K.G. 1981. *The principles of chemical equilibrium: with applications in chemistry and chemical engineering*. 4th ed. Cambridge [Eng.]; New York: Cambridge University Press.

9. Gunawardena, D.A. & Fernando, S.D. 2014. A thermodynamic equilibrium analysis of glucose conversion to hydrocarbons. *Chemical Engineering Communications*, 201(8): 1115–1124.

10. Jaworski, Z., Zakrzewska, B. & Pianko-Oprych, P. 2016. On thermodynamic equilibrium of carbon deposition from gaseous C-H-O mixtures: Updating for nanotubes. *Reviews in Chemical Engineering*, 33(3): 217–233.

11. Kiss, A.A. 2013. *Advanced distillation technologies: design, control, and applications*. Chichester, West Sussex: Wiley & Sons Ltd.

12. Kyle, B.G. 1984. *Chemical and process thermodynamics*. Englewood Cliffs, N.J: Prentice-Hall.

13. Lee, H.-G. 2012. *Materials thermodynamics: with emphasis on chemical approach*. Singapore; Hackensack, NJ: World Scientific.

14. Li, X., Grace, J.., Watkinson, A., Lim, C. & Ergüdenler, A. 2001. Equilibrium modeling of gasification: a free energy minimization approach and its application to a circulating fluidized bed coal gasifier. *Fuel*, 80(2): 195–207.

15. Mohnot, S. & Kyle, B.G. 1978. Equilibrium Gas-Phase Compositions and Carbon Deposition Boundaries in the CHO-Inert System. *Industrial & Engineering Chemistry Process Design and Development*, 17(3): 270–272.

16. Mountouris, A., Voutsas, E. & Tassios, D. 2006. Solid waste plasma gasification: Equilibrium model development and exergy analysis. *Energy Conversion and Management*, 47(13-14): 1723–1737.

17. Narayanan, K.V. 2013. *Textbook of chemical engineering thermodynamics.* New Delhi: Prentice-Hall of India Private Limited.

18. Natarajan, K. 2014. Computing equilibrium constants of chemical reactions – A new approach. *International Journal of ChemTech Research*, 7: 2361–2367.

19. Patel, B., Hildebrandt, D., Glasser, D. & Hausberger, B. 2007. Synthesis and Integration of Chemical Processes from a Mass, Energy, and Entropy Perspective. *Industrial & Engineering Chemistry Research*, 46(25): 8756–8766.

20. Prins, M.J., Ptasinski, K.J. & Janssen, F.J.J.G. 2003. Thermodynamics of gas-char reactions: first and second law analysis. *Chemical Engineering Science*, 58(3-6): 1003–1011.

21. Smallman, R.E. & Bishop, R.J. 2006. *Modern physical metallurgy and materials engineering science, process, applications*. Oxford: Butterworth Heinemann. http://www.dawsonera.com/depp/reader/protected/external/AbstractView/S9780080511993/S12.31/0 30 July 2017.

22. Stull, D.R., Westrum, E.F. & Sinke, G.C. 1987. *The chemical thermodynamics of organic compounds*. Malabar, Fla: Krieger.

23. Tay, D.H.S., Kheireddine, H., Ng, D.K.S., El-Halwagi, M.M. & Tan, R.R. 2011. Conceptual Synthesis of Gasification-Based Biorefineries Using Thermodynamic Equilibrium Optimization Models. *Industrial & Engineering Chemistry Research*, 50(18): 10681–10695.

24. Tay, D.H.S., Ng, D.K.S., Kheireddine, H. & El-Halwagi, M.M. 2011. Synthesis of an integrated biorefinery via the C–H–O ternary diagram. *Clean Technologies and Environmental Policy*, 13(4): 567–579.

25. Weinhold, F. 2009. *Classical and geometrical theory of chemical and phase thermodynamics*. Hoboken, N.J.: Wiley. http://site.ebrary.com/id/10296723 28 November 2016.

26. Yongdong, X. & Yan, X.-T. 2010. *Chemical vapour deposition: an integrated engineering design for advanced materials*. London; New York: Springer.

27. Zeleznik, F.J. & Gordon, S. 1968. Calculation of complex chemical equilibria. *Industrial & Engineering Chemistry*, 60(6): 27–57.

CHAPTER 4

RESULTS AND DISCUSSION

4.1. INTRODUCTION

In this study, chemical equilibria for a C-H-O system is developed using a stoichiometric equilibrium model to study and analyze biomass gasification. The framework is applicable for evaluating and predicting the equilibrium composition of syngas under different biomass gasification parameters. The equilibrium gas-phase composition at various H/O ratios are plotted as carbon deposition boundaries, which are useful for predicting whether or not solid carbon will form in a given process. The gas-phase equilibrium compositions for the C-H-O system in conjunction with material balance targets are applied in a case study for the conceptual design of an integrated biorefinery that produces DME from the syngas platform. This section therefore presents a discussion based on the results of the gas-phase equilibria of the C-H-O system as well as the conceptual design of the syngas-based DME biorefinery process.

4.2. EQUILIBRIUM GAS-PHASE COMPOSITION

The data for the equilibrium gas-phase composition at equilibrium with solid carbon (Graphite) in terms of mole fractions for H_2, CO, CO_2, CH_4, and H_2O is presented in Table A.2 in Appendix F. The equilibrium composition for the system was solved for the following parametric values:

T (K): 800, 900, 1000, 1200, 1500
Pressure, P: 1 atm.
Atomic ratio (H/O): 0.01, 0.1, 0.2, 0.6, 1, 1.5, 2, 2.5, 6, 10, 20, 30, 40, 50, 60, 70, 80, and 90

Overall, the data for the equilibrium composition is tabulated for 90 sets of parameter values of temperature, H/O ratio, and pressure. This covers a wide range of parameters to include practical values pertinent to biomass gasification systems performed at atmospheric pressure. The way the data is presented and tabulated is particularly useful in relation to

processes where there is variation of either oxygen or hydrogen. The equilibrium gas-phase composition is determined by the H/O ratio at any given temperature and pressure in the system.

4.2.1. Model validation

The equilibrium composition was calculated assuming ideal gas behaviour for the gas-phase components and thus the fugacity of all gases was taken as one. This assumption did not need to be validated because the non-ideality effect in the C-H-O system is negligible given the relatively high temperatures and low pressure considered in the study. The gas mole fraction deviation from ideality only gets considerable at high pressure and low temperature (Baron et al., 1976). Mohnot (1977) re-did the gas-phase calculations of the C-H-O system using the fugacity data at 25 atm. and 500 K. Even at such low temperature and relatively high pressure, the absolute error in mole fraction was in the range between the order of 10^{-4} to 10^{-3}, corresponding to a relative error of 0.1 % or less.

The computation of the equilibrium gas-phase composition considered only 6 species to be significant in the system. These species are CO_2, H_2O, CO, CH_4, H_2 and C (s). The calculation of the chemical equilibria for the C-H-O system is therefore limited only to the six species. In order to validate the accuracy of the equilibrium calculations based on this proposition, the equilibrium compositions of other minor species that are most likely to be present were calculated as shown in Appendix D. The calculations were done for the equilibrium mole fractions of methanol, ethane, ethylene and acetylene at 800, 900 and 1000 K for the same H/O values as those used in the equilibrium gas-phase composition of the major species. The results of the mole fractions of the equilibrium syngas compositions for the minor species are presented in Table A.4 (See Appendix F).

The mole fractions of these compounds are generally in the order of 10^{-6}, which is very small and therefore justifies their omission in the computation of the system's equilibria. Moreover, the results for the equilibrium gas-phase composition were also validated by comparing with data from published literature such as that by Baron et al. (1976) and Cairns and Tevebaugh

(1964). The calculated equilibrium syngas composition results showed excellent agreement with the literature results in the range that the data overlapped.

4.2.2. General trends in the equilibrium gas composition

The data for the mole fractions of the equilibrium syngas composition as a function of H/O ratio at 1 atm. and 800, 900, 1000, 1200 and 1500 K is presented in Figure 4.1.

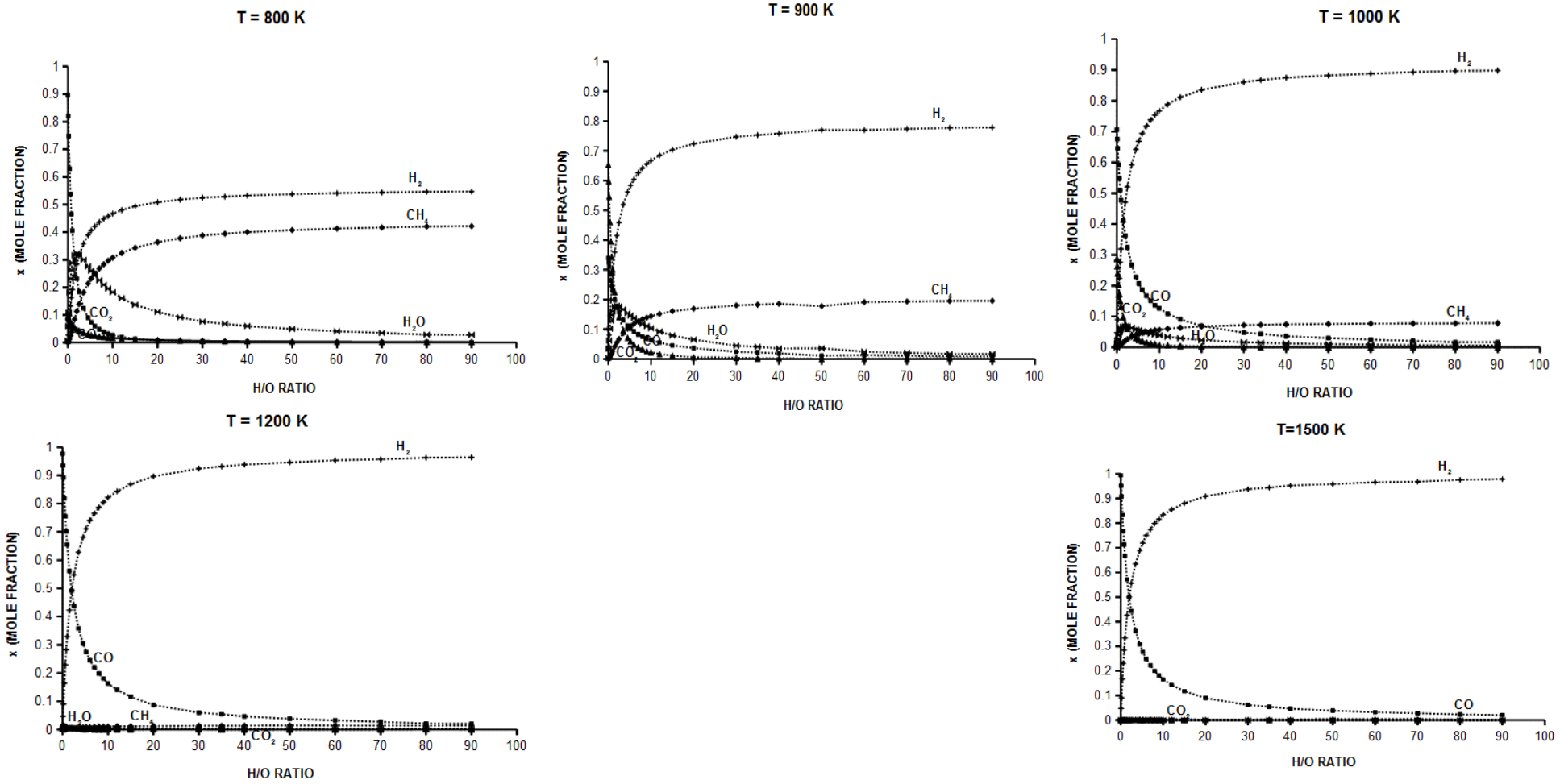

Figure 4.1. Mole fractions of gaseous species in equilibrium with solid carbon in the C-H-O system at 1 atm, 800, 900, 1000, 1200 and 1500 K for the H/O ratio between 0 - 90.

We see from Figure 4.1 that the mole fraction of CH_4 at all temperatures increases gradually as the H/O ratio increases from 0.01 to 90 as a result of the system's reduction in oxygen. On the other hand, the level of CH_4 generally decreases with increasing temperature due to the thermal instability of CH_4 at high temperatures. That is, methane decomposes to form carbon and hydrogen at high temperatures from the methanation reaction as shown in Equation 2.17.

The mole fraction of H_2 increases gradually over the entire temperature range as H/O ratio increases from 0.01 to 90. The amount of hydrogen also increases with increasing temperature owing to the decomposition of CH_4 in the methanation reaction. In addition, the level of H_2 increases as a result of the heterogeneous water-gas shift reaction (Equation 2.16), where char (C(s)) reacts with water vapor to produce H_2 and CO at higher equilibrium temperatures.

Figure 4.1 also shows that the amount of CO_2 decreases as the H/O ratio increases for the entire temperature range as a result of the water-gas shift reaction (Equation 2.3) and the Boudouard equilibrium (Equation 2.15). These reactions are also the cause for the rapid decrease in CO_2 as the temperature increases. Figure 4.1 also reveals that the mole fraction of CO at 800 K is less sensitive to the change in the H/O ratio. However, from 1000 to 1500 K, the amount of CO decreases noticeably as the H/O ratio increases from 0.01 to 90 and the mole fraction of CO is no longer influenced by temperature. This is because at these temperatures, the Boudouard equilibrium reaction shifts towards the formation of CO and the excess solid carbon in the system gets converted to CO. Another reduction reaction that takes place at these temperatures and lower H/O ratio is the water-gas shift reaction (Equation 2.3) which also results in the formation of CO.

Another important point to note from Figure 4.1 is that the mole fraction of H_2O increases as the H/O ratio increases. However, this happens until a certain maximum point for each temperature, whereupon it begins to drop gradually as the H/O ratio increases further. The stoichiometric point at which the mole fraction of H_2O is maximum is H/O = 2 at 800, 900 and 1000 K. The reason the amount of H_2O initially increases is because H_2O is the product of the shift reaction (Equation 2.16). Meanwhile, the subsequent decline in the mole fraction

of H_2O as the H/O ratio increases further is mainly because of the reduction in O_2 which leads to the formation of H_2 and CH_4.

4.2.3. Carbon deposition boundaries

Figure 4.2 shows the carbon deposition boundaries obtained from the equilibrium compositions on a C-H-O ternary diagram. The carbon deposition boundaries are presented at 1 atm. for 800, 900, 1000, 1200 and 1500 K. A large number of H/O values (i.e. 18) for each set of temperature values were used to ensure that accurate and smooth boundary curves are obtained.

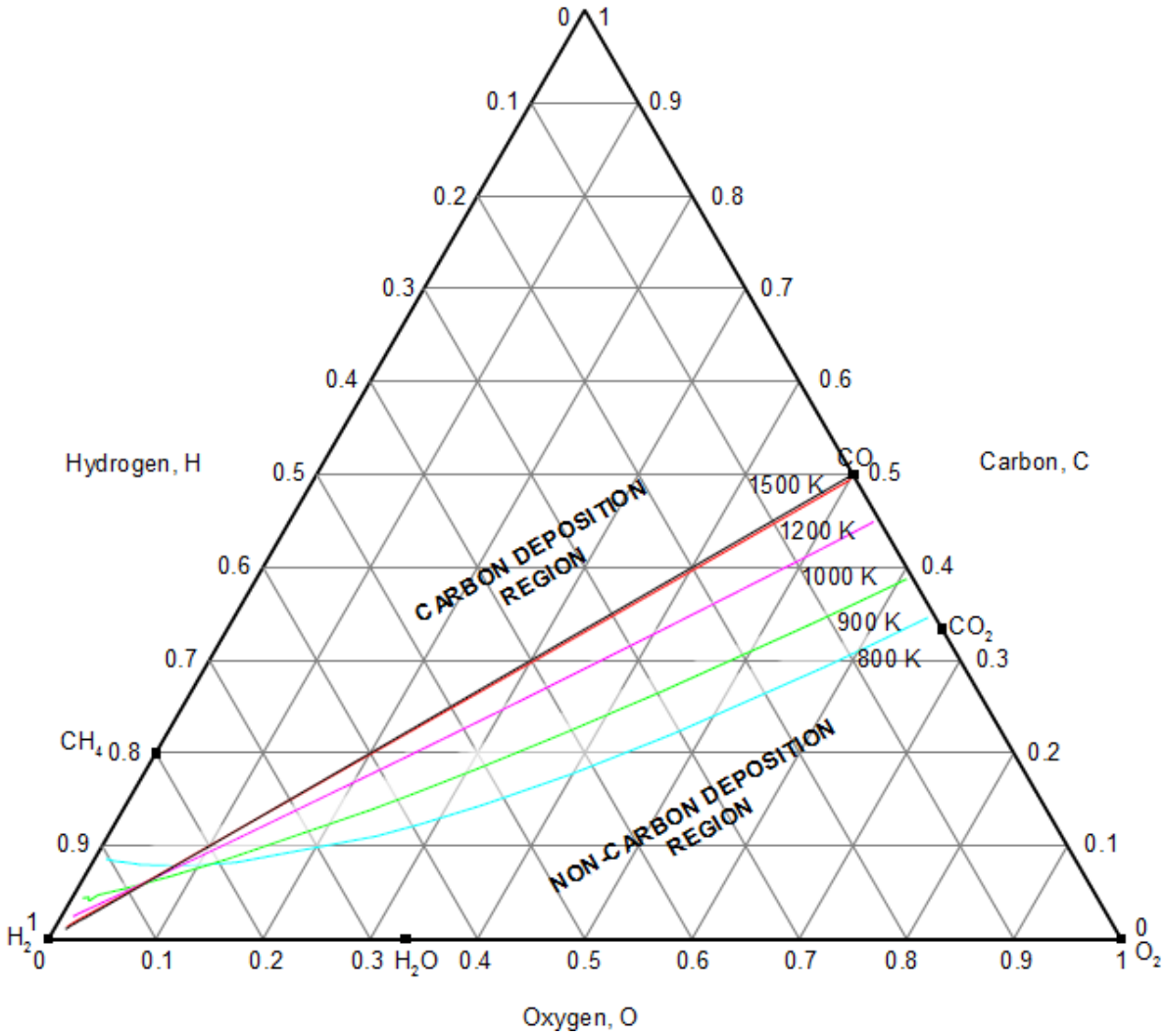

Figure 4.2. Carbon deposition boundaries at 1 atm. and 800, 900, 1000, 1200 and 1500 K.

We see from Figure 4.2 that carbon deposition regions become small at higher temperatures, indicative of the fact that the number of C-H-O systems that may result in carbon deposition reduce. At each of the carbon deposition boundaries, the gas phase mixture is in equilibrium with solid carbon in the form of graphite. The boundaries indicate safe operating conditions where carbon deposition can be avoided in biomass gasification processes. For a given composition above the carbon deposition boundary (i.e. towards the C vertex), carbon will be deposited in the system; conversely, if the composition is below the boundary, then there is no risk of carbon deposition as far as thermodynamics is concerned.

It can also be seen that there is a shift in the equilibrium gas-phase compositions towards more H_2 and CO as the temperature increases. Therefore, the carbon deposition boundaries are almost straight lines that connect CO and H_2 for 1200 K and 1500 K. For these temperatures, the gas-phase compositions may be estimated by means of a lever arm rule. However, at lower temperatures (800, 900 and 1000 K), there is higher amounts of CH_4, H_2O and CO_2 and the carbon deposition boundaries are curved. The gas-phase composition at these temperatures cannot be predicted only by means of graphic calculations like the lever arm rule.

4.3. CASE STUDY: CONCEPTUAL DESIGN OF A DIMETHYL ETHER BIOREFINERY

As previously mentioned, the processing of biomass feedstock into marketable, value-added products (e.g. biofuels, bio-chemicals, etc.) is an attractive alternative to fossil fuels. Therefore, the conceptual design of biomass conversion processes into biofuels like mixed alcohols, dimethyl ether (DME), methanol and Fischer-Tropsch fuels (FT fuels) is crucial in developing efficient and sustainable biorefineries. DME is selected as case study because it has not been widely studied using the graphical targeting approach presented in this study. Therefore, the case study considers the conceptual design of a biorefinery process that involves the conversion of lignocellulosic biomass feedstock into DME.

A back-to-front macroscopic process synthesis approach is proposed to determine the theoretical performance targets for the biorefinery. In this approach, the "*bigger picture*" is considered first and the details later (El-Halwagi, 2012). Overall process targets for the biorefinery are first determined and then systematic procedures are developed to achieve the targets prior to carrying out the detailed design. Overall material balance targets of the process are set by applying atomic species balance based on the process inputs and outputs. Sustainability metrics such as atom economy, carbon efficiency, etc. are also incorporated in the framework in order to provide insight into the process efficiency and feedstock utilization (Constable et al., 2002; Sheldon, 2011). The process targets together with the metrics enable the screening, evaluation and comparison of various process routes/alternatives.

Previous studies on the conceptual design of biorefineries such as Tay et al. (2011) have mainly focused on designing and optimizing individual processes such as gasification. However, it is possible that even though individual processes/technologies within the biorefinery may be optimum, the overall biorefinery process may not be optimum. Therefore, this study develops systematic tools for the conceptual design of a biorefinery based on overall process material balance as proposed by Patel et al. (2007). By first setting the overall targets upfront, the designer is able to dictate the material balance of the process, making it possible to ensure the design of a more efficient process in terms of feed-material utilization (Patel, 2015).

The method considers first the overall biorefinery and its targets, and then moves to focus on systematic procedures applied to individual technologies within the biorefinery to determine the overall targets. Material balance and thermodynamic equilibrium are applied for the conceptual design of a DME biorefinery in a graphical targeting approach to determine:

- The overall maximum material balance targets for the DME biorefinery process.
- Process benchmarks for equilibrium syngas composition and production rates required for DME synthesis.
- Optimum gasifier operating parameters for biomass gasification (e.g. type and amount of gasifying agents, temperature, etc.) that meets the targeted syngas composition.

4.3.1. Overall process targets for the DME biorefinery process

The case study considers a biorefinery process in which biomass is converted to DME. The objective is to ensure that maximum amounts of C, H and O in the biomass feedstock end up as DME by minimizing the production of by-products. The inputs required to produce the desired product, in this case DME, first need to be determined. Since a holistic approach is considered, the process inputs and outputs are limited only to compounds that are naturally available. Therefore, possible process inputs for the biorefinery are biomass, H_2O, CO_2, and O_2. Minor component flows such as nitrogen and sulphur in biomass are not taken into

account. Figure 4.3 shows the schematic of the overall material balance for the DME biorefinery process in which 1 mole of DME is produced.

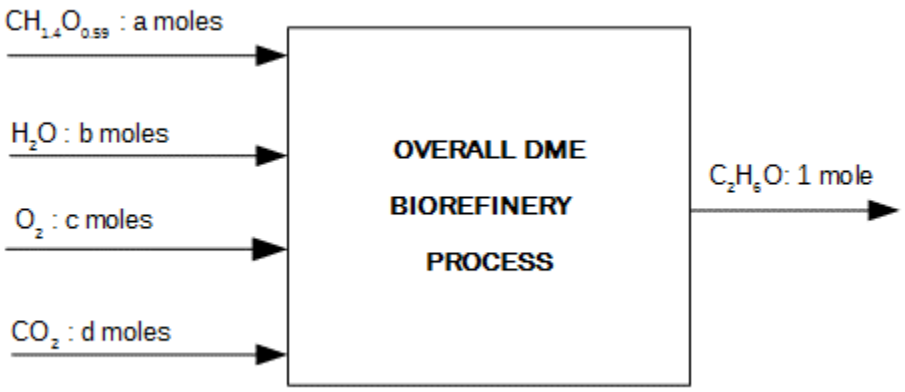

Figure 4.3. Schematic representation of an overall DME synthesis process

The material balance for the overall biorefinery process as shown in Figure 4.3 can be written as follows:

$$a\ CH_{1.4}O_{0.59} + b\ H_2O + c\ O_2 + d\ CO_2 - 1C_2H_6O = 0 \qquad (4.1)$$

where *a, b, c* and *d* are the respective amounts of biomass, water, O_2 and CO_2 required (if the coefficient is positive) or produced (if the coefficient is negative) in the process for converting biomass into 1 mole of DME. Writing an atomic balance for each species results in a system of three equations:

$$\text{Carbon: } a + d = 2 \qquad (4.2i)$$

$$\text{Hydrogen: } 1.4a + 2b = 6 \qquad (4.2ii)$$

$$\text{Oxygen: } 0.59a + b + 2c + 2d = 1 \qquad (4.2iii)$$

The three material balance equations are linear and can be plotted to give a visual presentation of the various material balance options for the process. Since we have four unknowns and three equations, we can vary the amount of biomass feedstock (i.e. choose values for variable *a*) and determine the values of *b, c*, and *d* from the set of equations. The plot for the material balance equations is shown in Figure 4.4.

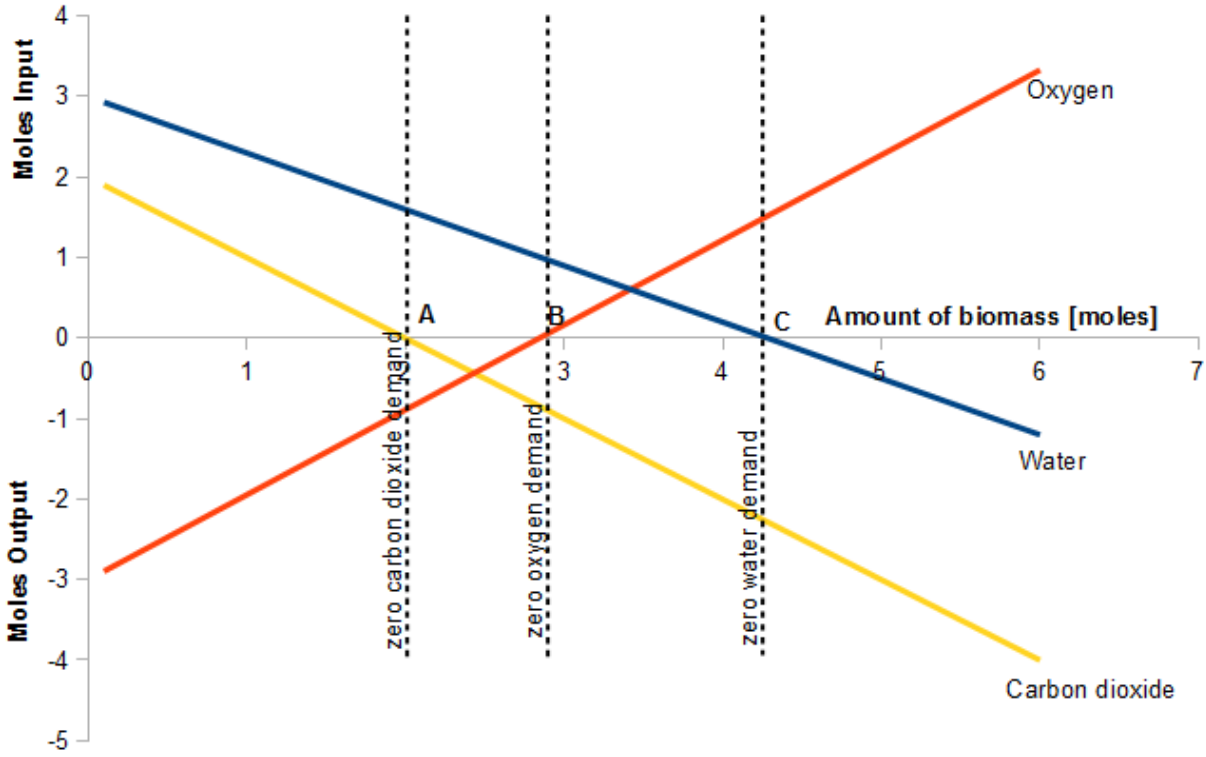

Figure 4.4. Material balance regions for the overall DME biorefinery process

From this Figure, the molar quantities of each component produced or required to produce one mole of DME can be determined as a function of the amount of biomass fed to the process. Important information regarding all possible DME processes that utilize or produce biomass, water, oxygen and carbon dioxide (as the case may be) are contained and represented as material balance regions in Figure 4.4. We can scan and screen all possible

process targets that describe the DME biorefinery and come up with a sensible process that meets specific desired objectives.

From Figure 4.4, Points A, B and C present important process targets whereby CO_2, O_2 and H_2O are respectively neither produced nor required. Material balance of processes that lie to the left of point B produce O_2, and therefore are considered not feasible (Patel et al., 2007). Material balances of processes to the right of point B on the other hand, are characterized by the production of larger amounts of CO_2. These include material balance targets at point C where H_2O is zero. Thus, point B marks an important material balance target for the process that describes the minimum amount of biomass feedstock required to achieve an O_2-neutral process with minimum amount of CO_2 produced.

We see that at point B, the molar quantities of biomass, H_2O, O_2 and CO_2 are 2.844, 1.009, 0, and 0.844 respectively. That is, the biorefinery requires 2.844 moles of biomass and 1.009 moles of H_2O to produce 1 mole of DME and 0.844 moles of CO_2. The process target at Point B can be represented on the C-H-O ternary diagram as shown in Figure 4.5. The measurements of the product and reactant line are presented in Table A.1 (Appendix A).

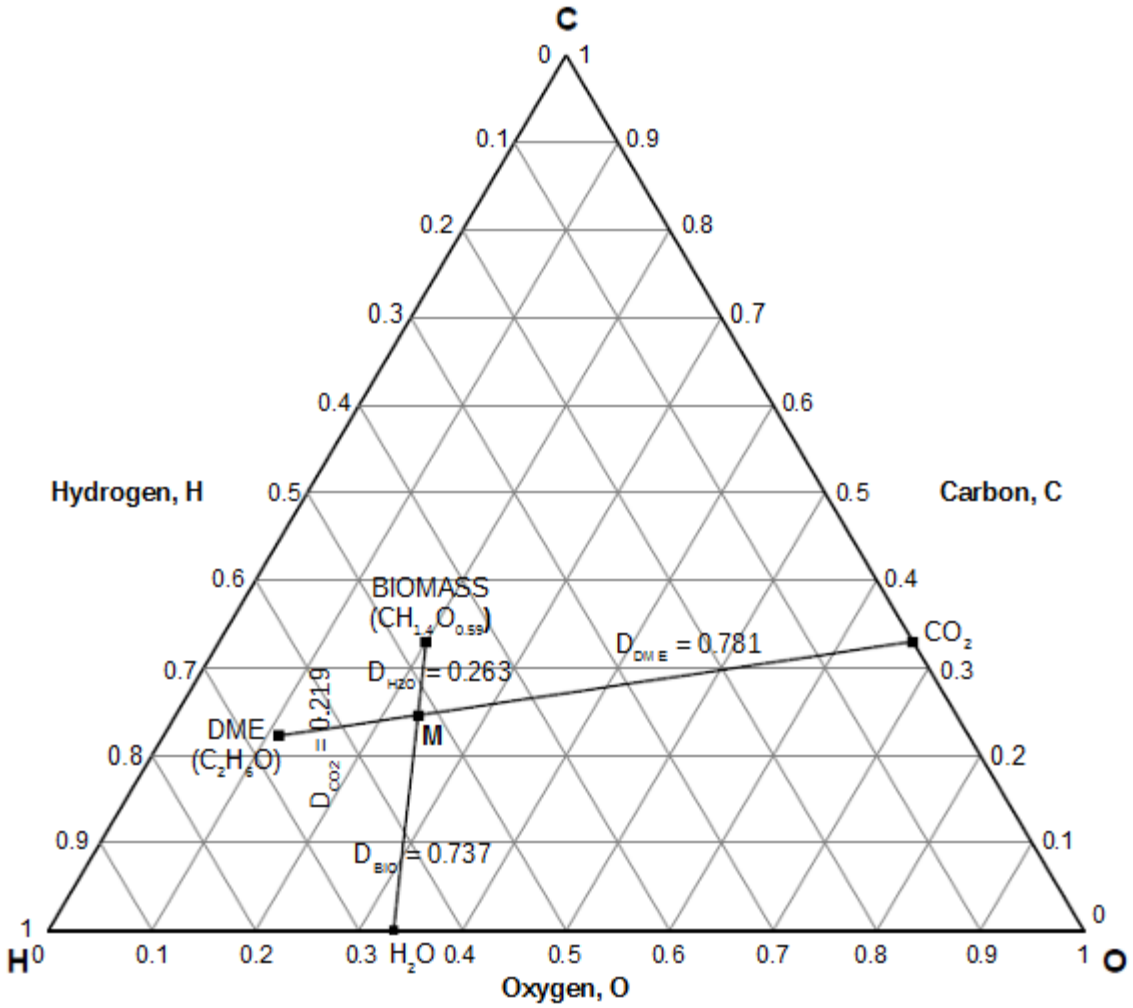

Figure 4.5. Overall DME biorefinery on a C-H-O ternary diagram

From Figure 4.5, the reactant and product lines intersect at Point M where there is a mixture of reactants (biomass and H_2O) and products (DME and CO_2). The lever rule can be used to determine the stoichiometric ratio of biomass:H_2O and DME:CO_2 in the process. For the reactant line, the relative distances of biomass and H_2O with respect to Point M are D_{BIO} = 0.737 and D_{H_2O} = 0.263 respectively. For the product line, the relative distances of DME and CO_2 with respect to Point M are D_{DME} = 0.781 and D_{CO_2} = 0.219 respectively. Solving Equation 3.21, the stoichiometric coefficients of biomass, H_2O, and CO_2 are respectively 2.844, 1.009 and 0.844 for the biorefinery process that produces 1 mole of DME.

From Figure 4.5, it can be deduced that introducing H_2 in the process will shift the reactant line and the equilibrium Point M towards the left of the DME-CO_2 product line, indicating that more DME is produced. Conversely, if O_2 is introduced, the reactant line together with Point M will shift toward the right of the DME-CO_2 product line, signifying that more CO_2 is produced. It can also be seen that, the stoichiometric coefficients obtained from solving Equation 3.21 correspond to the molar quantities of biomass, H_2O and CO_2 at the process target represented by Point B in Figure 4.4. Therefore, from Figures 4.4 and 4.5, the process target for the overall DME biorefinery process is given by the following material balance

$$2.844CH_{1.4}O_{0.59} + 1.009H_2O \Longrightarrow 1C_2H_6O + 0.844CO_2 \qquad (4.3)$$

The process targets reveal that a minimum of 2.844 moles of biomass require 1.009 moles of H_2O to produce 1 mole of DME and a minimum of 0.844 moles of CO_2. Based on a mass basis of 1 ton biomass feedstock, 0.28 tons of H_2O is required to produce 0.708 tons of DME and 0.572 tons of CO_2 as depicted in Figure 4.6.

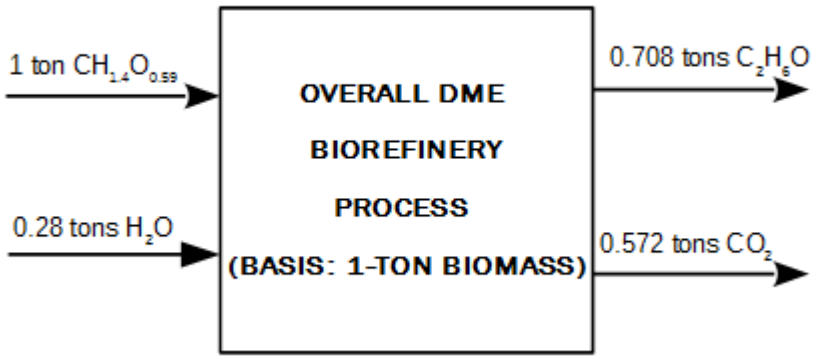

Figure 4.6. Process targets for the overall DME biorefinery on a mass basis of 1-ton biomass

It is important to note that Equation 4.3 is not the reaction that takes place in the biorefinery process; rather it is the overall material balance. This implies that the actual individual reaction(s) for the process may differ from Equation 4.3. The process targets for the DME biorefinery can be assessed using sustainability metrics for determining the efficiency and/or

the environmental performance of this process (Constable et al., 2002; Sheldon, 2011). These metrics are easily determined once the overall material balance of the process is known. Sustainability metrics that are used in this study for assessing and evaluating the utilisation of raw materials as well as waste generation are defined below and their sample calculation is presented in Appendix C.

$$\text{E-Factor} = \frac{\text{Mass of waste produced}}{\text{Mass of desired product}}$$

$$\text{Atom Economy} = \frac{\text{Mass of desired product}}{\text{Total mass of feed}}$$

$$\text{Carbon Efficiency} = \frac{\text{Moles of C in desired product}}{\text{Moles of C in feed}}$$

Based on the process targets from Equation 4.3, the atom economy and the E-factor for the biorefinery process are 55% and 81% respectively. The atom economy shows that just over half of the biomass fed to the process will be converted to DME. Moreover, the E-factor shows that the amount of DME produced in the biorefinery is only 20% more than the CO_2 by-product. The biorefinery also has a carbon efficiency of 70%, indicating that of the carbon introduced to the process, only 70% ends up in the desired product. Therefore, the metrics generally suggest that a lot of waste is being generated and thus the biomass feedstock is not efficiently converted to DME in the biorefinery.

Having set the material balance targets for the overall DME biorefinery, the next steps employ systematic graphical tools to gain insight into how these process targets can be achieved from the individual processes within the biorefinery, namely, the biomass gasification and DME synthesis process.

4.3.2. Process targets for the DME synthesis process

The overall biorefinery process for producing DME from the syngas platform basically involves two main processes - biomass gasification and the DME synthesis process. To achieve the overall process targets set in the previous step, we first consider the DME synthesis process. We determine the process targets of the DME synthesis process based on its inputs and outputs. DME is synthesized from syngas platform which typically comprises of H_2, CO, H_2O, CO_2 and traces of CH_4. Since CH_4 is usually present in extremely small amounts, it is not considered. Therefore, the inputs considered for the DME synthesis process are H_2, CO, H_2O and CO_2. Figure 4.7 presents the schematic of the DME synthesis process assuming that 1 mole of DME is produced from the process inputs.

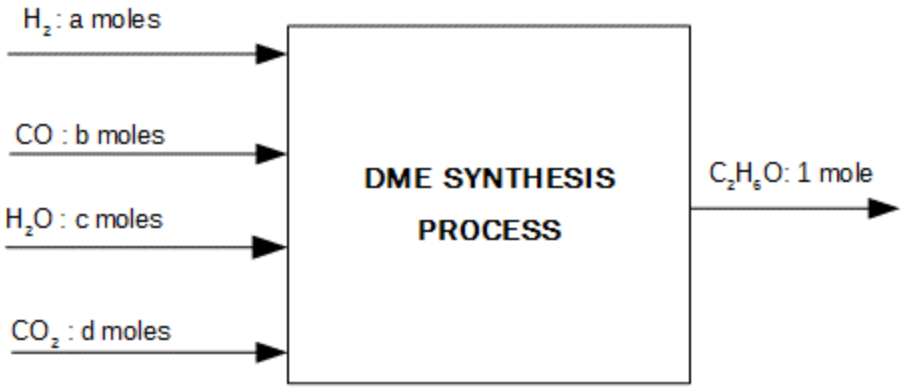

Figure 4.7. Schematic of DME synthesis process from syngas

The material balance for the DME synthesis process in Figure 4.7 can be written as follows:

$$a\ H_2 + b\ CO + c\ H_2O + d\ CO_2 - 1C_2H_6O = 0 \qquad (4.4)$$

where *a, b* and *c* are the respective amounts of H_2, CO, H_2O and CO_2 required (if the coefficient is positive) or produced (if the coefficient is negative) in the process of producing 1 mole of DME. Writing the atomic balance for each species in the system results in a system of three equations:

Carbon: b + d = 2 (4.5i)

Hydrogen: 2a + 2b = 6 (4.5ii)

Oxygen: b + c + 2d = 1 (4.5iii)

The three material balance equations are plotted to give the material balance regions for the various options of synthesizing DME from syngas (Figure 4.8). The molar quantities of each component produced or required to produce 1 mole of DME are given as a function of the amount of H_2 fed into the process. Using this material balance plot, we are able to establish feasible process regions from the many possible material balance options.

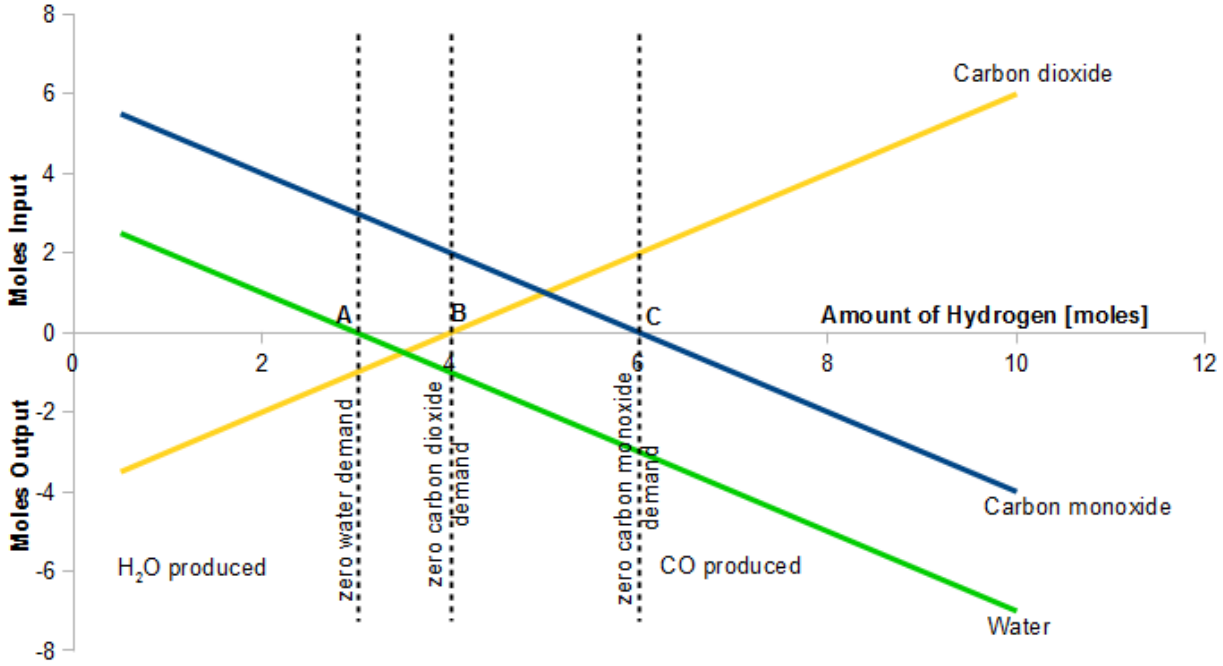

Figure 4.8. Material balance regions for the DME synthesis process

Based on Figure 4.8, three important material balance targets denoted as Points A, B and C are highlighted. Point A represents a process that neither requires nor produces H_2O. At this point, 3 moles of both H_2 and CO are required to produce 1 mole of DME and CO_2. This represents the direct or one-step DME synthesis route in which the H_2:CO ratio equals 1

(Huang et al., 2015). Material balances for processes to the left of Point A produce more CO_2 than the desired product, signifying that reactants are not efficiently converted to products.

Point B represents a process that does not produce or require CO_2. At Point B, 4 moles of H_2 and 2 moles of CO are required to produce 1 mole of DME and H_2O. This represents the overall reaction for the two-step or indirect DME synthesis route in which the H_2/CO ratio is 2 (*ibid.*). Material balance targets for processes that lie to the left of Point B release both H_2O and CO_2 as products, signifying generation of more waste in the process. This however excludes the process target represented by Point A where only CO_2 is produced and H_2O is zero. On the other hand, processes to the right of Point B produce more H_2O than the desired product, suggesting that reactants are not utilized efficiently. Therefore, all these processes, including Point C (where CO equals zero) are not considered.

Therefore, only two material balance targets representing the one-step/direct DME synthesis route (at point A) and the two-step/indirect DME synthesis route (at point B) are considered in the case study. This is consistent with the findings in the literature that show that the direct and indirect methods are the main routes used in the synthesis of DME (Aguayo et al., 2007; Luu et al., 2016). The one-step/direct and two-step/indirect DME synthesis process targets are represented on C-H-O ternary diagrams in Figures 4.9 and 4.10 respectively. The measurements of the product and reactant lines for the inverse lever rule are given in Table A.1 (See Appendix A).

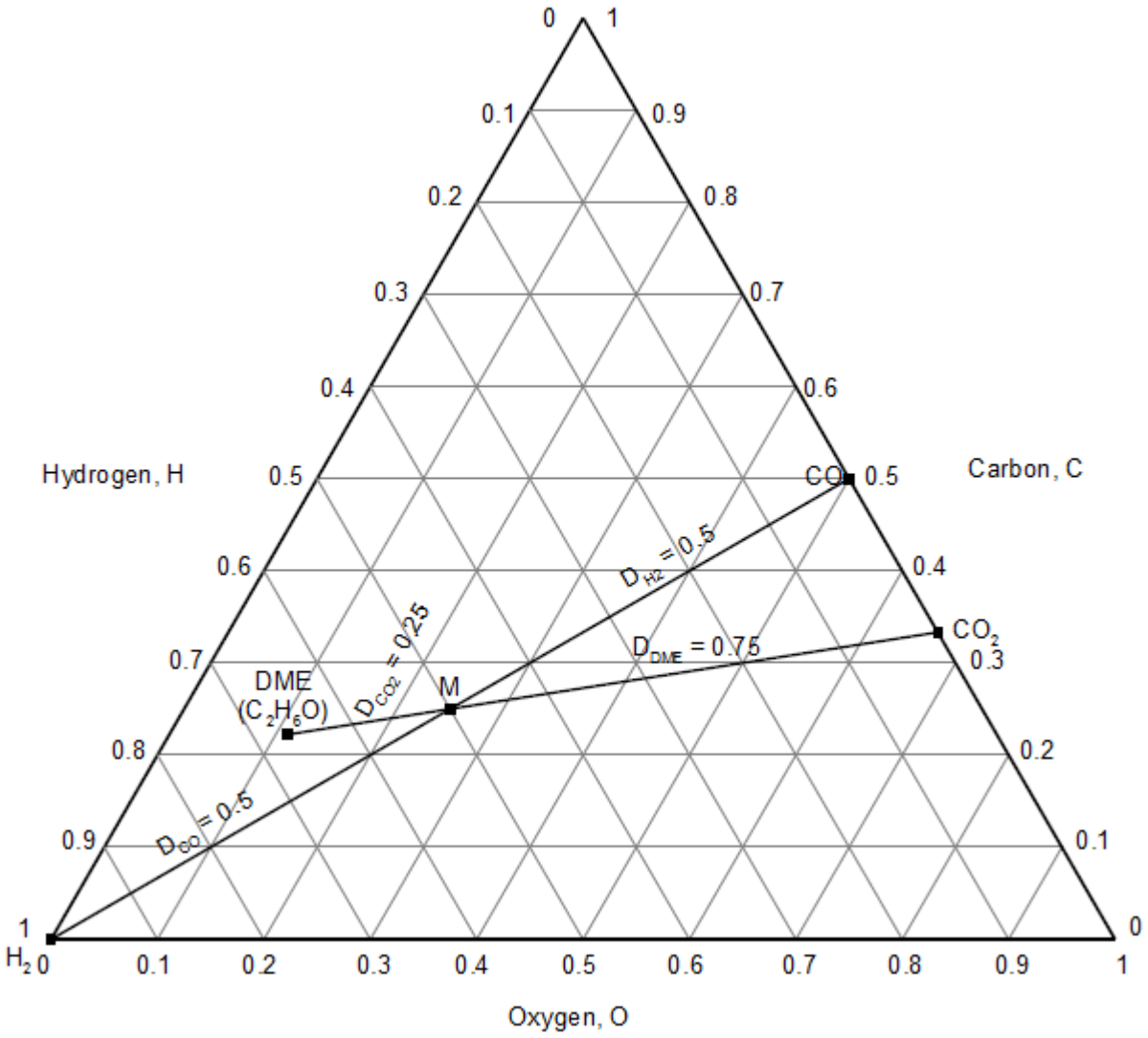

Figure 4.9. Process targets for the one-step/direct DME synthesis route

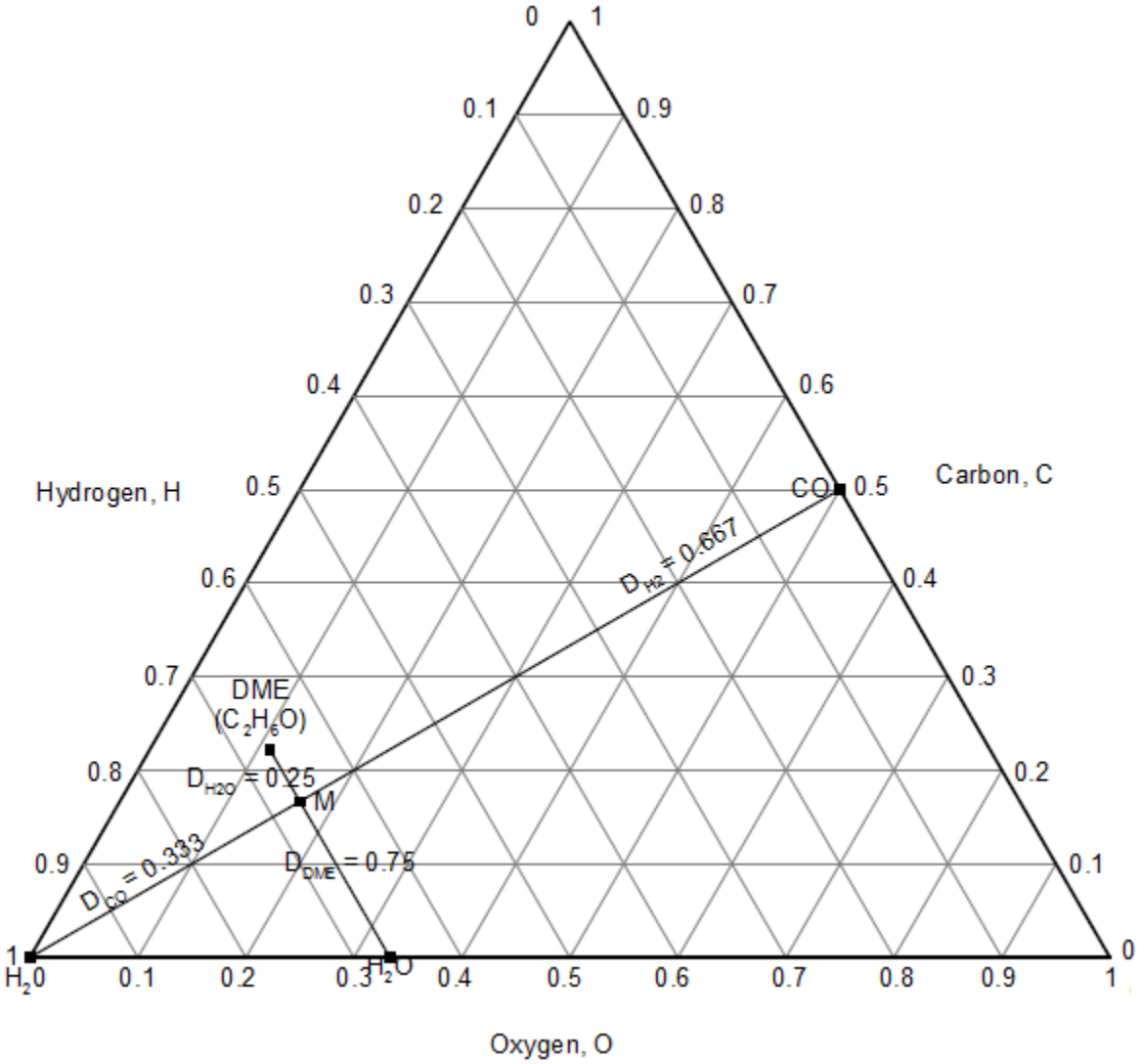

Figure 4.10. Process targets for the two-step/indirect DME synthesis route

Applying the inverse lever arm rule, we find that the stoichiometric coefficients from solving Equation 3.21 for Figures 4.9 and 4.10 correspond to the molar quantities presented by the process targets at Points A and B in Figure 4.8. Therefore, the two process targets for the synthesis of DME are given by the following material balance equations:

$$\text{Direct DME synthesis } (H_2/CO = 1): \quad 3H_2 + 3CO \Longrightarrow 1C_2H_6O + CO_2 \qquad (2.7)$$

$$\text{Indirect DME synthesis } (H_2/CO = 2): \quad 4H_2 + 2CO \Longrightarrow 1C_2H_6O + H_2O \qquad (2.6)$$

The material balance targets for the two process routes are compared using sustainability metrics to assess the efficiency of the conversion of reactants into products in Table 4.1.

Table 4.1. Comparison of material balance targets for the two DME synthesis processes

Overall material balance	Metrics		
	Carbon Efficiency (%)	Atom Economy (%)	E-Factor
Direct DME synthesis route	67	53	0.96
Indirect DME synthesis route	100	77	0.39

From Table 4.1, all the three metrics reveal that syngas is converted into DME more efficiently in the indirect route. The carbon efficiency in this process is 100% compared to 67% for the direct synthesis process. This indicates that all the carbon from syngas is converted into DME in the indirect route whereas only 67% ends up as DME in the direct method. With respect to the atom economy, only 53% of the total mass of syngas fed to the process ends up as DME in the direct method, whereas 72% of the total syngas is converted to DME in the indirect route. Moreover, more waste is generated in the direct synthesis process than in the indirect process as indicated by the value of the E-Factor that is close to 1 for the direct DME synthesis route.

4.3.3. Syngas composition targets requirements for DME synthesis

Now that the material balance targets for both the direct and indirect DME synthesis methods are determined, we proceed with the conceptual design of the biomass gasification process from which the syngas platform for the DME synthesis is produced. We have seen that the direct and indirect DME synthesis routes require syngas composition with H_2:CO ratios of 1:1 and 2:1 respectively. We use the equilibrium data in Table A.2 in Appendix F and Figure 4.1 to determine syngas with the required composition for the material balance targets of both

the direct and indirect DME synthesis. The equilibrium data also enables us to evaluate and determine optimum process variables in the biomass gasification process in order to achieve the required syngas composition targets for DME production.

From Table A.2, the syngas specifications for the DME process routes can be determined either directly or by interpolation of the H/O from the equilibrium data. Possible syngas compositions that fulfill the requirements for the indirect and direct DME synthesis routes at the different temperatures are summarized in Tables 4.2 and 4.3 respectively.

Table 4.2. Syngas compositions at 800, 900, 1000, 1200 and 1500 K and H/O ratios that meet the requirements for the indirect DME synthesis

T(K)	H/O (ratio)	Syngas composition					Atomic ratio			Required H_2/CO ratio
		x_{H_2}	x_{CO}	x_{CO_2}	x_{H_2O}	x_{CH_4}	C	H	O	
800	0.712	0.143	0.072	0.515	0.242	0.029	0.213	0.327	0.460	2.0
900	1.842	0.380	0.190	0.205	0.178	0.047	0.173	0.536	0.291	2.0
1000	3.272	0.571	0.285	0.047	0.065	0.032	0.165	0.640	0.195	2.0
1200	3.982	0.665	0.334	0.000	0.001	0.000	0.167	0.666	0.167	2.0
1500	3.969	0.663	0.335	0.000	0.000	0.000	0.168	0.664	0.167	2.0

Table 4.3. Syngas compositions at 800, 900, 1000, 1200 and 1500 K and H/O ratios that meet the requirements for the direct DME synthesis

T(K)	H/O (ratio)	Syngas composition					Atomic ratio			Required H_2/CO ratio
		x_{H_2}	x_{CO}	x_{CO_2}	x_{H_2O}	x_{CH_4}	C	H	O	
800	0.360	0.082	0.082	0.669	0.158	0.010	0.266	0.194	0.540	1.0
900	0.901	0.246	0.245	0.342	0.148	0.019	0.240	0.360	0.400	1.0
1000	1.599	0.409	0.410	0.097	0.067	0.017	0.241	0.467	0.292	1.0
1200	1.991	0.493	0.493	0.004	0.007	0.004	0.249	0.500	0.251	1.0
1500	1.996	0.499	0.500	0.000	0.000	0.001	0.250	0.500	0.250	1.0

The composition of the syngas produced at the different equilibrium temperatures is evaluated to determine syngas with the most desirable properties with regards to the intended application. The properties of syngas can be defined based on its composition, impurities as well as calorific value (Strezov and Evans, 2015). However, heating value is not critical for downstream application in DME synthesis as long as H_2/CO and impurities levels are satisfied (See Table 2.4).

Based on composition, the selection criteria for the optimum syngas composition considers factors such as the level of moisture (x_{H_2O}) and methane (x_{CH_4}) content, and most importantly, the amount of hydrogen (x_{H_2}) and carbon monoxide (x_{CO}). From Tables 4.2 and 4.3, the equilibrium syngas composition at 800, 900 and 1000 K generally has high moisture (x_{H_2O}) and methane (x_{H_2O}) content. In both cases, the mole fraction of H_2O at 800, 900 and 1000 K present a moisture content of more than 5%. Likewise, methane content at these temperatures is at least 1% of the overall composition. In addition, the syngas is also characterised by low concentrations of H_2 and CO. These factors make the syngas produced at these temperatures unfavourable for both the DME synthesis routes. On the other hand, equilibrium syngas composition at 1200 and 1500 K generally has higher mole fractions of both H_2 and CO. For both temperatures, the CH_4 as well as the moisture content are particularly low, both less than 1%. In fact, the traces of other species are almost non-existent at equilibrium at 1500 K.

Based on syngas composition as syngas quality index, biomass gasification at 1200 and 1500 K appears to produce ideal syngas composition for both the direct and indirect DME synthesis routes. For the case study, the composition at 1200 K is selected as optimum based on energy considerations. The syngas compositions required for the direct and indirect synthesis routes are plotted as Points P_1 and P_2 respectively on the C-H-O ternary diagram in Figure 4.11.

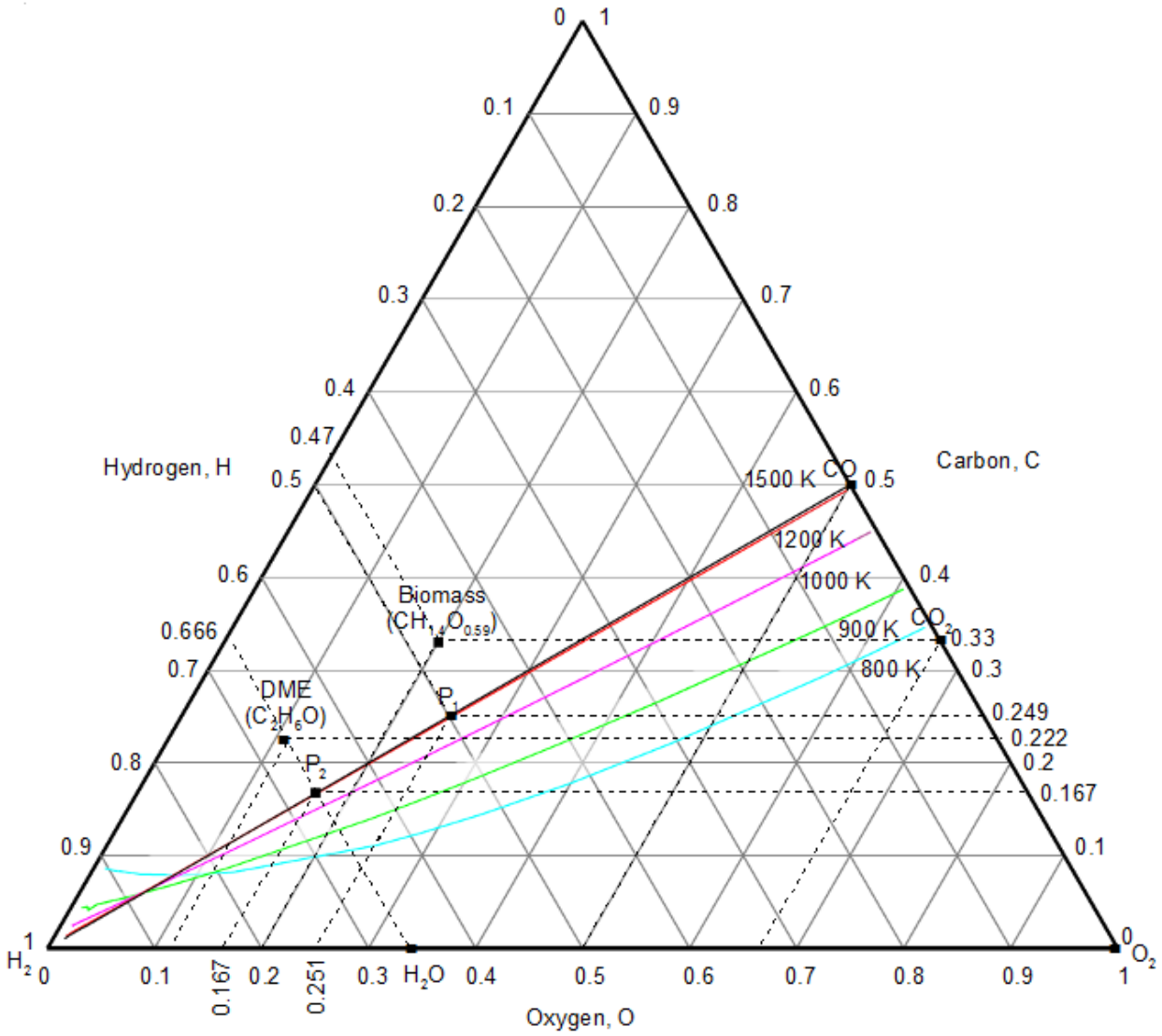

Figure 4.11. Targeting of syngas composition for the direct and indirect DME synthesis

From Figure 4.11, the atomic ratios at Point P_1 are 0.249 C, 0.5 H and 0.251 O. Similarly, Point P_2 is located at 0.167 C, 0.666 H and 0.167 O on the C-H-O ternary diagram. These two points represent target syngas compositions that fulfill the requirement for the direct and indirect DME synthesis. They are the compositions of syngas platform from biomass gasification required for the respective synthesis routes. Therefore, the syngas composition targets for both synthesis routes are achieved without carbon deposition when the biomass feedstock is gasified at 1 atm. and 1200 K.

4.3.4. Selection of optimum gasifying agent for biomass gasification

Gasification of biomass to produce syngas requires a gasifying medium. A number of gasifying agents can be used for biomass gasification, including steam, oxygen, CO_2 or a combination of these gasifying agents. In this section, we use the C-H-O ternary diagram with carbon deposition to determine the oxidant that produces the desired syngas composition for both the DME synthesis routes. We first consider biomass gasification using H_2O, O_2 and CO_2 on their own, and then we will later on look at co-feeding these gasifying agents.

4.3.4.1. Biomass gasification with individual agents: H_2O, O_2 and CO_2

We consider biomass gasification with H_2O, oxygen, and CO_2 separately. Figure 4.12 represents the biomass gasification process using CO_2, H_2O and O_2 on the C-H-O ternary diagram at the carbon deposition boundary for the selected optimum temperature (i.e. 1200 K). To represent each process, we draw three reactant lines joining biomass ($CH_{1.4}O_{0.56}$) to the respective gasifying agents. The three reactant lines intersect the 1200 K carbon deposition boundary, resulting in three different equilibrium composition points labeled Q, R and S. The equilibrium Points Q, R and S represent syngas produced when biomass is gasified with H_2O, O_2 and CO_2 respectively at 1 atm. and 1200 K.

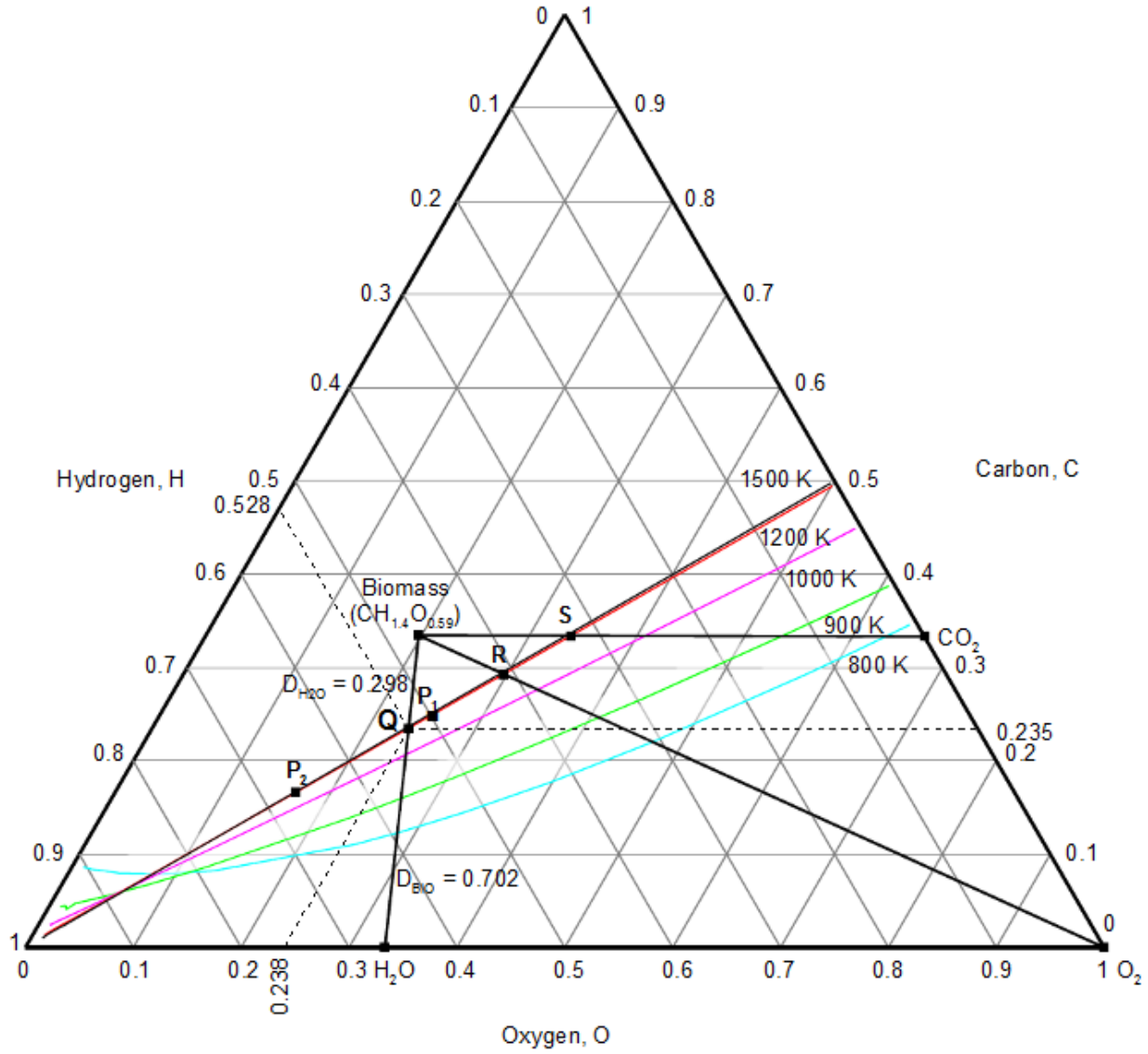

Figure 4.12. Biomass gasification with H_2O, CO_2 and O_2

We determine the optimum gasifying agent by evaluating the equilibrium gas compositions from each gasifying agent relative to the desired syngas compositions for the direct and indirect DME synthesis routes (P_1 and P_2 respectively). The gasifying agent that results in an equilibrium gas composition that is on or closest to P_1 and P_2 is considered optimum. From Figure 4.12, we see that none of the equilibrium points from the three gasifying agents is located on either P_1 or P_2. This means that gasifying biomass with H2O, O_2 or CO_2 at 1 atm. and 1200 K cannot produce syngas with the exact specification for both the one-step/direct and two-step/indirect DME synthesis routes. This is further illustrated in Table 4.4 with a

summary of the equilibrium gas compositions of the points resulting from biomass gasification with H_2O, CO_2 and O_2 at atmospheric pressure and 1200 K.

Table 4.4. Summary of equilibrium syngas compositions from biomass gasification with H_2O, CO_2 and O_2 at 1 atm. and 1200 K

Oxidant	Resultant Equilibrium point	H/O ratio	Atomic fractions			Equilibrium Syngas composition (mole fraction)					Syngas molar mass	H_2/CO
			C	H	O	x_{H_2}	x_{CO}	x_{CO_2}	x_{H_2O}	x_{CH_4}		
CO_2	S	1.004	0.33	0.335	0.334	0.332	0.653	0.008	0.006	0.001	19.078	0.508
O_2	R	1.408	0.291	0.415	0.294	0.408	0.577	0.006	0.006	0.003	16.976	0.707
H_2O	Q	2.218	0.235	0.528	0.238	0.519	0.466	0.004	0.006	0.004	13.913	1.113

From the data in Table 4.4, we see that the H_2/CO ratios of the resultant equilibrium syngas compositions from biomass gasification with O_2, CO_2 and H_2O are 0.505, 0.707 and 1.113 respectively. Meanwhile, the material balance targets for the direct and indirect DME synthesis routes are $H_2/CO = 1$ and $H_2/CO = 2$ respectively. Therefore, the syngas compositions produced from the three gasifying agents do not meet the requirements for the intended downstream applications. However, Point Q which represents the equilibrium syngas composition from biomass gasification with H_2O has the highest H_2/CO ratio (1.113) and it is located closest to the process targets for the direct and indirect DME synthesis routes (i.e. P_1 and P_2 respectively). This implies that biomass gasification with H_2O produces results with better syngas composition compared to O_2 and CO_2 as far as meeting the requirements for the DME synthesis targets are concerned.

From Figure 4.12, it can be deduced that it is feasible to produce syngas with H_2/CO ratio of 1 for the downstream direct DME production by co-feeding H_2O with either CO_2 or O_2. Co-feeding H_2O with either CO_2 or O_2 shifts the syngas equilibrium Point Q toward the syngas target for the direct DME synthesis process (i.e. P_1). However, producing syngas composition required for the downstream application in the indirect DME synthesis process from biomass gasification using any combination of the gasifying agents is infeasible. Instead, as can be seen in Figure 4.12, an additional source of H_2 (for example, CH_4) is required in order to achieve syngas with a H_2/CO ratio of 2. We will look at this process pathway in detail in section 4.3.6.

4.3.5. Integrated biorefinery based on the one-step/direct DME synthesis route

From the previous section, we found that biomass gasification with H_2O produces a syngas composition with the highest H_2/CO ratio (i.e. 1.113). However, this does not meet the required syngas composition target of $H_2/CO = 1$. But, we have seen from Figure 4.12 that in order to produce syngas with the exact H_2/CO ratio required for the direct DME synthesis route, H_2O needs to be co-fed with either CO_2 or O_2.

4.3.5.1. Biomass gasification: co-feeding H_2O with CO_2 and O_2

Material balance targets and regions for co-feeding H_2O with CO_2 and O_2 are presented in Figure A.1. (Appendix E). In this section, we use C-H-O ternary diagram to represent these material balances. From Figure 4.13, all possible co-feed streams of H_2O with CO_2 (H_2O/CO_2) are represented by a line that joins H_2O and CO_2. In the same manner, all possible co-feed streams of H_2O with O_2 (H_2O/O_2) are represented by a line that joins H_2O and O_2.

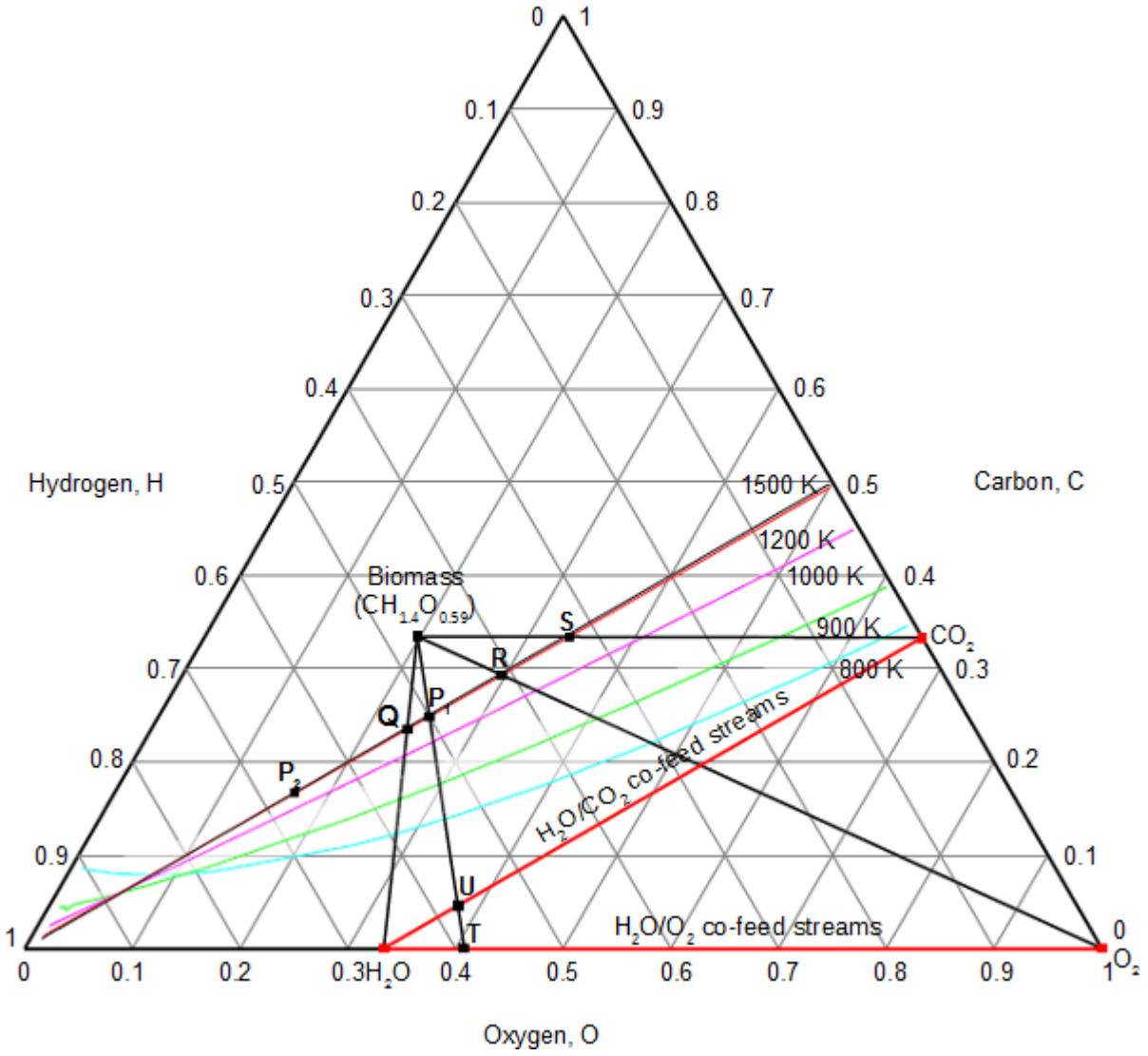

Figure 4.13. Biomass gasification by co-feeding H_2O with CO_2 or O_2

To determine the optimum co-feed streams for the biomass gasification process, a reactant line is drawn from biomass ($CH_{1.4}O_{0.59}$) through the target syngas composition for the direct DME synthesis route (i.e. Point P_1). As we can see from Figure 4.13, the reactant line intersects two lines - one joining H_2O and CO_2 and the other joining H_2O and O_2. The two points of intersection are labelled U and T respectively. They represent the optimum co-feed streams that produce the target syngas composition for the one-step/direct DME synthesis process. Specifically, Point U represents the optimum co-feed stream of H_2O with CO_2 whereas Point T represents the optimum co-feed stream of H_2O with O_2 for the production of the target syngas composition.

Considering biomass gasification by co-feeding H_2O with O_2, we find that Point T is located at 0.594 H and 0.406 O on the C-H-O ternary plot. Therefore, this point can be considered as a C-H-O component represented by the empirical formula $H_{0.594}O_{0.406}$. Figure 4.14 represents the material balance for the gasification process on a C-H-O ternary diagram using the inverse lever arm rule. The measurements for the relative distances of biomass (D_{BIO}) and $H_{0.594}O_{0.406}$ (D_T) are given in Table A.1 (see Appendix A).

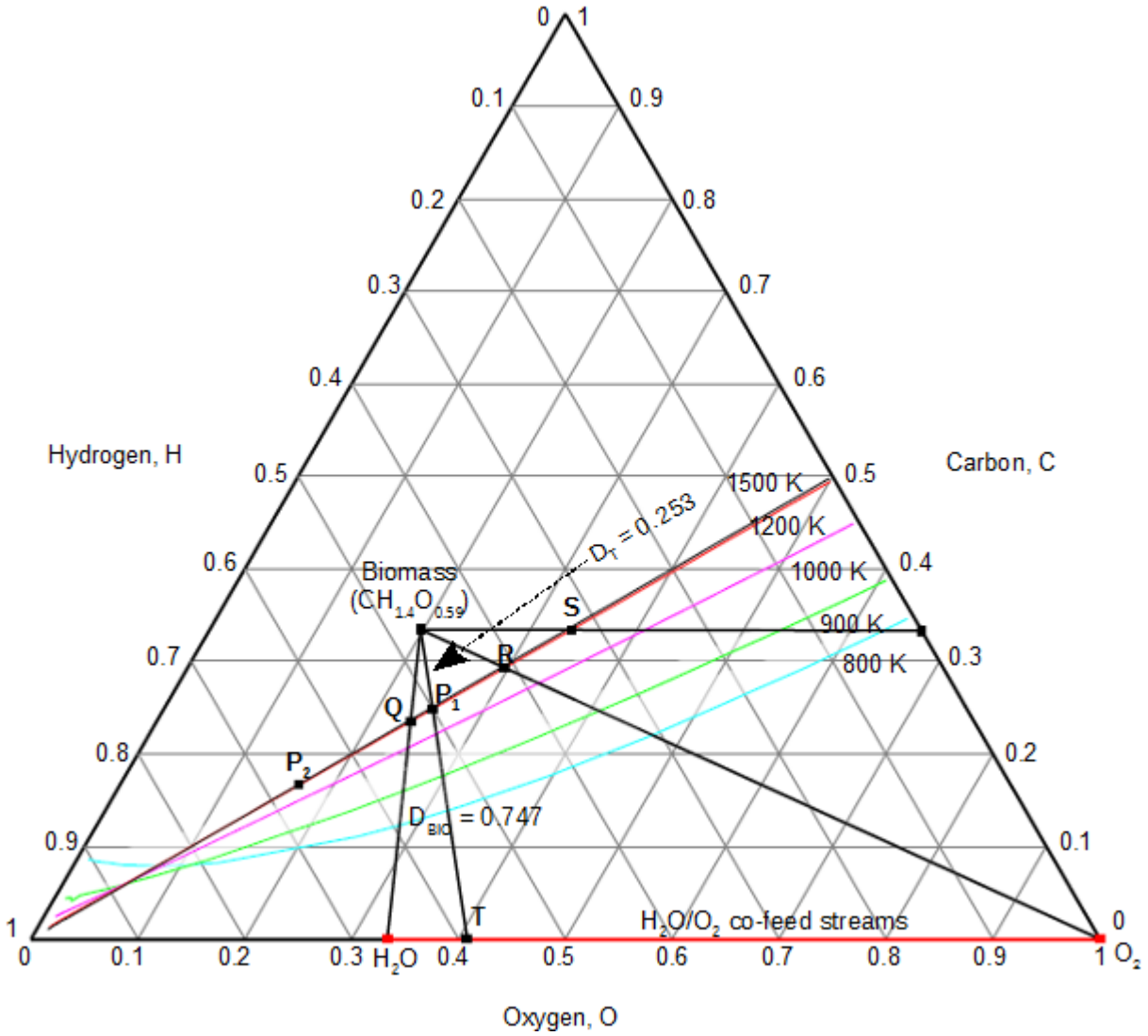

Figure 4.14. Material balance for biomass gasification with optimum H_2O/O_2 co-feed

From Figure 4.14, the relative distances of biomass and $H_{0.594}O_{0.406}$ with respect to Point P_1 are D_{BIO} = 0.747 and D_T = 0.253 respectively. From solving Equation 3.21, we find that the stoichiometric coefficient for $H_{0.594}O_{0.406}$ in the gasification of 1 mole of biomass is 1.011. That is, 1.011 moles of $H_{0.594}O_{0.406}$ is required to gasify 1 mole of biomass to produce syngas composition with H_2/CO = 1. To find the respective molar quantities of H_2O and O_2 in the optimum co-feed stream, we perform the material balance for the production of 1.011 moles of $H_{0.594}O_{0.406}$ from H_2O and O_2. The material balance is written as,

$$\gamma H_2O + \beta O_2 - 1.011\ H_{0.594}O_{0.406} = 0 \quad (4.6)$$

where γ and β are the respective molar quantities of H_2O and O_2 required to produce 1.011 moles of the optimum H_2O/O_2 co-feed stream ($H_{0.594}O_{0.406}$).

The atomic balance for the species involved becomes

$$\text{H balance: } 2\gamma = 0.6005 \quad (4.7i)$$

$$\text{O balance: } \gamma + 2\beta = 0.410 \quad (4.7ii)$$

and

$$\gamma = 0.3,$$

$$\beta = 0.055$$

Therefore, the material balance targets for the production 1.011 moles of $H_{0.594}O_{0.406}$ in Equation 4.6 corresponds to

$$0.3\ H_2O + 0.055\ O_2 \Longrightarrow 1.011\ H_{0.594}O_{0.406} \quad (4.8)$$

That is, 0.3 moles of H_2O and 0.055 moles of O_2 are required to produce 1.011 moles of the optimum H_2O/O_2 co-feed stream ($H_{0.594}O_{0.406}$). As we can see, the molar amounts of H_2O and O_2 required for the gasification process are the same as those at Point A in Figure A.1. (see Appendix E). Therefore, based on Equation 4.8 and Figure A.1, the material balance of the gasification process with the optimum co-feed of H_2O and O_2 is

$$1CH_{1.4}O_{0.59} + 0.3\ H_2O + 0.055\ O_2 - H_2 - CO = 0 \quad (4.9)$$

The material balance shows that 0.3 moles of H_2O and 0.055 moles of O_2 are required to gasify 1 mole of biomass in order to produce syngas with the required syngas composition for the downstream application in the one-step/direct DME synthesis process.

Following the same approach, the material balance for the biomass gasification with H_2O co-fed with CO_2 is represented on the C-H-O ternary diagram in Figure 4.15. The Point U, representing the optimum H_2O/CO_2 co-feed stream for the biomass gasification process is located at 0.045 C, 0.577 H and 0.378 O on the C-H-O ternary diagram. Point U can therefore be considered as a C-H-O component represented by the empirical formula $C_{0.045}H_{0.577}O_{0.378}$. The measurements for the reactant line joining biomass ($CH_{1.4}O_{0.59}$) and $C_{0.045}H_{0.577}O_{0.378}$ are given in Table A.1 (Appendix A).

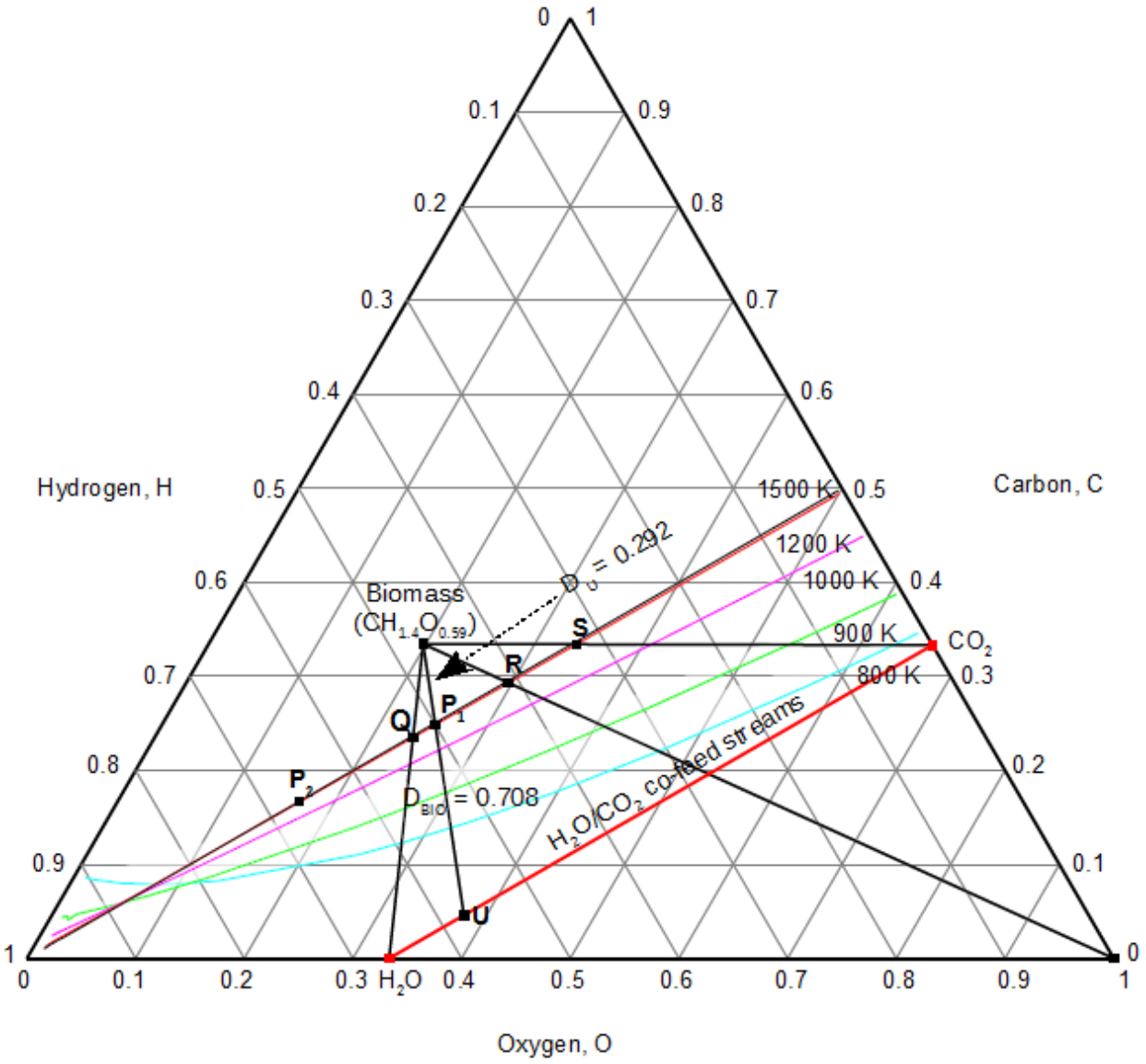

Figure 4.15. Material balance for biomass gasification with optimum H_2O/CO_2 co-feed

From Figure 4.15, the relative distances of biomass and $C_{0.045}H_{0.577}O_{0.378}$ with respect to Point P_1 are $D_{BIO} = 0.708$ and $D_U = 0.292$. By solving Equation 3.21 for the stoichiometric coefficients, we find that 1.23 moles of $C_{0.045}H_{0.577}O_{0.378}$ are required to gasify 1 mole of biomass in order to produce syngas composition with $H_2/CO = 1$ (Point P_1). To find the respective molar quantities of H_2O and CO_2 in the optimum H_2O/CO_2 co-feed stream, we perform material balance for producing 1.23 moles of $C_{0.045}H_{0.577}O_{0.378}$ from H_2O and CO_2. The material balance is written as

$$\gamma H_2O + \beta CO_2 - 1.230\ C_{0.045}H_{0.577}O_{0.378} = 0 \quad (4.10)$$

where γ and β are the respective molar quantities of H_2O and CO_2 required to produce 1.230 moles of the optimum H_2O/CO_2 co-feed stream.

The atom balance for the species then becomes,

$$\text{H balance: } 2\gamma = 0.70971 \quad (4.11i)$$

$$\text{O balance: } \gamma + 2\beta = 0.46494 \quad (4.11ii)$$

and

$$\gamma = 0.355,$$

$$\beta = 0.055$$

Therefore, the material balance for producing 1.23 moles of $C_{0.045}H_{0.577}O_{0.378}$ from H_2O and CO_2 in Equation 4.10 corresponds to

$$0.355\ H_2O + 0.055\ CO_2 \Longrightarrow 1.230\ C_{0.045}H_{0.577}O_{0.378} \quad (4.12)$$

That is, 0.355 moles of H_2O and 0.055 moles of CO_2 are required to produce 1.23 moles of the optimum H_2O/CO_2 co-feed stream ($C_{0.045}H_{0.577}O_{0.378}$). Again, the molar amounts of H_2O and CO_2 required in the gasification process are the same as those at Point B in Figure A.1 in Appendix E. Therefore, from Equation 4.12 and Figure A.1, the material balance of the gasification process with the optimum co-feed of H_2O and CO_2 is given by

$$1CH_{1.4}O_{0.59} + 0.355\ H_2O + 0.055\ CO_2 \Longrightarrow 1.055\ H_2 + 1.055\ CO \quad (4.13)$$

This means that 0.355 moles of H_2O and 0.055 moles of CO_2 are required to gasify 1 mole of biomass in order to produce syngas with composition required for the one-step/direct DME synthesis.

The two process targets involving the biomass gasification with the optimum H_2O/O_2 co-feed (Equation 4.9) and H_2O/CO_2 co-feed (Equation 4.13) are able to produce the required syngas composition target for the direct DME synthesis route. Sustainability metrics for the two process targets are given in Table 4.5.

Table 4.5. Metrics for the overall biomass gasification process: H_2O co-feed with CO_2 or O_2

Biomass gasification material balance	Metrics		
	Carbon Efficiency (%)	Atom Economy (%)	E-Factor
Equation 4.9: $1CH_{1.4}O_{0.59} + 0.3H_2O + 0.055O_2 \Longrightarrow H_2 + CO$	100	100	0
Equation 4.13: $1CH_{1.4}O_{0.59} + 0.355H_2O + 0.055CO_2 \Longrightarrow 1.055H_2 + 1.055CO$	100	100	0

From the results in Table 4.5, the metrics for the material balance targets of the two gasification processes are the same. Both material balance targets have 100% atom economy, 100% carbon efficiency and 0 E-Factor. This means that in both processes, all the raw materials end up in the desired product syngas.

However, in section 4.3.1, the overall material balance for the DME biorefinery (i.e. Equation 4.3) does not require nor produce O_2 as is the case in the biomass gasification with the H_2O/O_2 co-feed (Equation 4.9). Therefore, the material balance for biomass gasification with H_2O/O_2 co-feed is disregarded. That is, the case study considers biomass gasification process using a combination of H_2O and CO_2 at a molar ratio of $H_2O/CO_2 = 6.455$. As previously indicated, the material balance targets show that 1 mole of biomass requires 0.355 moles of H_2O and 0.055 moles of CO_2 to produce 1.055 moles of both H_2 and CO. Based on a mass basis of 1-

ton biomass, 0.280 tons H_2O and 0.106 tons CO_2 are required to produce 0.092 ton H_2 and 1.293 ton CO, as depicted in schematically in Figure 4.16.

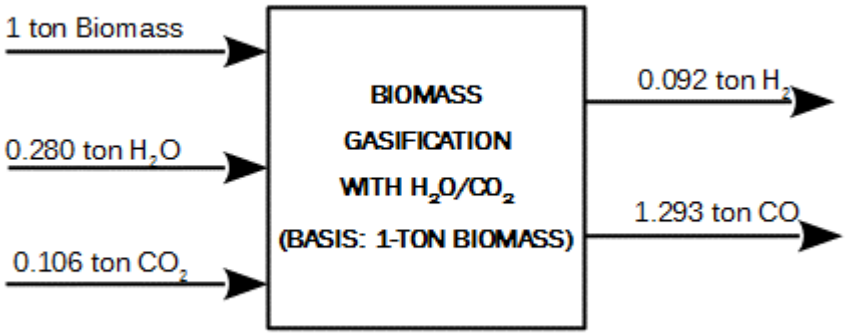

Figure 4.16. Schematic of biomass gasification with optimum H_2O/CO_2 co-feed on a mass basis of 1 ton biomass

In section 4.3.2, it was found that the material balance of the one-step/direct DME synthesis route is given by

$$3H_2 + 3CO \Longrightarrow C_2H_6O + CO_2 \qquad (2.7)$$

We can apply material balance and scale up the direct DME synthesis process to a process feed of 0.092 tons H_2 (46.191 moles) and 1.293 tons CO (46.191 moles) produced from the gasification of 1 ton of biomass feedstock (See Figure 4.16). The scaled up material balance corresponds to

$$46.191H_2 + 46.191CO \Longrightarrow 15.397C_2H_6O + 15.397CO_2$$

In terms of mass basis, the scaled up direct DME synthesis process requires 0.092 tons H_2 and 1.293 tons CO to produce 0.708 tons DME and 0.677 tons CO_2 as shown schematically in Figure 4.17.

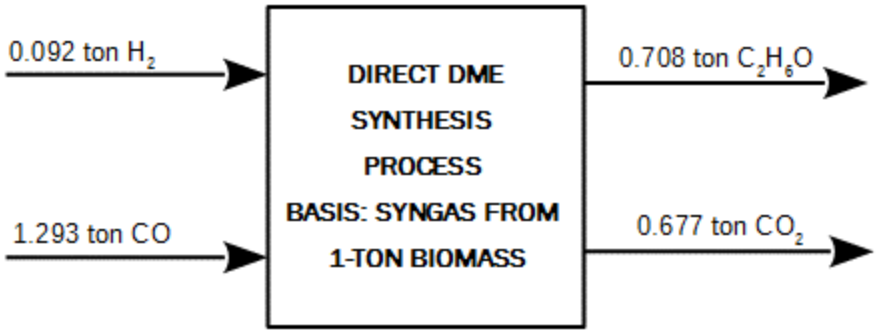

Figure 4.17. Schematic of the direct DME synthesis process on a mass basis of 1-ton biomass feedstock gasified

Based on the process targets from Figures 4.16 and 4.17, we can develop a simplified block flow diagram and material balance for the integrated biorefinery based on the one-step/direct DME synthesis route as shown in Figure 4.18.

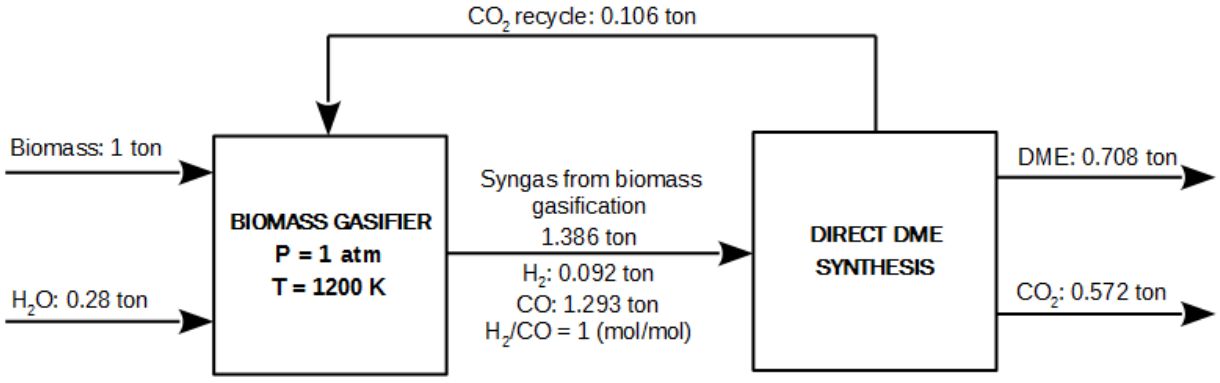

Figure 4.18. Simplified block flow diagram and material balance for the integrated biorefinery based on direct DME synthesis route

Comparison between the process targets for the overall DME biorefinery in Figure 4.6 and the integrated biorefinery in the block flow diagram reveals some interesting points regarding the approach presented in this study: We can see that the overall material balance in Figure 4.6 presents a summary of the integrated biorefinery. The process targets for the overall DME production show a sum of 0.572 tons of CO_2 by-product. This value is the difference between the 0.677 tons of CO_2 produced in the direct DME synthesis process and the 0.106 tons CO_2 recycled to the gasification process as shown in the block flow diagram.

4.3.5.2. Summary of process targets for the integrated biorefinery based on the direct DME synthesis route

The results obtained from the case study for the direct DME synthesis integrated biorefinery are summarised in Table 4.6. Lignocellulosic biomass feedstock ($CH_{1.4}O_{0.59}$) is first gasified by co-feeding H_2O and CO_2 at 1200 K and atmospheric pressure. The optimum H_2O/CO_2 molar ratio of 6.455 (2.642 (w/w)) is required for the biomass gasification process in order to achieve the desired syngas composition for the downstream application in the one-step/direct DME synthesis.

Syngas with the H_2/CO ratio of 1 is produced from biomass gasification at the total rate of 1.386 ton/ton of biomass. Syngas produced from the gasifier is fed to the direct DME synthesis process where 0.708 tons of DME is produced along with 0.677 tons of CO_2 by-product. The DME integrated biorefinery recycles 0.106 ton of CO_2 to the biomass gasification process and generates a minimum waste of 0.572 tons CO_2 per ton of biomass feedstock. According to the sustainability metrics discussed in section 4.3.1, the calculated sustainability metrics for the overall one-step/direct DME integrated biorefinery are 55%, 70% and 0.81 atom economy, carbon efficiency and E-Factor respectively.

Table 4.6. Summary of results for the direct DME synthesis integrated biorefinery case study

Idealized Integrated biorefinery	
Overall DME process	
Process Input/Feed: Biomass	1-ton dry ash free (daf)
H_2O	0.28 tons
CO_2	0.106 tons
Product: Dimethyl ether (DME)	0.708 tons
By-product: Carbon dioxide (CO_2)	0.572 tons
Biomass Gasification	
Process parameters: Pressure (atm.)	1
Temperature (K)	1200
Oxidant (s)	H_2O/CO_2
H_2O/CO_2 molar ratio	6.455 (2.642 (w/w)))
Process Inputs/Feed: Biomass	1-ton dry ash free (daf)
H_2O	0.28 ton
CO_2	0.106 ton
Product (s): Syngas	
H_2	0.092 ton
CO_2	1.293 ton
Production rate (ton/ton of biomass)	1.386
One-step/Direct DME synthesis	
Process Input/Feed: Syngas	
H_2	0.092 ton
CO_2	1.293 ton
H_2/CO (mol/mol)	1
Product(s): Dimethyl Ether (DME)	0.708 ton
By-product(s): Carbon dioxide (CO_2)	0.572 ton
Recycle stream(s): CO_2	0.106 ton

4.3.6. Integrated biorefinery based on the two-step/indirect DME synthesis route

In section 4.3.4, it had been shown that producing syngas with a H_2/CO ratio of 2 (for the downstream indirect DME synthesis route) is infeasible from biomass gasification with all three oxidants (i.e. H_2O, O_2 and CO_2). It was also found that it is not feasible to produce the desired syngas composition even when considering a combination of these oxidants. Biomass gasification with H_2O produced syngas with the highest H_2/CO ratio (i.e. 1.113) compared to CO_2 and O_2. However, the syngas platform from biomass gasification with H_2O is deficient in H_2 and therefore an addition source of H_2 is required. To produce the syngas composition target of $H_2/CO = 2$, we consider co-feeding biomass with CH_4 as a source of H_2.

The process inputs for the overall indirect production of DME therefore comprise of biomass, H_2O and CH_4. The material balance for producing 1 mole of DME can be written as

$$a\ CH_{1.4}O_{0.59} + b\ H_2O + c\ CH_4 - 1C_2H_6O = 0 \qquad (4.14)$$

where *a, b* and *c* are the respective amounts of biomass ($CH_{1.4}O_{0.59}$), H_2O and CH_4 required (if the coefficient is positive) or produced (if the coefficient is negative) in the process of producing 1 mole of DME.

Performing the atomic balance for each species, we get

$$\text{C balance: } a + c = 2 \qquad (4.15i)$$

$$\text{H balance: } 1.4a + 2b + 4c = 6 \qquad (4.15ii)$$

$$\text{O balance: } 0.59a + b = 1 \qquad (4.15iii)$$

From the material balance, we have three equations and three variables. Thus, the degree of freedom is 0 and the equations can be solved for the three variables a, b and c. Solving the set of equations, the overall biorefinery based on the two-step/indirect DME synthesis process is represented by the following material balance

$$1.058CH_{1.4}O_{0.59} + 0.376\ H_2O + 0.942\ CH_4 \Longrightarrow 1C_2H_6O \qquad (4.16)$$

The overall material balance for the DME biorefinery is represented on the C-H-O ternary diagram in Figure 4.19. The stream that represents the optimum co-feed of H_2O and CH_4 is first located on the C-H-O ternary diagram: A reactant line is projected from biomass through DME (C_2H_6O). The point where the reactant line intersects the line that joins H_2O and CH_4 forms the optimum co-feed stream of H_2O and CH_4. This point is labeled V on the C-H-O ternary diagram in Figure 4.19. By tracing the point, we find that it is located at 0.1603 C, 0.7558 H and 0.0639 O on the C-H-O ternary diagram. Therefore, the point can be considered as a C-H-O component represented by an empirical formula $C_{0.1603}H_{0.7558}O_{0.0639}$.

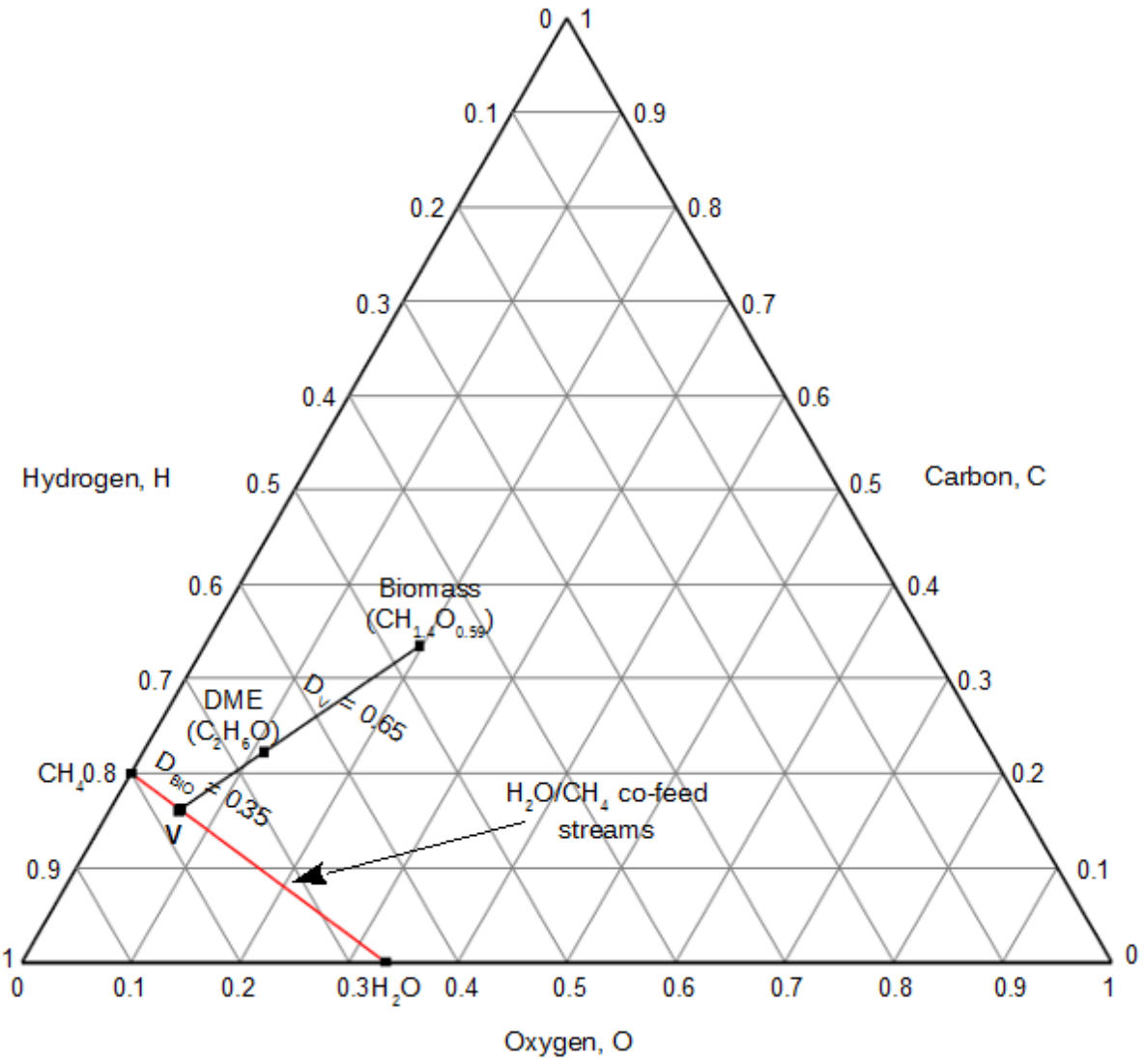

Figure 4.19. Material balance for the overall two-step/indirect DME synthesis biorefinery

The material balance of the overall two-step DME synthesis biorefinery in which biomass is co-fed with the optimum mixture of H_2O and CH_4 ($C_{0.1603}H_{0.7558}O_{0.0639}$) to produce DME is determined by using the lever rule. The measurements for the relative distances of the reactant line are given in Table A.1 (See Appendix A). The relative distances of biomass and $C_{0.1603}H_{0.7558}O_{0.0639}$ with respect to DME (C_2H_6O) are D_{BIO}= 0.35 and D_V= 0.65. The stoichiometric coefficient for the material balance of a process that produces 1 mole of DME from biomass and the optimum mixture of H_2O and CH_4 is 5.874. The material balance targets

reveal that 1.058 mole of biomass requires 5.874 moles of the optimum H_2O/CH_4 stream to produce 1 moles of DME.

We determine the respective molar quantities of H_2O and CH_4 in the optimum co-feed stream by doing material balance for producing 5.874 moles of $C_{0.1603}H_{0.7558}O_{0.0639}$ from H_2O and CH_4. The material balance is written as follows,

$$\gamma H_2O + \beta CH_4 - 5.874C_{0.1603}H_{0.7558}O_{0.0639} = 0 \qquad (4.17)$$

where γ and β are the respective molar quantities of H_2O and CH_4 required to produce 5.874 moles of the optimum H_2O/CH_4 stream. Doing the atomic balance for each component, we get

$$\text{C balance: } \beta - 0.942 = 0 \qquad (4.18i)$$

$$\text{O balance: } \gamma - 0.376 = 0 \qquad (4.18ii)$$

and

$$\gamma = 0.376$$

$$\beta = 0.942$$

Therefore, the material balance for the optimum H_2O/CH_4 co-feed stream in Equation 4.17 corresponds to

$$0.376H_2O + 0.942CH_4 \Longrightarrow 5.874C_{0.1603}H_{0.7558}O_{0.0639} \qquad (4.19)$$

So, the material balance targets for the process that produces 1 mole DME from the two-step/indirect synthesis method is given as,

$$1.058CH_{1.4}O_{0.59} + 0.376H_2O + 0.942CH_4 \Longrightarrow 1C_2H_6O \qquad (4.16)$$

The biorefinery targets show that 1.058 moles of biomass require 0.376 moles of H_2O and 0.942 moles of CH_4 to produce 1 mole of DME (C_2H_6O). In terms of a mass basis of 1 ton

biomass, 0.28 tons of H_2O and 0.623 tons of CH_4 are required to produce 1.903 tons of DME as depicted schematically in Figure 4.20.

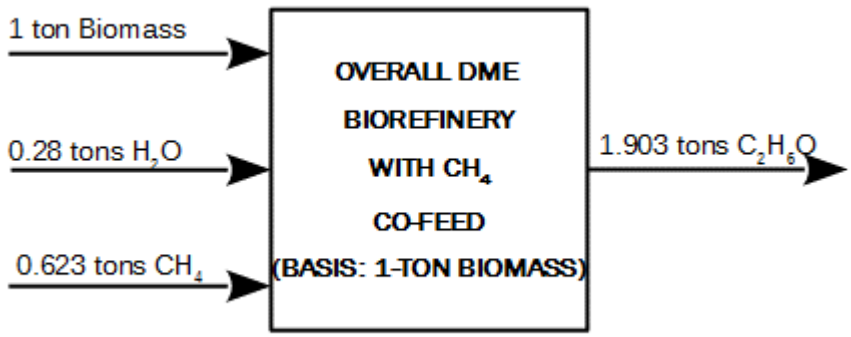

Figure 4.20. Schematic of the overall biorefinery: biomass co-feed with H_2O and CH_4

When we evaluate and assess the process targets using sustainability metric, we find that the atom economy, carbon efficiency and E-Factor are 100%, 100% and 0 respectively. The metrics indicate that the process is 100% efficient in terms of converting reactant into products. That is, all the feed material to the process is converted into the desired product without any waste generation.

Having set the process targets for the overall biorefinery process that is based on the indirect DME synthesis, we endeavor to gain insights into how the targets can be achieved through the individual processes involved (i.e. biomass gasification and indirect DME synthesis).

4.3.6.1. Process targets for biomass gasification with CH_4 co-feed

Biomass gasification is the initial process in the DME integrated biorefinery. For the biomass gasification process, we consider co-feeding CH_4 and H_2O to achieve syngas composition of $H_2/CO = 2$. Biomass gasification by co-feeding CH_4 was proposed by Nakyai et al. (2017) to increase the syngas yield of hydrogen in biomass air-steam gasification. The material balance targets for the biomass gasification process with CH_4 co-feed are determined in Appendix E.

We illustrate the material balance of the gasification process on the C-H-O ternary diagram in Figure 4.21. The optimum co-feed stream of H_2O and CH_4 is first located on the C-H-O diagram. A reactant line is projected from biomass through the syngas equilibrium point where $H_2/CO = 2$ (i.e. Point P_2). The point where the reactant line intersects the line joining H_2O and CH_4 forms the optimum co-feed stream for producing the desired syngas composition target. The point is labeled W on the C-H-O ternary diagram in Figure 4.21. By tracing the point location on the C-H-O ternary diagram, we find that this stream is located at 0.107 C, 0.737 H and 0.156 O. Therefore, the optimum co-feed stream can be considered as a C-H-O component represented by the empirical formula $C_{0.107}H_{0.737}O_{0.156}$.

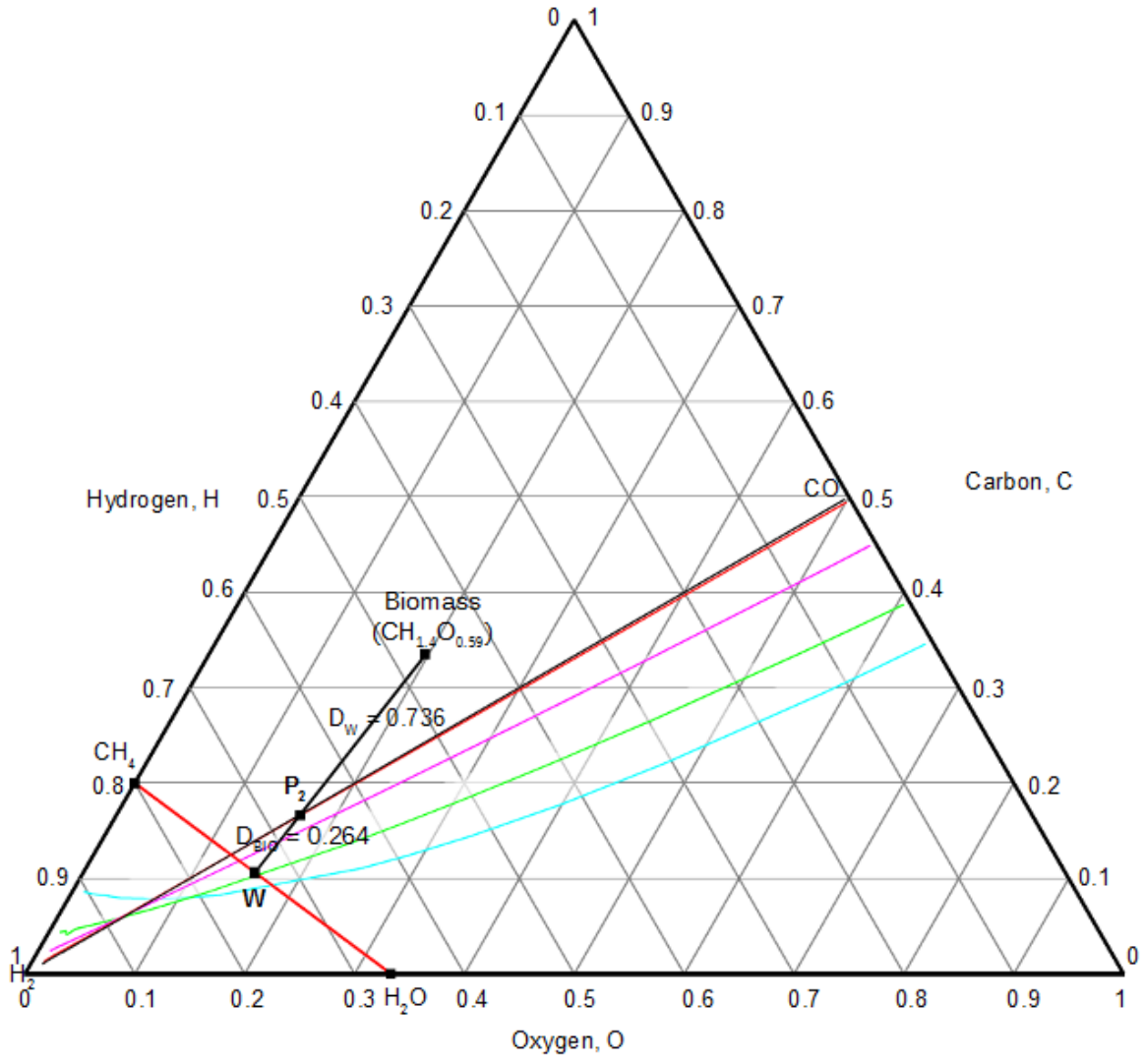

Figure 4.21. Biomass gasification with optimum H_2O/CH_4 co-feed

The material balance of the gasification process that produces syngas composition with a H_2/CO ratio of 2 is determined using the lever arm rule. The relative distances of biomass and $C_{0.107}H_{0.737}O_{0.156}$ with respect to the desired syngas composition at P_2 are measured as D_{BIO}= 0.264 and D_W= 0.736 (See Table A.1 in Appendix A). The stoichiometric coefficient for the material balance of the gasification of 1 mole of biomass with the optimum co-feed of H_2O and CH_4 is 8.317. That is, to produce the required syngas composition for the downstream indirect DME synthesis, 1 mole of biomass requires 8.317 moles of $C_{0.107}H_{0.737}O_{0.156}$.

We determine the respective molar quantities of H_2O and CH_4 in the optimum co-feed stream by doing material balance for producing 8.317 moles of $C_{0.107}H_{0.737}O_{0.156}$ from H_2O and CH_4. The material balance is written as follows

$$\gamma H_2O + \beta CH_4 - 8.317C_{0.107}H_{0.737}O_{0.156} = 0 \qquad (4.20)$$

where γ and β are the respective molar quantities of H_2O and CH_4 required to produce 8.317 moles of the optimum H_2O/CH_4 co-feed stream ($C_{0.107}H_{0.737}O_{0.156}$).

Performing the atomic balance for each component, we have

$$\text{C balance: } \beta - 0.89 = 0 \qquad (4.21i)$$

$$\text{O balance: } \gamma - 1.3 = 0 \qquad (4.21ii)$$

and

$$\gamma = 1.3,$$
$$\beta = 0.89$$

Therefore, the material balance for producing 8.317 moles of $C_{0.107}H_{0.737}O_{0.156}$ in Equation 4.20 corresponds to

$$1.3\ H_2O + 0.89\ CH_4 \Longrightarrow 8.317\ C_{0.107}H_{0.737}O_{0.156} \qquad (4.22)$$

As it can be seen from Equation 4.22, the molar amounts of H_2O and CH_4 required for the biomass gasification are the same as those calculated algebraically (See Appendix E). Therefore, the material balance for the gasification of 1 mole of biomass with the optimum H_2O and CH_4 co-feed is given as

$$1CH_{1.4}O_{0.59} + 1.3\ H_2O + 0.89\ CH_4 \Longrightarrow 3.78\ H_2 + 1.89\ CO \qquad (4.23)$$

The process targets for the biomass gasification using the optimum co-feed of H_2O/CH_4 shows that 1.3 moles of H_2O and 0.89 moles of CH_4 are required to gasify 1 mole of biomass in order to produce 3.78 moles of H_2 and 1.89 moles of CO. On a mass basis of 1 ton biomass, 1.025 tons of H_2O and 0.623 tons of CH_4 are required to produce 0.331 tons of H_2 and 2.317 tons CO. The material balance targets are represented schematically in Figure 4.22.

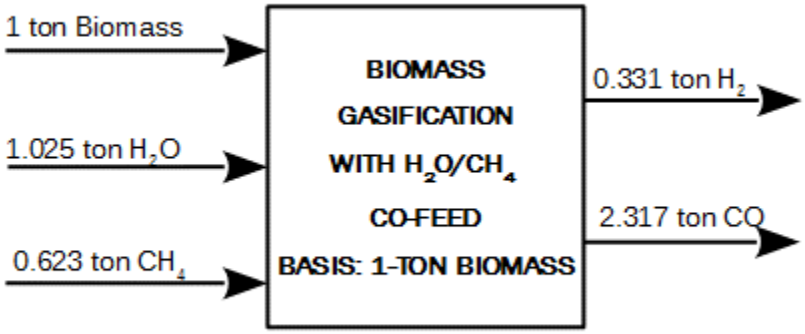

Figure 4.22. Schematic of the biomass gasification with optimum H_2O/CH_4 co-feed

In Section 4.3.2, it was found that the material balance of the two-step/indirect DME synthesis route is given as

$$4H_2 + 2CO \Longrightarrow C_2H_6O + H_2O \qquad (2.6)$$

We can apply material balance and scale up the indirect DME synthesis process to a process feed that corresponds to 1 ton of biomass gasified. This is equivalent to feeding 0.331 tons

(165.3 moles) H_2 and 2.317 tons (82.75 moles) CO from the biomass gasification process into the indirect DME synthesis process. The scaled up material balance for the indirect DME synthesis process then becomes

$$165.5\ H_2 + 82.75\ CO \Longrightarrow 41.375\ C_2H_6O + 41.375\ H_2O \qquad (4.24)$$

In terms of a mass basis of 1 ton biomass feedstock, 0.331 ton of H_2 and 2.317 ton of CO are required to produce 1.903 ton of DME and 0.745 ton of H_2O. The material balance for the two-step/indirect DME synthesis process that corresponds to a mass basis of 1 ton of biomass gasified is shown schematically in Figure 4.23.

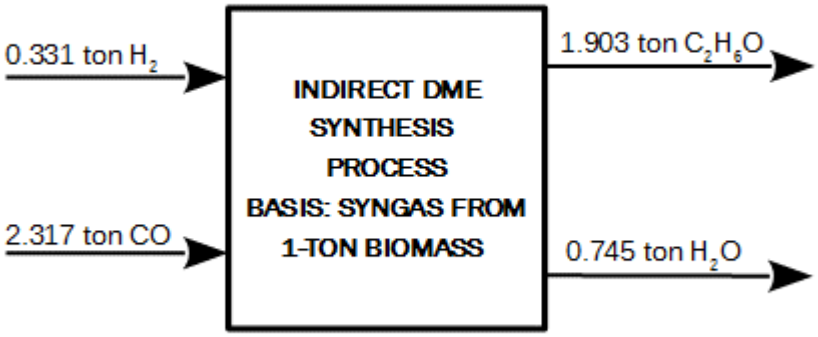

Figure 4.23. Schematic of the indirect DME synthesis process on a mass basis of 1 ton biomass feedstock gasified

We use the previous results obtained for the material balance targets of the biomass gasification in Figure 4.22 and the indirect DME synthesis process in Figure 4.23 to develop a complete DME integrated biorefinery process which is based on the two-step/indirect route in Figure 4.24.

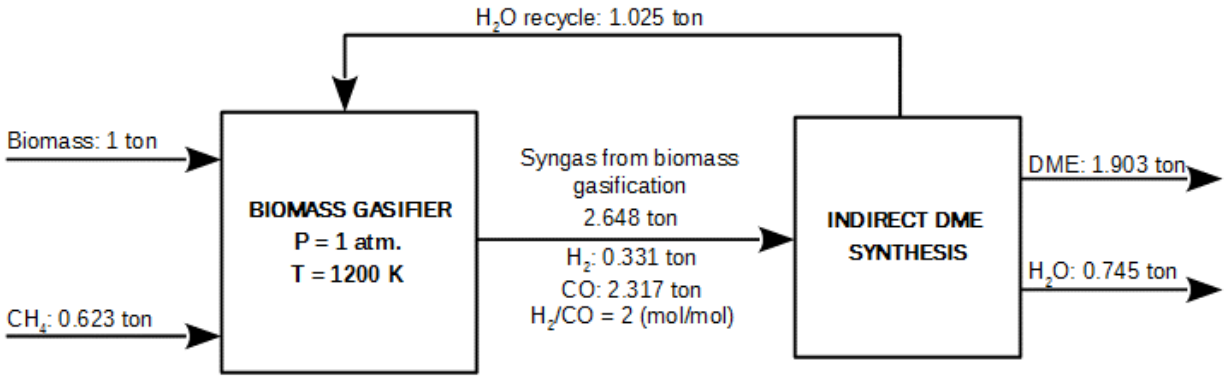

Figure 4.24. Simplified block flow diagram and material balance for integrated biorefinery based on indirect DME synthesis route

It is important to note that the schematic for the overall indirect DME synthesis biorefinery in Figure 4.20 presents an overview of the individual processes shown in the block flow diagram (Figure 4.24). Based on the overall DME biorefinery process in Figure 4.20, 1 ton of biomass and 0.28 tons of H_2O are required to produce 1.903 tons of DME. However, Figure 2.24 shows that the integrated biorefinery process requires 1.025 tons of H_2O for the biomass gasification and produces 0.745 tons of H_2O in the indirect DME synthesis process. The difference between the amounts of H_2O required and produced in the two processes is 0.28 ton and this amount corresponds to the H_2O feed reflected in the overall DME biorefinery process (See Figure 4.20). 1.025 tons of H_2O is recycled from the indirect DME synthesis step to the gasification stage.

4.3.6.2. Summary of process targets for the integrated biorefinery based on indirect DME synthesis route

The results obtained in the case study for the indirect DME synthesis integrated biorefinery are summarised in Table 4.7. Based on Figure 4.24, lignocellulosic biomass feedstock ($CH_{1.4}O_{0.59}$) is first gasified by co-feeding H_2O and CH_4 at 1200 K and atmospheric pressure. The optimum H_2O/CH_4 ratio of 1.645 (w/w) is required for the biomass gasification process to achieve the required syngas composition of H_2/CO = 2. Syngas is produced from the

biomass gasification at the total rate of 2.648 ton/ton of biomass. Syngas is fed into the indirect DME synthesis process where 1.903 tons of DME is produced along with 0.745 tons of H_2O as by-product. The integrated biorefinery recycles 1.025 tons of H_2O to the gasification process. The result for the amount of DME produced in this case study is more than three times that reported by Tay et al. (2011) for the indirect DME synthesis route.

Table 4.7. Summary of results for the indirect DME synthesis integrated biorefinery case study

Idealized Integrated biorefinery	
Overall DME process	
Process Input/Feed: Biomass	1-ton dry ash free (daf)
H_2O	0.28 tons
CH_4	0.623 tons
Product: Dimethyl ether (DME)	1.903 tons
By-product (s): N/A	
Biomass gasification	
Process parameters: P (atm.)	1
T (K)	1200
Oxidant (s)	H_2O/CH_4
H_2O/ CH_4 molar ratio	1.641 (1.645 (w/w))
Process Inputs/Feed: Biomass	1-ton dry ash free (daf)
H_2O	1.025 ton
CH_4	0.623 ton
Product (s): Syngas	
H_2	0.331 ton
CO	2.317 ton
Production rate (ton/ton of biomass)	2.648
Indirect DME synthesis process	
Process Input/Feed: Syngas	
H_2	0.331 ton
CO_2	2.317 ton
H_2/CO (mol/mol)	2
Product (s): Dimethyl Ether (DME)	1.903 ton
By-product: H_2O	0.745 ton
Recycle stream(s): H_2O	1.025 ton

REFERENCES

1. Aguayo, A.T., Ereña, J., Mier, D., Arandes, J.M., Olazar, M. & Bilbao, J. 2007. Kinetic Modeling of Dimethyl Ether Synthesis in a Single Step on a CuO−ZnO−Al2O3/γ-Al2O3 Catalyst. *Industrial & Engineering Chemistry Research*, 46(17): 5522–5530.

2. Baron, R.E., Porter, J.H. & Hammond, O.H. 1976. *Chemical equilibria in carbon-hydrogen-oxygen systems*. Cambridge, Mass: MIT Press.

3. Cairns, E.J. & Tevebaugh, A.D. 1964. CHO Gas Phase Compositions in Equilibrium with Carbon, and Carbon Deposition Boundaries at One Atmosphere. *Journal of Chemical & Engineering Data*, 9(3): 453–462.

4. Constable, D.J.C., Curzons, A.D. & Cunningham, V.L. 2002. Metrics to 'green' chemistry - which are the best? *Green Chem.*, 4(6): 521–527.

5. El-Halwagi, M.M. 2012. *Sustainable design through process integration: fundamentals and applications to industrial pollution prevention, resource conservation, and profitability enhancement*. Boston, MA: Butterworth-Heinemann.

6. Huang, M.-H., Lee, H.-M., Liang, K.-C., Tzeng, C.-C. & Chen, W.-H. 2015. An experimental study on single-step dimethyl ether (DME) synthesis from hydrogen and carbon monoxide under various catalysts. *International Journal of Hydrogen Energy*, 40(39): 13583–13593.

7. Luu, M.T., Milani, D., Wake, M. & Abbas, A. 2016. Analysis of di-methyl ether production routes: Process performance evaluations at various syngas compositions. *Chemical Engineering Science*, 149: 143–155.

8. Mohnot, S.M. 1977. *Equilibrium gas-phase compositions and carbon deposition boundaries in the CHO inert system*. Kensas State University.

9. Nakyai, T., Authayanun, S., Patcharavorachot, Y., Arpornwichanop, A., Assabumrungrat, S. & Saebea, D. 2017. Exergoeconomics of hydrogen production

from biomass air-steam gasification with methane co-feeding. *Energy Conversion and Management*, 140: 228–239.

10. Patel, B. 2015. A Thermodynamic Targeting Approach for the Synthesis of Sustainable Biorefineries. In *Computer Aided Chemical Engineering*. Elsevier: 1283–1288. http://www.linkinghub.elsevier.com/retrieve/pii/B9780444635778500590 28 April 2017.

11. Patel, B., Hildebrandt, D., Glasser, D. & Hausberger, B. 2007. Synthesis and Integration of Chemical Processes from a Mass, Energy, and Entropy Perspective. *Industrial & Engineering Chemistry Research*, 46(25): 8756–8766.

12. Sheldon, R.A. 2011. Utilisation of biomass for sustainable fuels and chemicals: Molecules, methods and metrics. *Catalysis Today*, 167(1): 3–13.

13. Strezov, V. & Evans, T.J. eds. 2015. *Biomass processing technologies*. Boca Raton: CRC Press, Taylor & Francis Group.

14. Tay, D.H.S., Kheireddine, H., Ng, D.K.S., El-Halwagi, M.M. & Tan, R.R. 2011. Conceptual Synthesis of Gasification-Based Biorefineries Using Thermodynamic Equilibrium Optimization Models. *Industrial & Engineering Chemistry Research*, 50(18): 10681–10695.

15. Tay, D.H.S., Ng, D.K.S., Kheireddine, H. & El-Halwagi, M.M. 2011. Synthesis of an integrated biorefinery via the C–H–O ternary diagram. *Clean Technologies and Environmental Policy*, 13(4): 567–579.

CHAPTER 5

CONCLUSIONS

5.1. INTRODUCTION

The overall aim of the study was to develop a systematic graphical targeting approach for the conceptual design of sustainable gasification-based integrated biorefineries. This aim was presented in two parts. Firstly, by developing a stoichiometric equilibrium model for biomass gasification that can be used to evaluate and predict the equilibrium composition of syngas. Secondly, to apply the developed stoichiometric equilibrium model in a case study for the conceptual design of a syngas-based biorefinery that produces DME.

This part of the study therefore revisits the main objectives of the dissertation, summarizes the main findings of the research work and then gives conclusions on the basis of the findings. Recommendations will also be discussed.

5.2. SUMMARY OF FINDINGS

The C-H-O system was investigated by developing an equilibrium model based on thermodynamics to represent the biomass gasification process at 1 atm. and 800, 900, 1000, 1200 and 1500 K. Only 6 species, namely, CO, H_2, CO_2, C (s), H_2O and CH_4 were found to be present in significant amounts. The system was found to consist of two phases which are defined by three chemically independent components/constituents (i.e. C, H and O). The phase rule analysis revealed that the C-H-O system has a maximum degree of freedom of three. Thus, temperature, pressure and H/O ratio were specified to describe the gas-phase equilibrium state of the C-H-O system.

The equilibrium syngas composition was found to have high methane and moisture content at lower temperatures (i.e. 800, 900 and 1000 K) while insignificant traces of these species are found at 1200 and 1500 K. Higher temperatures (1200 and 1500 K) were shown to produce syngas composition that is predominantly CO and H_2. For all temperatures, the H_2/CO ratio of the equilibrium gas composition increases as H/O ratio increases from 0.01 to 90.

When the equilibrium gas compositions were plotted as carbon deposition boundaries on the C-H-O ternary diagram, it was found that carbon deposition regions become small at higher temperatures and large at lower temperatures.

For the second part of this study, a back-to-front targeting approach was proposed and used in a case study for the conceptual design of a DME integrated biorefinery. The integrated biorefinery consists of two main processes, i.e. biomass gasification and the DME synthesis process. We found that the DME synthesis process has two main process targets, one based on the indirect synthesis route and another on the direct synthesis route. The direct and indirect DME synthesis routes require syngas platform with compositions $H_2/CO = 1$ and $H_2CO = 2$ respectively. The syngas composition targets for both synthesis processes could not be achieved from biomass gasification with individual oxidants (i.e. H_2O, CO_2 and O_2). However, biomass gasification with H_2O at 1200 K was found to produce better results with a H_2/CO ratio of 1.113.

For the biomass gasification process to achieve the syngas target required for the direct DME synthesis route, a mixture of H_2O and CO_2 with a molar ratio of $H_2O/CO_2 = 6.455$ is used as an oxidant. Based on the process targets for the biomass gasification and the direct DME synthesis process, a simplified flow sheet of the overall integrated biorefinery for the production of DME was developed. The biorefinery produces 0.708 tons of DME, 0.572 tons of CO_2 by-product and recycles 0.106 tons of CO_2 to the gasification process per ton of biomass feedstock. The overall process targets for the integrated biorefinery has 70% carbon efficiency and 55% atom economy.

In order to achieve the syngas composition target for the indirect DME synthesis route (i.e. $H_2/CO = 2$), an additional source of H_2 is required. Introducing CH_4 into the biorefinery results in an overall process targets with 100% carbon efficiency. Biomass gasification with a mixture of H_2O and CH_4 ($H_2O/CH_4 = 1.641$ mol/mol) as oxidant is used to produce syngas platform with the required composition of $H_2/CO = 2$. Overall, the integrated biorefinery based on the indirect DME synthesis route produces 1.903 tons of DME, 0.745 tons H_2O by-product, and recycles 1.025 tons of H_2O to the gasification process. Comparatively, the biorefinery that is

based on the indirect DME route produces more than twice the amount of DME than the direct route-based biorefinery.

5.3. CONCLUSIONS

Based on the results presented for the equilibrium model as well as the case study for the conceptual design of a DME biorefinery, the following conclusions can be made:

- From the general analysis, the C-H-O system is relatively simple as it involves only 6 chemical species of interest, i.e. five gaseous species in equilibrium with solid carbon (graphite). The choice for using the equilibrium constant and material balance approach (as opposed to the Gibbs energy minimization approach) for analysing and calculating the chemical equilibria was therefore appropriate.

- The C-H-O ternary diagram offers a quick and useful graphical tool for representing both chemical equilibrium and overall material balance. When equilibrium compositions are plotted on the C-H-O ternary diagram as carbon deposition boundaries, they provide a visual representation of process conditions that need to be avoided when designing and operating processes. In addition, the C-H-O ternary diagram allows one to illustrate and determine the overall material balance targets through the use of the inverse lever arm rule.

- The chemical equilibria allow a quick way of estimating, evaluating and predicting the syngas composition under different biomass gasification conditions. That is, biomass gasification processes can rapidly be assessed for various process parameters (temperature, types of oxidants, etc.) that produce required downstream syngas platform.

- The back-to-front approach provides a very useful tool for determining the maximum production rates and targets of the final product prior to detailed design using minimum information about the process. Applying overall material balance targets

enables the chemical engineer/process designer to make crucial decisions at the early stages of the design process by dictating the process flowsheet such that the utilization of raw materials is maximized.

- Incorporating sustainability metrics into the material balance targets provides meaningful insights into optimum utilization of feedstock as well as the process efficiency.

5.4. RECOMMENDATIONS

The calculation for the chemical equilibria considers a system that is entirely made up of only C, H and O and does not account for the effect of inerts. Thus, the results of the model may not well represent processes such as biomass gasification in which gases like nitrogen can exist as inert. We therefore recommend that the approach presented in this study should be considered for the C-H-O-N system in which N_2 is taken into account as an inert.

The process targets for the biorefinery processes have been determined in terms of mass only. Further future work should also focus on setting the biorefinery process targets based on energy and entropy as well. This is because even though the biorefinery processes appear attractive from a material balance perspective, there is also a possibility that they may not be feasible in terms of energy and work perspective. That is, they may require additional energy and work to convert the raw materials into products.

More than double the amount of DME is produced from the integrated biorefinery based on the indirect DME synthesis route compared to the direct DME route. The indirect route-based biorefinery is more efficient in terms of converting raw materials into the desired product (i.e. DME) as indicated by the sustainability metrics. Therefore, it is recommended that research and development efforts in designing gasification-based biorefineries for producing DME should be focused on the indirect DME synthesis route. This is however recommended under the caveat that natural gas (methane) is also available.

Biorefineries operating at the process targets determined in the study have efficient conversion of raw materials to the desired products (i.e. DME) and minimum generation of waste and therefore require less complex equipment for handling. This in turn translates into both minimum operating and capital costs of the biorefinery. Therefore, future work should incorporate capital and operating cost estimations.

APPENDIX A: SAMPLE CALCULATIONS FOR MOLAR RATIOS AND STOICHIOMETRIC COEFFICEINT

Biomass ($CH_{1.4}O_{0.59}$)

Total number of atoms in $CH_{1.4}O_{0.59}$ = 1 C atom + 1.4 H atom + 0.59 O atom = 2.99 atoms
Resultant atomic ratios:

$$\text{Carbon: } \frac{1}{2.99} = 0.334 \quad \text{(A.1i)}$$

$$\text{Hydrogen: } \frac{1.4}{2.99} = 0.468 \quad \text{(A.1ii)}$$

$$\text{Oxygen: } \frac{0.59}{2.99} = 0.197 \quad \text{(A.1iii)}$$

Water (H_2O)

Total moles in H_2O = 0 C atom + 2 H atoms + 1 O atom = 3 atoms
Resultant atomic ratios:

$$\text{Carbon: } \frac{0}{3} = 0 \quad \text{(A.2i)}$$

$$\text{Hydrogen: } \frac{2}{3} = 0.667 \quad \text{(A.2ii)}$$

$$\text{Oxygen: } \frac{1}{3} = 0.333 \quad \text{(A.2iii)}$$

Carbon dioxide (CO_2)

Total moles in CO_2 = 1 C atom + 2 O atom = 3 atoms
Resultant atomic ratios

$$\text{Carbon: } \frac{1}{3} = 0.333 \quad \text{(A.3i)}$$

$$\text{Hydrogen: } \frac{0}{3} = 0 \quad \text{(A.3ii)}$$

$$\text{Oxygen: } \frac{2}{3} = 0.667 \quad \text{(A.3iii)}$$

Oxygen (O_2)

Total moles in O_2 = 2 O atom = 2 atoms

Resultant atomic ratios:

$$\text{Carbon: } \frac{0}{2} = 0 \quad \text{(A.4i)}$$

$$\text{Hydrogen: } \frac{0}{2} = 0 \quad \text{(A.4ii)}$$

$$\text{Oxygen: } \frac{2}{2} = 1 \quad \text{(A.4iii)}$$

Sample calculations of stoichiometric coefficients using the lever arm rule for the biomass combustion process is shown below:

Generally,

$$\text{Lever arm } (D_{CH}) = \frac{\text{Segment length/distance from point M}}{\text{Total measured length/distance}}$$

From the reactant line in Figure 3.9

$$\text{Biomass lever arm } (D_{Bio}) = \frac{63.88 \text{ mm}}{108.97 \text{ mm}} = 0.586$$

$$O_2 \text{ lever arm } \left(D_{O_2}\right) = \frac{45.09 \text{ mm}}{108.97 \text{ mm}} = 0.414$$

NB: The O_2 lever arm (D_{O_2}) can alternatively be given as 1 - 0.586 = 0.414

From the product line in Figure 3.10

$$CO_2 \text{ lever arm } (D_{CO_2}) = \frac{52.98 \text{ mm}}{90.05 \text{ mm}} = 0.588$$

$$H_2O \text{ lever arm } (D_{H_2O}) = 1 - 0.589 = 0.412$$

Determining the stoichiometric coefficients (SC), we use Equation 3.21

$$\frac{\text{Length, } D_{CH}}{\text{Total length between reactant or product}} = \frac{(\text{Stoichiometric coefficient, SC}) \times (\text{Number of atoms in CH})}{\text{Total number of atoms for all reactants or products}} \tag{3.40}$$

For O_2 stoichiometric coefficient,

$$O_2 \text{ lever arm } (D_{O_2}) = \frac{45.09 \text{ mm}}{108.97 \text{ mm}} = 0.414$$

Number of atoms in O_2 = 2

For the combustion of 1 mole of biomass, the total number of atoms in reactants becomes $2 \times SC_{O_2} + 2.99$

Therefore, from Equation 3.21 we get

$$\frac{45.09 \text{ mm}}{108.97 \text{ mm}} = \frac{(SC_{O_2}) \times 2}{2.99 + 2(SC_{O_2})}$$

and

$$SC_{O_2} = 1.055$$

CO_2 stoichiometric coefficient is calculated as follows:

$$CO_2 \text{ lever arm } \left(D_{CO_2}\right) = \frac{52.98 \text{ mm}}{90.05 \text{ mm}} = 0.588$$

Number of atoms in $CO_2 = 3$

For the combustion of 1 mole of biomass, the total number of atoms in reactants using the stoichiometric coefficient of O_2 is

$$2 \times SC_{O_2} + 2.99 = 2 \times 1.055 + 2.99 = 5.1$$

Therefore, from Equation 3.21 we get

$$\frac{52.98 \text{ mm}}{90.05 \text{ mm}} = \frac{(SC_{CO_2}) \times 3}{5.1}$$

and

$$SC_{CO_2} = 1.000$$

Likewise, H_2O stoichiometric coefficient is calculated as follows:

$$H_2O \text{ lever arm } \left(D_{H_2O}\right) = \frac{37.02 \text{ mm}}{90.05 \text{ mm}} = 0.412$$

Number of atoms in $H_2O = 3$

For the combustion of 1 mole of biomass, the total number of atoms in reactants using the stoichiometric coefficient of O_2 becomes

$$2 \times SC_{O_2} + 2.99 = 2 \times 1.055 + 2.99 = 5.1$$

Therefore, from Equation 3.21 we get

$$\frac{37.07\ \text{mm}}{90.05\ \text{mm}} = \frac{(SC_{CO_2})\times 3}{5.1}$$

and

$$SC_{H_2O} = 0.700$$

NB: The stoichiometric coefficient of H_2O can also be calculated from Equation 3.21 using the total number of atoms in the products. In this case, the total number of atoms in the products using the stoichiometric coefficient of CO_2 becomes

$$3\times SC_{H_2O} + 3\times SC_{CO_2} = 3\times SC_{H_2O} + 3$$

Using Equation 3.21, we get

$$\frac{37.07\ \text{mm}}{90.05\ \text{mm}} = \frac{(SC_{H_2O})\times 3}{3 + 3(SC_{H_2O})}$$

and

$$SC_{H_2O} = 0.700$$

Therefore, the material balance for the biomass combustion process corresponds to Equation 3.20

$$1CH_{1.4}O_{0.59} + 1.055O_2 - 0.7H_2O - 1CO_2 = 0 \qquad (3.41)$$

The lever arm rule measurements and their respective relative distances for the product and reactant lines in all the processes referred to in the study are summarized in Table A.1 below.

Table A.1. Summary of lever arm measurements, relative distance and stoichiometric coefficients

Figure 4.5	Overall DME biorefinery			
	Compounds	Measured Segment (mm)	Relative distance	SC (moles)
Reactants	Biomass	28.87	0.737	2.844
	H_2O	10.28	0.263	1.009
Products	DME	59.8	0.781	1 (basis)
	CO_2	16.81	0.219	0.844
Figure 4.9	One-step/Direct DME synthesis route			
Reactants	H_2	48.3	0.5	3
	CO	48.3	0.5	3
Products	DME	51.63	0.75	1 (basis)
	CO_2	17.21	0.25	1
Figure 4.10	Two-step/Indirect DME synthesis route			
Reactants	H_2	64.4	0.667	4
	CO	32.20	0.333	2
Products	DME	18.54	0.75	1 (basis)
	H_2O	6.18	0.25	1
Figure 4.14	Biomass gasification with H_2O/O_2 co-feed			
Reactants	Biomass	26.9	0.747	1 (basis)
	$H_{0.594}O_{0.406}$	9.1	0.253	1.011
Products[a]	H_2			
	CO			
Figure 4.15	Biomass gasification with H_2O/CO_2 co-feed			
Reactants	Biomass	21.07	0.708	1 (basis)
	$C_{0.045}H_{0.577}O_{0.378}$	8.67	0.292	1.23
Productsa	H_2			
	CO			
Figure 4.19	Biomass co-feed with H_2O and CH_4			
Reactants	Biomass	26.059	0.35	1.058
	$C_{0.1603}H_{0.7558}O_{0.0639}$	14.031	0.65	5.874
Products[a]	DME			1
Figure 4.21	Biomass gasification with H_2O/CH_4 co-feed			
Reactants	Biomass	7.79	0.264	1

	$C_{0.107}H_{0.737}O_{0.0.156}$	21.67	0.736	8.317
Products[a]	H_2			
	CO			

[a] Stoichiometric coefficients for products determined algebraically

APPENDIX B: ANALYSIS OF THE CHEMICAL EQUILIBRIUM SYSTEM

Determination of the number of components, C

MATLAB statement for determining the atom matrix rank

>>rank ([1 0 2; 0 2 1; 1 0 1; 1 4 0; 1 0 0; 0 2 0])

Ans. = 3

Thus, the rank of the atom matrix = 3

Determination of independent reactions (r)

From the analysis of the C-H-O system, it was found that the system consists of 6 chemical species (i.e. N = 6). These species are CO, CO_2, H_2O, CH_4, C(s) and H_2. It was also found that the system has 3 phase rule components (C), namely C, H, and O.

The relationship between the number of components C, the number of chemical species N and the number of independent reactions, r, is given by

$$C = N - r \tag{3.42}$$

Rearranging the equation gives

$$r = N - C$$

Given C = 3 and N = 6, then

$$r = 6 - 3 = 3$$

That is, there are three independent reactions in the system. The next step is to determine the set of independent reactions. The formation reactions for the molecular species present in the system (i.e. H_2O, H_2, C(s), CO_2, CO and CH_4) are written as follows:

$$C + 0.5O_2 = CO \quad \text{(A.5i)}$$

$$C + O_2 = CO_2 \quad \text{(A.5ii)}$$

$$H_2 + 0.5O_2 = H_2O \quad \text{(A.5iii)}$$

$$C + 2H_2 = CH_4 \quad \text{(A.5iv)}$$

Because elemental oxygen does not appear as part of the N species, it is eliminated from the set of independent formation reactions. By choosing any of the above equations that has an oxygen molecule, for instance Equation A.5i, the following substitutions and rearrangements of the atomic species can be done:

$$C + 0.5O_2 = CO \quad \text{(A.5i)}$$

$$0.5O_2 = CO - C \quad \text{(A.5v)}$$

Substituting Equation A.5v into all the equations that consist of molecular oxygen, we get the following:

Equation A.5ii becomes

$$C + 2(CO - C) = CO_2$$

$$C + 2CO - 2C = CO_2$$

$$2CO = C + CO_2 \quad \text{(A.5vi)}$$

Equation A.5iii becomes

$$H_2 + CO - C = H_2O$$

$$H_2 + CO = C + H_2O \quad \text{(A.5vii)}$$

This results in the following set of three independent reactions;

$$2CO = C + CO_2 \quad \text{(A.5vi)}$$

$$H_2 + CO = C + H_2O \quad \text{(A.5ii)}$$

$$C + 2H_2 = CH_4 \quad \text{(A.5iv)}$$

The three independent reactions are the Boudouard equilibrium, Heterogeneous water gas shift reaction and Hydrogenation gasification/Methanation respectively.

From the phase rule expression in Equation 3.33

$$F = 2 - \pi + N - r \quad (3.43)$$

Given N = 6, π = 2 and r = 3

$$F = 2 - 2 + 6 - 3 = 3 = 3$$

The phase rule shows that there are three degrees of freedom. Therefore, to be able to define the system at equilibrium, three variables need to be specified. Temperature, pressure and one atomic ratio will define the system.

APPENDIX C: SAMPLE CALCULATIONS OF SUSTAINABILITY METRICS

$$\text{E-Factor} = \frac{\text{Mass of waste produced}}{\text{Mass of desired product}}$$

$$\text{Atom Economy} = \frac{\text{Mass of desired product}}{\text{Total mass of feed}} \times 100$$

$$\text{Carbon Efficiency} = \frac{\text{Moles of C in desired product}}{\text{Moles of C in feed}} \times 100$$

From the definitions of the sustainability metrics, the following sample calculations can be done from the overall material balance targets for DME production:

$$2.844CH_{1.4}O_{0.59} + 1.009H_2O \Longrightarrow 1C_2H_6O + 0.844CO_2 \tag{4.3}$$

$$\text{E-Factor} = \frac{(0.844\ \text{mol})\times(44\ \text{g/mol})}{(1\ \text{mol})\times(46\ \text{g/mol})} = 0.81$$

$$\text{Atom Economy} = \frac{(1\ \text{mol})\times(46\ \text{g/mol})}{(2.844\ \text{mol})\times(22.84\,\text{g/mol})+(1.009\ \text{mol})\times(18\ \text{g/mol})}\times 100 = 55\%$$

$$\text{Carbon Efficiency} = \frac{2}{2.844}\times 100 = 70\%$$

APPENDIX D: SAMPLE EQUILIBRIUM CALCULATIONS FOR MOLE FRACTIONS OF TRACE SPECIES

For any given species, $C_\alpha H_\beta O_\gamma N_\theta$, the formation reaction becomes (Mohnot, 1977)

$$\alpha C + \frac{\beta}{2}H_2 + \frac{\gamma}{2}O_2 + \frac{\theta}{2}N_2 = C_\alpha H_\beta O_\gamma N_\theta \tag{A.6}$$

Where α, β, γ and θ are the number of respective atoms in the species molecule

The mole fraction of the species is given by

$$x_{C_\alpha H_\beta O_\gamma N_\theta} = K_f P^{(\beta+\gamma+\theta)/2}\sqrt{x_{H_2}^{\beta} x_{O_2}^{\gamma} x_{N_2}^{\theta}} \tag{A.7}$$

where,

$$K_f = \exp\left(\frac{-\Delta G^f}{RT}\right) \tag{3.23}$$

Taking methanol for example, the formation reaction becomes

$$C + \frac{4}{2}H_2 + \frac{1}{2}O_2 + \frac{0}{2}N_2 = CH_3OH \tag{A.8}$$

The equation corresponds to

$$C(c) + 2H_2(g) + \frac{1}{2}O_2(g) = CH_3OH(g) \tag{A.8}$$

At 800 K, ΔG^f = -21.1 kcal/mole (Stull et al., 1987),

But,

$$K_f = \exp\left(\frac{-\Delta G^f}{RT}\right) \tag{3.23}$$

$$K = \exp\left(\frac{-(-21100)}{1.987(800)}\right) = 5.82\times10^5$$

Therefore, from Equation A.7, the mole fraction of methanol becomes

$$x_{CH_3OH} = K_{f(CH_3OH)} P^{(4+1+0)/2} \sqrt{x_{H_2}^4 x_{O_2}^1 x_{N_2}^0} \tag{A.9}$$

$$x_{CH_3OH} = K_{f(CH_3OH)} P^{2.5} (x_{H_2}^2)\left(x_{O_2}\right)^{\frac{1}{5}} \tag{A.9}$$

The mole fraction of O_2 is required to be able to determine the mole fraction of methanol

Considering the CO_2 formation,

$$C(c) + O_2(g) = CO_2\ (g) \qquad \text{(A.5ii)}$$

$$K = \frac{x_{CO_2}}{x_{O_2}} \qquad \text{(A.10)}$$

Rearranging the expression of the equilibrium constant,

$$x_{O_2} = \frac{x_{CO_2}}{K} \qquad \text{(A.11)}$$

At 800 K, ΔG^f for CO_2 formation is -94.54 kcal/mol (Stull et al., 1987)

and

$$K = \exp\left(\frac{-(-94540)}{1.987(800)}\right) = 6.75\times10^{25}$$

From above equations, the values for the mole fraction of CO_2 (x_{CO_2}) are found in Table A.2. The mole fraction of O_2 is then calculated using the values of the equilibrium constant for the formation of CO_2 in the same way at 900 and 1000 K. Based on Table A.2, for H/O = 0.01 at 800 K,

$$x_{O_2} = \frac{x_{CO_2}}{K} = \frac{0.896}{6.75\times10^{25}} = 1.328\times10^{-26}$$

The data of the mole fraction of O_2 at the same H/O ratios used in the calculation of the equilibrium composition are presented in Table A.4. Using values from Table A.2, the mole fraction of methanol at equilibrium can be calculated as follows:

$$x_{CH_3OH} = K_{f(CH_3OH)}P^{(4+1+0)/2}\sqrt{x_{H_2}^4 x_{O_2}^1 x_{N_2}^0} \Longrightarrow x_{CH_3OH} = K_{f(CH_3OH)}P^{2.5}(x_{H_2}^2)\left(x_{O_2}\right)^{\frac{1}{5}}$$

Then,

$$x_{CH_3OH} = \left(5.82\times10^{5}\right)\left(1^{2.5}\right)\left(0.03^{2}\right)\left(1.328\times10^{-26}\right)^{0.5} = 6.032\times10^{-13}$$

The rest of the data for the mole fraction of methanol are presented in Table A.4. The same procedure is applied for determining the mole fractions of ethane (C_2H_6), ethylene (C_2H_4) and acetylene (C_2H_2) and the results are also presented in Table A.4.

APPENDIX E: DETERMINAION OF MATERIAL BALANCE REGIONS AND TARGETS

(a) Biomass gasification: co-feeding H_2O with CO_2 and O_2

We consider the gasification of 1 mole of biomass with H_2O, CO_2 and O_2 to produce syngas with composition requirements for the downstream direct DME synthesis process. Process inputs considered are H_2O, CO_2, O_2, H_2 and CO. The material balance for the gasification therefore corresponds to

$$1CH_{1.4}O_{0.59} + a\ H_2O + b\ CO_2 + c\ O2 - d\ H_2 - e\ CO = 0 \qquad (A.12)$$

where *a, b, c, d,* and *e* are the amounts of H_2O, CO_2, O_2, H_2 and CO respectively required (if the coefficient is positive) or produce (for a component with a negative coefficient) in the gasification process of 1 mole of biomass. Writing an atomic balance for the overall process, we get

$$\text{Carbon: } b - d = -1 \qquad (A.13i)$$

$$\text{Hydrogen: } 2a - 2e = -1.4 \qquad (A.13ii)$$

$$\text{Oxygen: } a + 2b + 2c - d = -0.59 \qquad (A.13iii)$$

There are five unknown and three mass balance equations. Therefore, the degree of freedom in this system is two. We reduce the degree of freedom to one by introducing the material balance constraint imposed by the direct DME synthesis process in section 4.3.2, i.e. $H_2/CO = 1$. This constraint is expressed from Equation A.12 as

$$d = e \text{ or } d - e = 0 \qquad \text{(A.13iv)}$$

such that there are four material balance equations and five unknown variables. The four equations are plotted by varying the amount of H_2O fed to the process, i.e. choosing values for *a,* and determining the values of *b, c, d* and e as shown in Figure A.1.

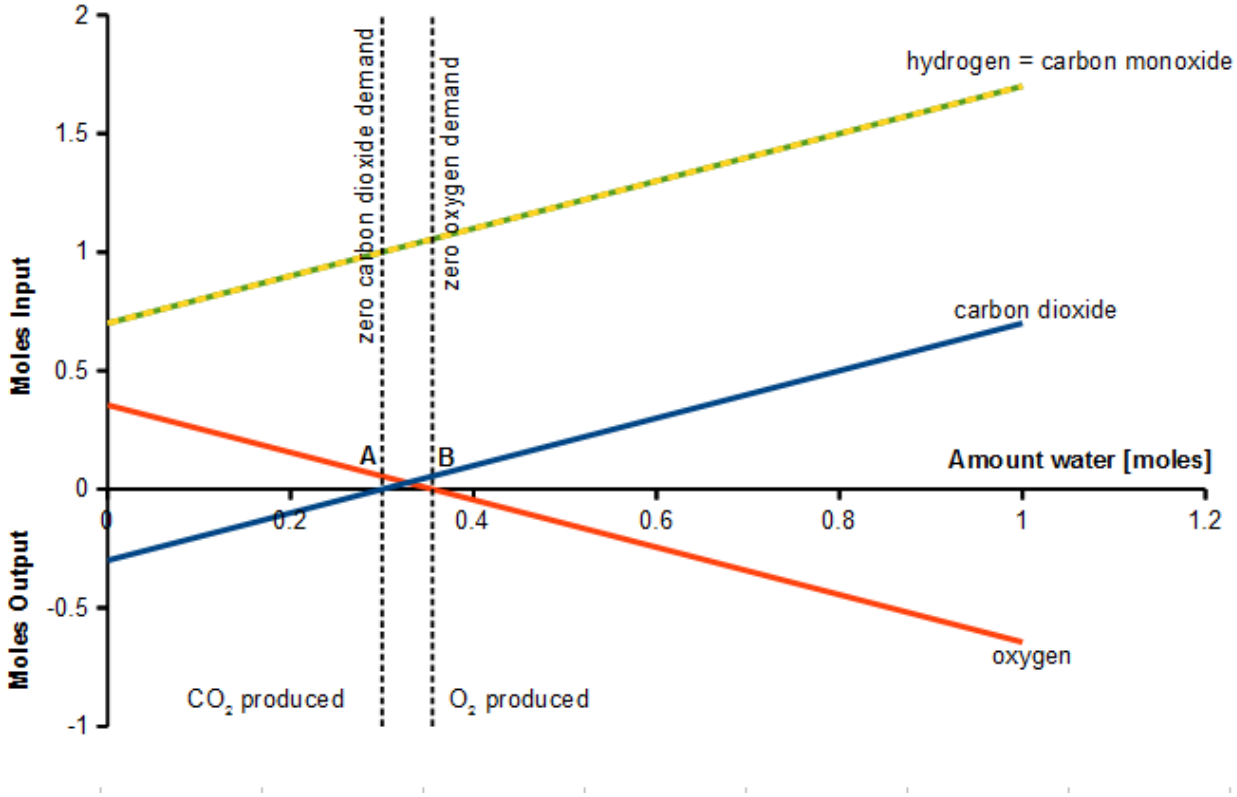

Figure A.1. Material balance regions for the biomass gasification with H_2O co-feed with CO_2 and O_2

From Figure A.1, Points A and B present important material balance targets for the gasification process where CO_2 and O_2 are respectively neither required nor produced. It can be seen that process regions to the left of A produce CO_2 and this is not desirable for the environment. Process targets to the right of B produce O_2 and are considered not feasible. At Point A where CO_2 is zero, the molar quantities of O_2, H_2O, H_2 and CO are respectively 0.055, 0.3, 1, and 1. The material balance target at this point corresponds to

$$1CH_{1.4}O_{0.59} + 0.3\ H_2O + 0.055\ O_2 - H_2 - CO = 0 \qquad (A.14)$$

Equation A.14, represents a biomass gasification process that involves co-feeding H_2O with O_2.

At Point B where O_2 is zero, the molar quantities of H_2O, CO_2, H_2 and CO are respectively 0.355, 0.055, 1.055 and 1.055 and the process target is represented by the following material balance

$$1CH_{1.4}O_{0.59} + 0.355\ H_2O + 0.055\ CO_2 - 1.055\ H_2 - 1.055\ CO = 0 \qquad (A.15)$$

Equation A.15 represents a biomass gasification process in which H_2O is co-fed with CO_2.

(b) Biomass gasification with CH_4 co-feed

To achieve a syngas composition of $H_2/CO = 2$, biomass gasification with CH_4 co-feed is considered. Based on 1 mole of biomass feedstock gasified, the material balance of the process corresponds to

$$1CH_{1.4}O_{0.59} + a\ H_2O + b\ CH_4 - c\ H_2 - d\ CO = 0 \qquad (A.16)$$

where *a, b,* c and *d* are the respective amounts of H_2O, CH_4, H_2 and CO required (if the coefficient is positive) or produced (if the coefficient is negative) in the process for converting 1 mole of biomass to syngas that has a composition of $H_2/CO = 2$.

Writing an atomic balance for each species, we get

$$\text{C balance: } b - d = -1 \qquad (A.17i)$$

$$\text{H balance: } 2a + 4b - 2c = -1.4 \qquad (A.17ii)$$

$$\text{O balance: } a - d = -0.59 \qquad (A.17iii)$$

There are four variables and three material balance equations. Therefore, there is one degree of freedom in this system. We reduce the degree of freedom to zero by introducing the material balance constraint imposed by the indirect DME synthesis process target. That is, $H_2/CO = 2$ as shown in section 4.3.2. This constraint is expressed from Equation A.16 as

$$c = 2d \text{ or } c - 2d = 0 \qquad \text{(A.18)}$$

Solving the four material balance equations, we find the material balance target for the biomass gasification process as

$$1CH_{1.4}O_{0.59} + 1.3\ H_2O + 0.89\ CH_4 \Longrightarrow 3.78\ H_2 + 1.89\ CO \qquad \text{(A.19)}$$

APPENDIX F: EQUILIBRIUM GAS-PHASE COMPOSITIONS

Table A.2. Equilibrium composition of major species at 1atm and 800, 900, 1000, 1200 and 1500 K

T(K)	H/O	Mole fractions				
		x_{H_2}	x_{CO}	x_{CO_2}	x_{H_2O}	x_{CH_4}
800	0.010	0.003	0.094	0.896	0.007	0.000
	0.100	0.028	0.090	0.821	0.060	0.001
	0.200	0.053	0.086	0.749	0.108	0.004
	0.600	0.133	0.073	0.538	0.231	0.025
	1.000	0.193	0.063	0.406	0.288	0.051
	1.500	0.244	0.055	0.300	0.317	0.084
	2.000	0.284	0.048	0.232	0.323	0.114
	2.500	0.315	0.043	0.184	0.319	0.139
	6.000	0.421	0.025	0.060	0.245	0.250
	10.000	0.467	0.016	0.027	0.182	0.307
	20.000	0.509	0.009	0.007	0.111	0.364
	30.000	0.525	0.006	0.005	0.076	0.388
	40.000	0.533	0.005	0.003	0.060	0.400
	50.000	0.538	0.004	0.001	0.049	0.407
	60.000	0.541	0.003	0.001	0.041	0.413
	70.000	0.544	0.003	0.001	0.035	0.417
	80.000	0.547	0.002	0.002	0.029	0.421
	90.000	0.547	0.002	0.001	0.028	0.422
	0.010	0.004	0.339	0.653	0.004	0.000

900	0.100	0.043	0.324	0.598	0.034	0.000
	0.200	0.081	0.310	0.546	0.061	0.002
	0.600	0.200	0.264	0.395	0.129	0.013
	1.000	0.284	0.230	0.301	0.160	0.026
	1.500	0.359	0.199	0.225	0.175	0.042
	2.000	0.415	0.176	0.175	0.179	0.056
	2.500	0.459	0.157	0.141	0.176	0.067
	6.000	0.604	0.092	0.048	0.137	0.118
	10.000	0.667	0.063	0.023	0.103	0.144
	20.000	0.723	0.036	0.006	0.065	0.169
	30.000	0.747	0.024	0.004	0.044	0.180
	40.000	0.758	0.019	0.002	0.035	0.186
	50.000	0.770	0.011	0.000	0.036	0.177
	60.000	0.770	0.013	0.001	0.024	0.191
	70.000	0.774	0.011	0.001	0.021	0.193
	80.000	0.777	0.009	0.002	0.017	0.195
	90.000	0.779	0.009	0.001	0.017	0.196
1000	0.010	0.006	0.706	0.287	0.000	0.000
	0.100	0.048	0.676	0.263	0.013	0.000
	0.200	0.090	0.646	0.240	0.023	0.001
	0.600	0.224	0.548	0.173	0.049	0.005
	1.000	0.320	0.478	0.132	0.061	0.010
	1.500	0.407	0.412	0.098	0.067	0.016
	2.000	0.471	0.363	0.076	0.069	0.021
	2.500	0.521	0.324	0.061	0.067	0.026
	6.000	0.694	0.187	0.021	0.052	0.047

	10.000	0.768	0.127	0.009	0.039	0.057
	20.000	0.835	0.070	0.003	0.023	0.068
	30.000	0.861	0.048	0.002	0.017	0.072
	40.000	0.875	0.036	0.002	0.013	0.075
	50.000	0.882	0.030	0.000	0.011	0.076
	60.000	0.888	0.025	0.000	0.009	0.077
	70.000	0.893	0.021	0.001	0.007	0.078
	80.000	0.897	0.017	0.002	0.006	0.078
	90.000	0.898	0.017	0.000	0.006	0.079
1200	0.010	0.005	0.976	0.018	0.000	0.000
	0.100	0.047	0.935	0.017	0.001	0.000
	0.200	0.090	0.892	0.015	0.002	0.000
	0.600	0.230	0.755	0.011	0.005	0.000
	1.000	0.329	0.655	0.008	0.006	0.002
	1.500	0.423	0.562	0.006	0.007	0.003
	2.000	0.493	0.492	0.005	0.006	0.004
	2.500	0.548	0.437	0.004	0.006	0.005
	6.000	0.740	0.245	0.002	0.004	0.008
	10.000	0.822	0.163	0.001	0.003	0.010
	20.000	0.896	0.087	0.001	0.003	0.012
	30.000	0.924	0.060	0.001	0.001	0.013
	40.000	0.938	0.047	0.001	0.001	0.014
	50.000	0.946	0.038	0.000	0.001	0.015
	60.000	0.953	0.033	0.000	0.000	0.014
	70.000	0.957	0.027	0.000	0.001	0.014
	80.000	0.962	0.021	0.001	0.001	0.014

	90.000	0.964	0.020	0.001	0.001	0.015
1500	0.010	0.005	0.994	0.001	0.000	0.000
	0.100	0.048	0.952	0.001	0.000	0.000
	0.200	0.091	0.908	0.001	0.000	0.000
	0.600	0.231	0.768	0.001	0.000	0.000
	1.000	0.333	0.667	0.000	0.000	0.000
	1.500	0.426	0.571	0.000	0.001	0.001
	2.000	0.500	0.499	0.000	0.000	0.000
	2.500	0.556	0.443	0.001	0.000	0.000
	6.000	0.750	0.249	0.001	0.000	0.000
	10.000	0.834	0.165	0.001	0.000	0.000
	20.000	0.910	0.090	0.001	0.000	0.000
	30.000	0.938	0.061	0.001	0.000	0.000
	40.000	0.953	0.046	0.001	0.000	0.000
	50.000	0.959	0.038	0.000	0.000	0.003
	60.000	0.966	0.032	0.000	0.000	0.002
	70.000	0.969	0.028	0.000	0.000	0.003
	80.000	0.976	0.023	0.001	0.000	0.000
	90.000	0.979	0.020	0.001	0.000	0.000

Table A.3. Atom percentages of C, H and O for the equilibrium gas composition at 1 atm and 800, 900, 1000, 1200 and 1500 K

T(K)	H/O	C	H	O
800	0.010	0.346	0.007	0.647
	0.100	0.319	0.068	0.613
	0.200	0.293	0.128	0.578
	0.600	0.221	0.307	0.472
	1.000	0.177	0.425	0.398
	1.500	0.144	0.523	0.333
	2.000	0.124	0.590	0.286
	2.500	0.111	0.639	0.251
	6.000	0.082	0.784	0.134
	10.000	0.079	0.834	0.087
	20.000	0.080	0.874	0.046
	30.000	0.082	0.886	0.032
	40.000	0.083	0.893	0.024
	50.000	0.084	0.897	0.019
	60.000	0.085	0.899	0.016
	70.000	0.085	0.901	0.014
	80.000	0.086	0.902	0.012
	90.000	0.086	0.903	0.011
900	0.010	0.387	0.007	0.606
	0.100	0.362	0.066	0.572
	0.200	0.337	0.123	0.539

	0.600	0.266	0.296	0.438
	1.000	0.220	0.411	0.369
	1.500	0.183	0.510	0.308
	2.000	0.157	0.579	0.264
	2.500	0.139	0.630	0.231
	6.000	0.086	0.790	0.124
	10.000	0.068	0.851	0.081
	20.000	0.054	0.902	0.044
	30.000	0.049	0.921	0.030
	40.000	0.047	0.930	0.023
	50.000	0.041	0.936	0.017
	60.000	0.045	0.939	0.015
	70.000	0.044	0.942	0.013
	80.000	0.044	0.945	0.011
	90.000	0.044	0.946	0.010
1000	0.010	0.449	0.006	0.545
	0.100	0.426	0.056	0.518
	0.200	0.403	0.106	0.491
	0.600	0.333	0.261	0.406
	1.000	0.285	0.368	0.347
	1.500	0.242	0.465	0.294
	2.000	0.211	0.534	0.255
	2.500	0.188	0.587	0.225
	6.000	0.110	0.766	0.124
	10.000	0.078	0.839	0.083

	20.000	0.049	0.906	0.045
	30.000	0.039	0.930	0.031
	40.000	0.033	0.943	0.023
	50.000	0.030	0.950	0.019
	60.000	0.028	0.956	0.016
	70.000	0.026	0.960	0.014
	80.000	0.025	0.964	0.012
	90.000	0.024	0.965	0.011
1200	0.010	0.494	0.005	0.500
	0.100	0.473	0.048	0.479
	0.200	0.451	0.092	0.457
	0.600	0.381	0.233	0.386
	1.000	0.331	0.335	0.335
	1.500	0.283	0.430	0.287
	2.000	0.248	0.501	0.251
	2.500	0.221	0.556	0.223
	6.000	0.125	0.749	0.125
	10.000	0.084	0.832	0.084
	20.000	0.046	0.908	0.045
	30.000	0.033	0.936	0.031
	40.000	0.026	0.950	0.024
	50.000	0.022	0.958	0.019
	60.000	0.019	0.964	0.016
	70.000	0.016	0.969	0.014
	80.000	0.014	0.974	0.012

	90.000	0.013	0.976	0.011
1500	0.010	0.497	0.005	0.498
	0.100	0.476	0.048	0.476
	0.200	0.454	0.091	0.455
	0.600	0.384	0.231	0.385
	1.000	0.333	0.333	0.333
	1.500	0.286	0.428	0.286
	2.000	0.250	0.500	0.250
	2.500	0.222	0.556	0.222
	6.000	0.125	0.751	0.125
	10.000	0.083	0.834	0.083
	20.000	0.045	0.910	0.045
	30.000	0.031	0.938	0.031
	40.000	0.023	0.953	0.024
	50.000	0.020	0.961	0.019
	60.000	0.016	0.968	0.016
	70.000	0.015	0.971	0.014
	80.000	0.012	0.976	0.012
	90.000	0.010	0.979	0.011

Table A.4. Equilibrium gas composition of minor species at 1 atm and 800, 900 and 1000 K

T (K)	H/O	x_{O_2}	x_{CH_3OH}	$x_{C_2H_6}$	$x_{C_2H_4}$	$x_{C_2H_2}$
800	0.01	1.328E-26	6.032E-13	1.215E-12	1.834E-12	4.785E-15
	0.1	1.216E-26	5.030E-11	9.879E-10	1.597E-10	4.466E-14
	0.2	1.110E-26	1.721E-10	6.700E-09	5.723E-10	8.454E-14
	0.6	7.971E-27	9.187E-10	1.059E-07	3.604E-09	2.122E-13
	1	6.015E-27	1.681E-09	3.235E-07	7.589E-09	3.079E-13
	1.5	4.445E-27	2.309E-09	6.537E-07	1.213E-08	3.892E-13
	2	3.437E-27	2.751E-09	1.031E-06	1.643E-08	4.530E-13
	2.5	2.726E-27	3.014E-09	1.407E-06	2.022E-08	5.025E-13
	6	8.890E-28	3.074E-09	3.358E-06	3.611E-08	6.715E-13
	10	4.000E-28	2.538E-09	4.583E-06	4.443E-08	7.449E-13
	20	1.037E-28	1.535E-09	5.934E-06	5.279E-08	8.119E-13
	30	7.408E-29	1.380E-09	6.512E-06	5.616E-08	8.374E-13
	40	4.445E-29	1.102E-09	6.814E-06	5.788E-08	8.502E-13
	50	1.482E-29	6.481E-10	7.008E-06	5.897E-08	8.582E-13
	60	1.482E-29	6.554E-10	7.126E-06	5.963E-08	8.630E-13
	70	1.482E-29	6.627E-10	7.245E-06	6.030E-08	8.678E-13
	80	2.963E-29	9.475E-10	7.365E-06	6.096E-08	8.725E-13
	90	1.482E-29	6.700E-10	7.365E-06	6.096E-08	8.725E-13
	100	6.693E-30	4.525E-10	7.420E-06	6.126E-08	8.747E-13
900	0.01	7.036E-24	6.748E-13	5.085E-13	6.382E-12	2.700E-13
	0.1	6.444E-24	7.462E-11	6.317E-10	7.375E-10	2.903E-12
	0.2	5.883E-24	2.530E-10	4.222E-09	2.617E-09	5.468E-12
	0.6	4.256E-24	1.312E-09	6.356E-08	1.595E-08	1.350E-11

	1	3.243E-24	2.309E-09	1.820E-07	3.217E-08	1.917E-11
	1.5	2.424E-24	3.190E-09	3.676E-07	5.141E-08	2.423E-11
	2	1.886E-24	3.760E-09	5.678E-07	6.869E-08	2.801E-11
	2.5	1.519E-24	4.129E-09	7.683E-07	8.403E-08	3.098E-11
	6	5.172E-25	4.171E-09	1.751E-06	1.455E-07	4.077E-11
	10	2.478E-25	3.521E-09	2.358E-06	1.774E-07	4.502E-11
	20	6.465E-26	2.113E-09	3.003E-06	2.085E-07	4.880E-11
	30	4.310E-26	1.842E-09	3.312E-06	2.226E-07	5.042E-11
	40	2.155E-26	1.341E-09	3.460E-06	2.292E-07	5.117E-11
	50	-	-	-	-	5.198E-11
	60	1.078E-26	9.785E-10	3.627E-06	2.365E-07	5.198E-11
	70	1.078E-26	9.887E-10	3.684E-06	2.389E-07	5.225E-11
	80	2.155E-26	1.409E-09	3.727E-06	2.408E-07	5.245E-11
	90	1.078E-26	1.001E-09	3.756E-06	2.420E-07	5.258E-11
1000	0.01	6.028E-22	7.732E-13	4.200E-13	2.409E-11	7.982E-12
	0.1	5.524E-22	4.737E-11	2.151E-10	1.541E-09	6.386E-11
	0.2	5.041E-22	1.591E-10	1.418E-09	5.419E-09	1.197E-10
	0.6	3.634E-22	8.367E-10	2.186E-08	3.357E-08	2.980E-10
	1	2.772E-22	1.492E-09	6.372E-08	6.851E-08	4.257E-10
	1.5	2.058E-22	2.079E-09	1.311E-07	1.108E-07	5.414E-10
	2	1.596E-22	2.452E-09	2.032E-07	1.484E-07	6.266E-10
	2.5	1.281E-22	2.688E-09	2.750E-07	1.816E-07	6.931E-10
	6	4.411E-23	2.798E-09	6.500E-07	3.222E-07	9.232E-10
	10	1.890E-23	2.243E-09	8.809E-07	3.946E-07	1.022E-09
	20	6.301E-24	1.531E-09	1.132E-06	4.665E-07	1.111E-09
	30	4.201E-24	1.329E-09	1.241E-06	4.960E-07	1.145E-09

	40	4.201E-24	1.373E-09	1.303E-06	5.122E-07	1.164E-09
	50	-	-	-	1.173E-09	-
	60	-	-	-	1.181E-09	-
	70	2.100E-24	1.385E-06	5.335E-07	1.188E-09	-
	80	4.201E-24	1.403E-06	5.383E-07	1.193E-09	-
	90	-	-	-	1.195E-09	-